Marine Diesel engine response to ventilation loads

MT71 MSc. Thesis

E.J.C. Hendrix

Technische Universiteit Delft

TU Delft Delft University of Technology

Challenge the future

Marine Diesel engine response to ventilation loads

MT71 MSc. Thesis

by

E.J.C. Hendrix

in partial fulfillment of the requirements for the degree of

Master of Science
in Marine Technology

at the Delft University of Technology.

This study will be presented publicly on-line and is
to be defended on monday december 14^{th} 2020 at 11:00 AM.

Student number:	1357581	
Report number:	SDPO.20.006.m	
Thesis committee:	ir. K. Visser	TU Delft
	Dr.-Ing. S. Schreier	TU Delft
	Dr. ir. A. Vrijdag	TU Delft, supervisor

An electronic version of this thesis will be made available at http://repository.tudelft.nl/.

The cover image is taken by the author at Svolværingen on Tranøy (NO). This former whaler shows the 'wet' side of this thesis: A propeller on the stern of her hull, where ventilation can be drawn from the waterline and through the propeller-plane.

TU Delft Delft University of Technology

Det har jag aldrig provad förut
så det klarar jag säkkert!

PIPI LÅNGSTRUMP

(I've never tried that before
so I'm sure I can do it!)

List of Tables

1.1 Stakeholders affected by inability to describe an engine's ventilation-response. 3
1.2 Damagetypes found on thrusters during their regular services. Source:[1] 4
1.3 Risk as a product of effect (↑) and probability (→) 4
1.4 "Adverse conditions" mean sea conditions with the following parameters. Based on source: [2] 5
1.5 Steps in the development of theory by using simulation. Source: [3] 8

2.1 Evaluation and comparison of model technologies: engine core model. Source [4] . . . 19
2.2 Components connecting different domains related to propeller ventilation. (Abbreviations in nomenclature). 19

3.1 Resistance prediction methods according to Bentley (2014) [5] and [6]. 28
3.2 Ventilation scaling laws as posed by [7]. 31
3.3 Table summarising research efforts regarding propeller-ventilation. ≤≤is a range of static immersion ratio's, (eq,amp) is a sinusoidal immersion ratio with equilibrium eq and amplitude amp, u = unknown, $\underline{\leq\leq}$= range of highest peaks, T = thrust, M = torque, avg = average, bs = blade spindle, exp = experimental, the = theoretical, Azi = azimuthing thruster, O = open, D = Ducted, ∀ = for all values, δ = steering angle [deg], σ_v = ventilation number, C_{Li} = lift coefficient for ideal angle of attack, k_p = propeller-characteristic coefficients, Q_a = added torque (bias) and Q_f = friction torque. 34
3.4 Engine limits. 39

4.1 Relations waves-block MSS. source: [8] 44
4.2 Organisation of different wave-types in the waves-block. 45
4.3 Relations added wave force $\tau_{wave,x}$. 45
4.4 Relations equations of motion in x, z, ϑ-direction. 46
4.5 Further hydromechanic assumptions. 46
4.6 Relations of the propeller sub-model. 48
4.7 Relations governor consisting of limited PI-controller & fuelpump. 48
4.8 table 49
4.9 Relations limited heat-to-pressure estimator. 50
4.10 Relations shaft. 50
4.11 Applied characteristic rotational intertia (left) and 1^{th} order time-constant (right). . . . 52

5.1 Waves-block verification. 54
5.2 Seven summarising steps in the analyses of experiments 61

6.1 Variation of input-parameters for experiments A-D. 67
6.2 For experiment A, the hypotheses are posed that: 67
6.3 For experiment B, the hypotheses are posed that: 67
6.4 For experiment C, the hypotheses are posed that: 67
6.5 For experiment D, the hypotheses are posed that: 68
6.6 Characteristic properties of a ventilation event. 79

7.1 List of data-types, parameters and applications of 88

C.1 Dimensionless parameters. 101

D.1 Dimensions from Damen combi freighter 3850 product sheet. Source: [9] 106
D.2 Propulsion system from Damen combi freighter 3850 product sheet. Source: [9] 106

D.3 Performances from Damen combi freighter 3850 product sheet. Source: [9] 106

E.1 Selection of general data from subsection 3.3 Technical data - Wärtsilä 8L20. ME = Engine driving propeller, variable speed. Source: [10] 107
E.2 Selection of combustion air system data from subsection 3.3 Technical data - Wärtsilä 8L20. Note 1 At ISO 15550 conditions and 100% load. Flow tolerance 5%. Source: [10] 107
E.3 Selection of exhaust gas system data from subsection 3.3 Technical data - Wärtsilä 8L20. Note 2 At ISO 15550 conditions. Flow tolerance 5% and temperature tolerance 10^0C. Source: [10] 109

F.1 Summary of modelled prime-mover components and processes. 114

H.1 Data regarding design- and trial conditions of the hull, propeller and engine. Adapted from [11] and [12] 121

I.1 Main particulars of the propeller. Source: [7] 123

List of Figures

1.1 Thruster ventilation. Source: [1] . . . 1
1.2 Ventilation flow regimes, with the regimes relevant for DP indicated on the Ja axis. Adopted from Olofsson. Source:[13] . . . 2
1.3 Engine response to: A) still-water and added resistance and B) propeller ventilation. . . 6

2.1 Schematic layout of a geared medium-speed propulsion system. Source: [14] . . . 9
2.2 Typical propeller design point. Source: [15] . . . 10
2.3 Orientation of body axes relative to fixed axes in terms of ϑ, ψ, φ. Viewed from below xy plane. Source: [16] . . . 11
2.4 Block diagram of translational dynamics. Source: [17] . . . 11
2.5 Figure illustrating the connection between a frequency domain and time domain representation of waves in a long crested short term sea state. Source: [18] . . . 12
2.6 Boundary conditions. Source: [19] . . . 12
2.7 Open-water test results of B4-40 screw series. Source: [20] . . . 14
2.8 Flow thread speeds (in body-bound coordinate system . . . 14
2.9 Influence of submerged depth on open water characteristics (MP8701). Source [7] . . . 15
2.10 Relative blade thrust of open thruster and relative propeller shaft immersion; propeller shaft at highest position h/R=-0.15; amplitude/R=2.15; period=2 s. Source [21] . . . 15
2.11 Operating field for FP propeller. Source: [22] . . . 16
2.12 Torque-speed characteristics. (Of a synchronous machine). Source: [23] . . . 16
2.13 Low-pass(12 Hz) filtered relative blade thrust of open thruster and relative propeller shaft immersion; propeller shaft at highest position h/R=-0.15; amplitude h/R=2.15; period=2 s. Source: [21] . . . 17
2.14 Turbocharger in the propulsion system. . . . 18
2.15 Bond graphs for 3D rigid body motion. Source [24] . . . 20
2.16 Arrangement of subject matters according to Fossen. Source: [25] . . . 20
2.17 A coaster in head seas. Source: [26] . . . 21

3.1 Superposition of wave excitation, added mass, damping and restoring loads. Source [18] 24
3.2 Supeposition of two uni-directional harmonic waves. Source: [19] . . . 25
3.3 Different wave-properties. . . . 25
3.4 Time history including an possible freak wave event. Source [27] . . . 27
3.5 Resistance in waves. Source: [6] . . . 27
3.6 Ventilation addressing strategies and possibilities (dotted). . . . 29
3.7 Coordinate system. Source: [28] . . . 29
3.8 Effect of propeller immersion on blade spindle torque (atmospheric pressure). Source: [29] (Time horizontal, blade spindle torque vertical) . . . 30
3.9 Time trace of T_{Bx} during approximately one wave period. Source: [1] . . . 30
3.10 Comparison of time-averaged loadings of ducted and open thrusters. Source: [21] . . . 30
3.11 Thrust ratio for each blade angular position [–∘– = 16, — = 14, ...∆... = 12 Hz]. h/R = 1. Source: [30] . . . 30
3.12 Influence of ventilation on open water propeller diagram. Adopted from Pohl. Source: [31]. . . . 32
3.13 Ideal liftcoefficient estimated from incipient ventilation. Source: [32] . . . 32
3.14 Parameters a and b for determination of the minimum power line values for the different ship types . . . 35
3.15 Alternative descriptions of time. A: cycle time scale. B: crank angle scale. . . . 35

3.16 Use of: Comparison process of a turbocharged engine (shaded area, index z) with compressor-work (1-1 z-7-8-1) and turbine-work (3-4-8-6-3) for pure pressure-charging, translated from German. Colours adapted, from source: [33] 35
3.17 Relation between pressure ratio π_V and specific effective work w_e, respectively the required turbocharger efficiency η_{ATL} for Diesel engines, translated from German. Source: [33] 37
3.18 Ideal first-order model of turbine-compressor system. Source: [34] 37
3.19 Governor for a diesel engine, schematics of speed droop and isochronous control modes. Source: [35] 38
3.20 Combined torque/power control scheme. Source: [13]. 38
3.21 Example weighting functions $\alpha_1(n_r)$ and $\alpha_2(n_r)$ used in the combined speed/torque/power controller. Source: [13]. 38
3.22 Effect of Waves on a Propeller, a Quasi-Steady Approximation. Source: [19]. Adapted by author. 39
3.23 Block diagram of ship dynamics. Source: [17] 40

4.1 (Selection of) Effect of Waves on a Propeller, a Quasi-Steady Approximation. Source: [19]. Adapted by author. 41
4.2 Steps, {functions}, (parameters) and relations → in the model. 41
4.3 Structure of the model with input (orange) sub-models (magenta) and output (blue). . 42
4.4 Sketch of different types of propeller ventilation. (Left) By formation of a free-surface vortex. (Right) Surface-piercing. Source: [30]. 43
4.5 Conceptual model of: A experimental setup, B estimated immersion $\hat{h}/R$. 43
4.6 Vessel-motion sub-model. 45
4.7 Sub-model of a possibly ventilating propeller. 47
4.8 Influence of submerged depth on open water characteristics (MP8701). Source: [7] . . 47
4.9 Prime-mover sub-model. 49
4.10 Nominal pV-diagram of Seiliger-cycle as used in Diesel A model. 49
4.11 Thrust- and torque loop of the model. 52

5.1 Superposition of two uni-directional harmonic waves with the MSS-toolbox from [8]. . . 54
5.2 Resultant force $F_{x,res}$, acceleration $\dot{x}$ and speed $\dot{x}$ for a sinusoidal variations of thrust T_p in the absence of waves. 55
5.3 Wave-height, heave- and pitch motions for three amplitudes ζ_a with $\omega = 2\pi/11[rads^{-1}]$ at $\dot{x} = 0[ms^{-1}]$. 55
5.4 Immersion-related parameters wave-height ζ, static immersion of 2.5 [m] and motions z and ϑ vary the propeller-shaft immersion h/R. Wave period $T = 11[s]$. 56
5.5 Thrust variation for $J = 0[-]$ and $Fr_p = 0.2[-]$ with h/R [-] varying as in figure 5.4 . . 57
5.6 Characteristic turbine-compressor parameters for sinusoidal 25[%] nominal variations with periods of 3 [s]. 58
5.7 Response to 20 [%] increase and 30 [%] decrease of engine speed setpoint $n_{e,set}$. . . 59
5.8 Envelope of the prime-mover sub-model. 60
5.9 Open-water diagram for model subjected to ventilating load. 61
5.10 Envelope and operational point for model subjected to ventilating load. 62
5.11 Response of the model subjected to ventilating load. 64

6.1 Adverse Torsethaugen spectrum, response amplitude operators and ω_e-values for experiment A. 66
6.2 Open-water diagram for experiment A. 68
6.3 Prime-mover response during 20 [s] time frame for experiment A. 69
6.4 Detail of figure 6.3. 70
6.5 Results for lower wave frequencies ω in experiment A. 72
6.6 Open-water diagram for experiment B. 73
6.7 Prime-mover response for experiment B. 74
6.8 Results for higher wave frequencies ω in experiment B. 75
6.9 Open-water diagram for experiment C. 76
6.10 Prime-mover response for experiment C. 77

6.11 Results for different wave amplitudes ζ_a in experiment C. 78
6.12 Open water diagram for experiment D. 79
6.13 Prime-mover response for experiment D. 80
6.14 Results for an adverse Torsethaugen spectrum in experiment D. 81

7.1 Propeller-shaft immersion ratio h/R and advance coefficient J in experiment A. (Reproduced from figures 6.2 & 6.5). 85
7.2 Open-water diagram for experiment A. (Figure 6.2 reproduced). 85
7.3 Prime-mover response during 20 [s] time frame for experiment A. (Figure 6.3 reproduced). 86
7.4 Prime-mover response for experiment C. (Reproduced figure) 86
7.5 Results for an adverse Torsethaugen spectrum in experiment D. (Reproduced from figure 6.14) 87

D.1 Combi freighter 3850 standard. Source: [9] 105

E.1 Operating field for FP Propeller (DAAF007340). Source: [10] 108
E.2 Maximum recommended load increase rates for variable speed engines. Source: [10] . 108

F.1 Block diagram of ship dynamics. Source: [17] 112

H.1 Maxsurf-Holtrop based predictions, 2^{nd} order and 3^{rd} order still-water resistance curves. 119
H.2 Operational envelope of diesel engine with propeller load curves for different gearbox ratio's i_{gb} and resistance estimates. 120

I.1 Influence of submerged depth on open water characteristics. Source: [7] 123
I.2 Rate of revolution on open water characteristics. Source: [7] 124
I.3 Rate of revolution on open water characteristics. Source: [7] 124
I.4 Adapted from source: [7] 125
I.5 Adapted from source: [7] 125

J.1 Torsethaugen frequency spectrum with H_s = 4m and ω_p = 1rad/s, spreading function with ψ_0 = -30° and s = 4, number of frequencies and directions N = 20 and M = 10, frequency cutoff factor ξ = 2.5 and wave direction limit ψ_{lim} = 20°. 127
J.2 Wave spectrum with wave energy limit κ = 0.005. The frequencies and directions of the components, which are shown as red stars, are chosen at random 127
J.3 Realization of a Torsethaugen spectrum with 200 wave components. 128
J.4 Realization of a Torsethaugen spectrum with 100 wave components. 128
J.5 Realization of a Torsethaugen spectrum with 50 wave components. 128
J.6 Realization of an 50-component adverse Torsethaugen spectrum with the MSS-toolbox from [8]. 129

Nomenclature

Abbreviations

NO_x	Nitrogen oxides
SO_2	sulphur dioxide
CO_2	Carbon dioxide
CPP	Controlable pitch propeller
DP	Dynamic positioning
EEDI	Energy efficiency design index
FPP	Fixed pitch propeller
ITTC	International towing tank conference
MEPC	Marine environment protection committee
PIV	Particle image velocimetry
TIFF	Tooth interior fatigue fracture

Domains

cc	combustion (related) chemistry
el	electrics
fm	fluid mechanics
hm	hydromechanics
hy	hydraulics
me	(Newtonian) mechanics
th	thermodynamics

Greek symbols

α	Crank-angle	[-]
$\epsilon_{i\zeta_a}$	Phase-shift between translation or rotation i and wave component with amplitude ζ_a	[rad]
η_{GB}	Gearbox efficiency $\frac{Q_p[Nm]}{Q_e[Nm]}$	[-]
λ	Wave length.	[m]

λ_{afr}	Air-to-fuel ratio	[-]
ω	Circular (or angular) wave frequency	$[rads^{-1}$
ϕ	Phase angle (evenly distributed between 0 and 2π)	[rad]
ψ	Wave direction	[°]
σ	Cavitation number, *"dimensionless pressure coefficient"* ([7]), or *"nondimensional pressure at mean shaft immersion"* ([36])	[-]
τ	Characteristic 1^{th} order time constant	[s]
ξ	Wave-spectrum frequency cutoff factor	[-]
ζ	Wave height (positive above still-water level)	$[m]$
X	Fuelrack setting	[mm]

Indexes

0	Undisturbed
$\{e\}$	Earth-bound inertial coordinate system, {n} for North-East-down by Fossen (2011) [25]
$\{e\}$	Earth-bound inertial coordinate system
{s}	Seakeeping reference frame of motion around a constant equilibrium state
a	amplitude
e	engine
gb	gearbox
P	Partially ventilating
p	propeller
q	Segment of the frequency domain
r	Segment of the directional domain
S	Superventilating (or fully-ventilated regime)
sw	Still-water (or calm-water) (resistance)
T	Transmission (gearbox and shaft bearings)

General nomenclature

$\dot{x}$	Hull speed in x-direction (scalar)	$[ms^{-1}]$
A_e/A_0	Propeller expanded area ratio	[-]
i	Gearbox ratio $\frac{n_e[rs^1]}{n_p[rs^1]}$	[-]

m_1	Charged mass at the closing of the cylinder	$[kgcycle^{-1}]$
P/D	Propeller blade pitch-ratio	[-]
P_B	Brake engine power	[W]
T_6	Temperature of the mass in the cylinder at the opening of the exhaust valve	$[K]$
u_w	Horizontal flow speed of multiple wave components in the x,y,z,-reference frame, in x-direction.	$[ms^{-1}]$
z_p	Propeller immersion below still-water level	[m]
g	Gravitational acceleration constant	$[ms^{-2}]$
h/R	Dimensionless propeller shaft immersion	[-]
k	Wave number	$[radm^{-1}]$
S	Propeller slip ratio	[-]
t	Thrust-deduction factor	[-]
V	Forward velocity of a vessel (vector)	$[ms^{-1}]$
w	Wake-factor	[-]

Propulsion system components

AX	axle
DE	(marine) Diesel engine
EG	electrical grid
EM	electrical machine
GB	(reduction) gearbox
GT	gas turbine
HU	hull

Abstract

Ventilation events are the result of masses of air being transported from the water surface along the hull, through the propeller plane. Previous research in literature has shown that ventilation induces large and sudden variations of the load on the propeller. The response of the propulsion system had not been documented before. This is a problem with practical and theoretical relevance as both operators and designers of ships and propulsion systems cannot predict the response of these systems to these significant and sudden variations of the propeller-load. The problem can manifest itself in different ways. A first example lies in a possible loss of propulsion and the damages that could incur. A second example lies in the possible installation of too much engine power to respond to unpredictable load-variations such as those incurred by ventilation events.

Increased understanding of the relation between wave properties, -height and -frequency, and the response of a marine Diesel engine, -speed and -torque, subjected to wave-induced ventilation, is the goal of this thesis and leads to the main research question: *How does a marine Diesel engine respond to off-design loads, and in particular to frequently varying loads resulting from propeller ventilation?* It focuses on the response of the prime-mover to variations of the propeller-load imposed by ventilation events. The scope of this thesis covers a monohull coaster with a medium-speed marine Diesel engine moving forward in head seas.

A model is proposed based on the description of immersion by Journée and Massie (2001) [19]. It consists of three sub-models that describe vessel-motion, the propeller and the prime-mover. The vessel-motion is described with a combination of potential-flow based methods and viscous theory. A quasi-static approach is proposed to describe the influence of ventilation on propeller-functioning. The prime-mover is modelled with a closed-cylinder process and an idealised first-order turbo-charger model that applies the exhaust-flow temperature of the closed-cylinder process to describe the charge-pressure.

Three limits to this model lie in the application of vessel-motion data in a limited, positive domain, the application of 1^{th} quadrant propeller data and the propeller envelope. This model uses input consisting of waves and the engine speed setpoint. The output consists of the rotational speed and produced torque of the prime-mover subjected to ventilation. Verification showed responses comparable to, and in the range and time frame of experimental results by Koushan (2007) [21]. Validation efforts lie beyond the scope of this thesis.

Experiments by means of simulations have been performed for two engine speed setpoints and different wave-types describing head seas: Regular waves characterised by low frequencies, -characterised by high frequencies and -characterised by different wave amplitudes. A final experiment subjected the model to an adverse long-crested wave-spectrum for ocean waves.

The research at hand found that the propeller immersion-ratio couples imposed waves and vessel-motions, to the inception of ventilation events. The quasi-static approach to model the influence of ventilation on propeller-functioning provided a reasonable estimate in verification, although further validation efforts are still required.
The main research question led to the answer that:

Frequently varying loads resulting from propeller ventilation can induce a significant shift in the operational point in the propellers open-water diagram and engines PV diagram and increase of the variations of engine speed n_e and -torque Q_e.

The final chapter also provides a number of pointers for a further validation effort, possible improvements to the proposed method and advice regarding further research.

Contents

List of Tables v

List of Figures vii

Abstract xv

1 Introduction 1
1.1 Propeller ventilation . . . 1
1.2 Problems regarding propeller ventilation . . . 3
1.3 Missing theoretical description . . . 6
1.4 Goal and scope of research . . . 7
1.5 Research questions . . . 7
1.6 Research approach . . . 8

2 Theoretical background 9
2.1 Ventilation and the marine propulsion system . . . 9
2.2 Vessel-motion theory . . . 11
2.3 Propeller theory . . . 14
2.4 Prime-mover theory . . . 16
2.5 Connecting components . . . 19
2.6 Detailed scope of research . . . 21

3 Literature research 23
3.1 Vessel-motion literature . . . 23
3.2 Propeller literature . . . 28
3.3 Prime-mover literature . . . 34
3.4 Modelling interaction in literature . . . 39
3.5 Summary . . . 40

4 A quasi-static ventilation model 41
4.1 The quasi-static approach . . . 41
4.2 Vessel-motion sub-model . . . 45
4.3 Propeller sub-model . . . 47
4.4 Prime-mover sub-model . . . 48
4.5 Selecting a suitable vessel-design . . . 50
4.6 Summary . . . 51

5 Model verification 53
5.1 Introduction . . . 53
5.2 Input-signals . . . 53
5.3 Verification of the vessel-motion . . . 54
5.4 Verification of the propeller . . . 56
5.5 Verification of the prime-mover . . . 58
5.6 Verification of the model . . . 60
5.7 Conclusion . . . 62

6 Experiment by simulation 65
6.1 Experimental setup and hypotheses . . . 65
6.2 Experiment A: Lower wave frequencies ω . . . 68
6.3 Experiment B: Higher wave frequencies ω . . . 73
6.4 Experiment C: Wave amplitude ζ_a . . . 76
6.5 Experiment D: Adverse Torsethaugen wave spectrum . . . 79
6.6 Interpretation of results . . . 82

7 Conclusions and recommendations **83**
7.1 Brief summary of research 83
7.2 Conclusions and answers to main research question 84
7.3 Recommendations 87

Bibliography **93**

A EEDI - Energy efficiency design index **97**

B Fourier transform equations **99**

C Dimensionless parameters **101**

D Damen Combi freight carrier 3850 **105**

E Wärtsilä 20 **107**

F Different modelling details **111**

G On turbo-charger modelling **117**

H Propulsion system matching **119**

I Propeller air ventilation and performance of ventilated propeller **123**

J Modelling waves **127**

K Equations of motion and RAO's **131**

L Analysis of ventilation events **135**

1

Introduction

This chapter serves as an introduction to a research on the response of a marine Diesel engine to ventilation loads. The research is performed to gather information for those that want to improve their understanding about comparable systems subjected to the same boundary conditions. Welman *et. al.* (2005) [37] identifies three qualities of constructive research: Observations take place in a systematic order so that all observations can be weighed equally. Results are gathered in a controlled manner and a structured method ensures that peers can reproduce the results of the work.
With these intentions, section 1.1 introduces propeller ventilation before sections 1.2 and 1.3 treat it's relevance by discussing *problems* and *missing theory* regarding propeller ventilation. Sections 1.4 - 1.6 treat the *goal and scope*, *research questions* and *approach* of this research effort.

1.1. Propeller ventilation

This section describes propeller-ventilation before discussing it's *causes* and resulting *load variations*.

Propeller ventilation influences the working mechanism of the propeller. Carlton (2007) [15] describes ventilation implicitly: "...if the propeller tip immersion becomes so small that the propeller tends to draw air from the surface, termed ventilation, along some convenient path such as along the hull surface or down a shaft bracket." Figure 1.1 illustrates the presence of the water surface and the transport of air during ventilation of a pulling thruster. I derive the following working-definition:

Definition 1. *Ventilation is the transport of a mass of air through the propeller plane.*

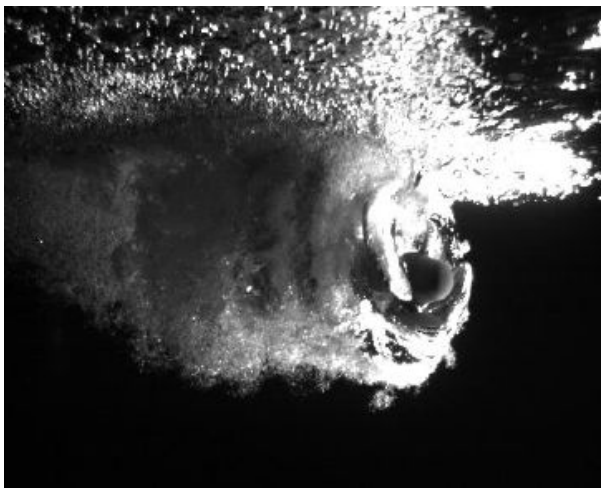

Figure 1.1: Thruster ventilation. Source: [1]

Causes of propeller ventilation

In addition to so-called *out-of-water* events that break the water surface as mentioned by Califano (2010) [30], four other possible sources of air can cause propeller ventilation.

1. The air that is dissolved in seawater.

2. Violent vessel-motion and wave interaction at the bow of a ship can introduce air to the inflow of the propeller.

3. Different systems can introduce air to the propeller flow: Either with the intent to reduce frictional resistance, or as with Prairie(Agouti)-Masker systems, to reduce the emission of sound as posed by for example patent US9410403 B2 [38]. These systems and previous sources are considered insignificant or outside the scope of this research effort.

4. The air as described by Carlton (2007) [15] above: The air, consisting of bubbles that break the water surface along the waterline of the vessel, that is transported towards the suction-(front) side of a propeller and transported through the propeller plane before they can dissolve or rise through the water surface again.

These sources of air result in propeller ventilation which results in variations of the propeller load.

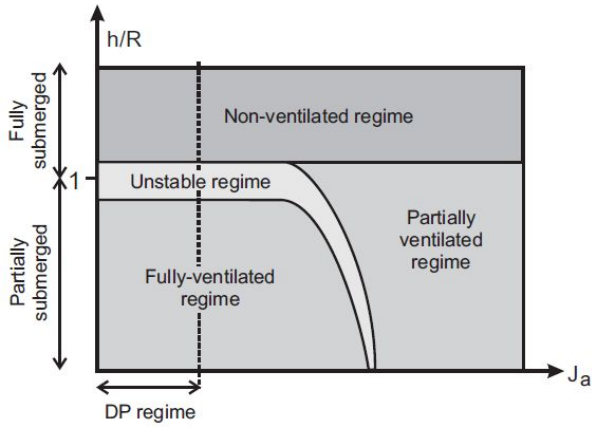

Figure 1.2: Ventilation flow regimes, with the regimes relevant for DP indicated on the Ja axis. Adopted from Olofsson. Source:[13]

Load variations

A mixture of air and seawater has significantly different physical properties such as density and compressibility, than a flow of seawater that only contains a relatively small amount of dissolved air. Instead of a uniform flow of water, ventilation thereby subjects the propeller to a two-phase flow of *seawater* that holds a certain mass of *air*. This flow has physical properties that are not covered in regular calculations regarding propeller functioning.
Minsaas *et al.* (1983) [32] recognised the static dimensionless propeller-immersion h/R as a governing parameter in the description of ventilation. Other research on both static- and dynamic immersion has since shown that propeller ventilation varies as a function of immersion, such as summarised in figure 1.2 from Smogeli (2006) [13].
The different ventilating regimes that occur as a result of different immersions, induce different propeller load fluctuations. Koushan (2004) [39] reports that these load variations can vary from 0 - 100 [%] of the average force experienced by a non-ventilated propeller.

This work continues with the *fourth* source of air as a result of reduced immersion h/R: propeller ventilation consisting of a transport of air bubbles that break the water surface along the waterline of the vessel and are transported through the propeller plane where they can incur a significant fluctuations of the propeller load.

1.2. Problems regarding propeller ventilation

This section addresses the practical relevance of this work by treating *operational problems* and *damages*, before *design problems* related to propeller ventilation are posed as a bridge to the theoretical relevance discussed in section 1.3.

Table 1.1 indicates that different stakeholders are affected by their inability to describe an engine's response to propeller ventilation. This makes the occurrence of ventilation an *unexpected* problem.

A/An ...	can not...
ship designer	design a propulsion system less affected by ventilation.
ship operator	estimate speed reduction and operational losses.
engine designer	optimise control strategies.

Table 1.1: Stakeholders affected by inability to describe an engine's ventilation-response.

IMO (2012) [40] further describes how the world fleet in December 2010 consisted of 104,304 propelled sea-going ships of no less than 100 GT. A part of this vast number consists of the world cargo carrying fleet that measured 55,138 ships in 2011. Next to these already vast numbers, smaller ships may also experience propeller ventilation and it can be concluded that a great number of ships during their lifetime may experience wave-induced ventilation events.
Klein Woud and Stapersma (2002) [11] further indicate that the application of the marine Diesel engine is widespread in this fleet. The influence of wave-induced ventilation events on the functioning of these engines remains undescribed. The the public domain lacks a method to couple such load-variations to the functioning of the engine and it's following response.

This indicates that the practical- and theoretical side of this work are applicable to a large number of vessels, strengthening it's relevance.

Operational problems

Operational problems imposed by ventilation are considered a *direct response*- or *efficiency*-related.

Direct response - loss of propulsion Klein Woud and Stapersma (2002) [11] describe how propulsion is an important operational function of a vessel. Experiencing ventilation, a propeller can loose a significant part of its capability to propel a vessel and thereby to control the vessels heading and speed. In particular, it leads to non-ideal voluntary and involuntary speed reductions and loss of control of a vessel. This may result in dangerous situations and possibly in significant damages to the vessel as the operational function of propulsion is provided less well or not at all.
As operators experience ventilation in challenging operational conditions such as adverse sea conditions, their possibilities to respond to ventilation are limited. A clear description of an ideal direct response to ventilation and the loss of propulsion resulting from it, lacks in the public domain to-date.

Direct response - turbocharger A complicating factor in the operators response to ventilation lies in the widespread application of turbochargers as described by Stapersma (2009) [41]. These are applied as they improve fuel-efficiency, lower the specific fuel consumption and thereby lower the price per unit power. As Hoornaert (2014) [42] describes, a principle disadvantage of a turbocharged engine is that the turbocharger introduces a memory effect in the propulsion system when a load-increase occurs. It's response-delay is introduced as a result of the turbochargers rotational inertia. This disadvantage can cause the propulsion systems inability to immediately provide a required load.

Efficiency - uncertainty and costs A marine propeller operating under non-ideal conditions, functions less efficient. A vessel operator can expect:

- Larger fuel-consumption and larger operational costs.
- Unknown reduction of speed and predictability.

As discussed by Minsaas (1983) [32], the influence of seastates inducing ventilation events and reducing propulsion efficiency can be significant if summed over the lifetime of a fleet of ships.

Thereby, an owner may experience significant operational losses as a result of the reduced propulsive qualities of a ventilating propeller.

Efficiency - airborne emission As discussed by Stapersma (2009) [41], the combustion of marine fuels results in the emission of CO_2. Iso 8217 (2017) [43] further shows that DMX, another name for marine gas oil, holds up to 1 [%, mass] of sulphur. Significant reductions of the vessels fuel efficiency may therefore result in the increase of airborne emissions of toxic substances such as CO_2, and SO_x.

Damages

A propulsion system subjected to ventilation may suffer from component damages or malfunctioning. A clear example lies in the damage that may occur to a propeller blade under the load variation that can occur during a propeller revolution. Van Beek and van Terwisga (2006) [29] state that: *"This load variation, but especially the pressure distribution on the blade tip area and consequently on the blade spindle torque is effected by the occurrence of cavitation and sometimes ventilation."* Five possible damage- and malfunctioning modi as a result of ventilation loads are:

1. **Propeller blade damage** The violent conditions of large pressure fluctuations to which a propeller is subjected in a ventilating regime can result in damages to one or multiple propeller blades which in term reduces the propellers capability to propel the vessel and it's efficiency.
2. **Propeller blade loss** A propeller or -blade repeatedly subjected to ventilation can thereby be damaged repeatedly and may eventually fail completely. This neglects losses as a result of the grounding of a vessel as a result of loss of control of the vessel in shallower waters.
3. **Engine failure or malfunctioning** Violent propeller loading as a result of ventilation imposes both low- and high-frequency engine-load variations. *"Combination of these low-and high-frequency fluctuations at such a short time lead to high impact on mechanical parts of power transmission."* Koushan (2007) [21]. A mechanical connection between a propeller and a prime-mover transmits these load fluctuations to the prime-mover that in turn experiences accelerations or deceleration's and in turn not be able to provide the required torque.
4. **Engine damages** An engine that is loaded with large loads that may be outside the engines design envelope may experience damage to it's components.
5. **Gear damages** As Dang *et al.* (2013) [1] report in table 1.2, damage to a thruster as observed during regular thruster service is not limited to the propeller and it's blades but can also consist of damages to connected gears, bearings and ducts. Ventilation-induced loads can also impact these components.

Components	Percentage of damages
Propellers	24%
Gears	12%
Bearings	11%
Ducts	3%
Steering gears	0%

Table 1.2: Damagetypes found on thrusters during their regular services. Source:[1]

high			high
med		med	
low	low		
	low	med	high

Table 1.3: Risk as a product of effect (↑) and probability (→)

Damages as listed above and in table 1.2, can vary from a nuisance, via costly affair to potentially dangerous situations. Table 1.3 indicates that such events, even if they occur seldomly with a low probability, can impose a large risk to the vessel nonetheless.

Design problems

This section elaborates on the problems that ventilation imposes on the design of a vessel and it's propulsion system. Two contradicting design goals are posed before the current method to address ventilation in the design-stage is discussed.

EEDI versus Minimum power line To limit the emission of greenhouse gasses, nation states can adopt legislation from the IMO and it's Marine Environment Protection Committee (henceforth MEPC). Publication IMO-MEPC (2009) [44] introduces the Energy Efficiency Design Index (henceforth EEDI) and how it is to be calculated. Summarising equation A.1 with equation 1.1, it is a ratio between emitted amount of CO_2 as a result of the combustion of fuel, and the amount of transport work that a vessel can do by combusting this amount of fuel. This in term depends on the installed engine power P_i, the fuel specific carbon dioxide emission C_i and the specific fuel consumption SFC_i per engine and fueltype i. By imposing such a legal upper-limit on the EEDI value of a newly built vessel, a government can try to reduce the emission of greenhouse gasses.

$$EEDI = \frac{CO_2\ emission}{transportwork} = \frac{\Sigma_{i=1}^{n} P_i \cdot C_i \cdot SFC_i}{f_i \cdot Capacity \cdot V_{ref} \cdot f_w} \tag{1.1}$$

On the other hand, legislation such as the IMO-MEPC interim guidelines (2016) [45] impose a lower limit to the installed amount of engine power to limit the movement towards even smaller engines that are cheaper, but may not be able to provide sufficient propulsion in adverse conditions. Although they may be experienced seldomly, adverse loading conditions, as defined by IMO-MEPC (2015) [2] and shown in table 1.4, impose a unique peak requirement on the capabilities of a propulsion system.

Ship length, L_{pp}, m	Significant wave height h_s, m	Peak wave period T_P, s	Mean wind speed V_w, m/s
Less than 200	4.0	7.0 to 15.0	15.7
$200 \leq\ L_{pp} \leq 250$	Parameters linearly interpolated depending on the ship's length		
More than L_{pp} = 250	5.5	7.0 to 15.0	19.0

Table 1.4: "Adverse conditions" mean sea conditions with the following parameters. Based on source: [2]

These upper- and lower- limits on a design do not explicitly take ventilation-induced load variations into account. On the other hand ventilation-induced load fluctuations pose a problem for *both* the use of smaller turbocharged engines resulting from the upper-limit, and the requirement to provide sufficient propulsion in adverse conditions from the lower-limit.

Sea margin versus detailed description During the design process of a vessel and it's propulsion system, assumptions are made regarding a certain 'design condition' to which the vessel will be subjected during it's lifetime.

To include a capability to cope with unknown, larger loads called *off-design loads*, a margin is included in the required amount of installed power. Babicz (2015) [22] describes this sea margin as "*A provision for an increased resistance caused by wind, sea state, fouling of hull and propeller, shallow water currents, etc.*". As the precise size and combination of these loads, which vary throughout a docking-cycle and also incorporate ventilation induced loads, are unknown, it is unclear precisely how much power is actually required to safely propel the vessel. Propulsion system design therefore uses the sea-margin as a safety margin for unknown loads.

On the other hand, if such effects can be described, they can be accounted for directly with a detailed description, instead of an estimated margin. This would result in a smaller margin which has different operational benefits. The operational problems related to the turbocharger mentioned on page 3 could be prevented if a design can be improved by improving it's response to ventilation events. Another example of improved design by accounting directly for the influence of propeller-ventilation on the propulsion system lies in the design of better engine-control strategies by engine designers, as pointed to in table 1.1.

In summary: Propeller ventilation can impose significant *operational problems*, *damages* to equipment and *design problems* that affect all stakeholders in table 1.1. It's influence on the functioning of the propulsion system is only implicitly accounted for by the sea-margin and not described in the public domain to date. Section 1.3 investigates this missing description further.

1.3. Missing theoretical description

This section briefly explains the theoretical gap in the description of engine response to wave-induced ventilation events in the public domain to date.
Previous research efforts such as those by Koushan (2007) [21] and Dang and Brouwer (2013) [1] have established the variation of propeller loads and their connected gears and bearings.
Other efforts such as those by Smogeli (2006) [13] have focussed on response strategies for electrically controlled propulsors.
Although much is known about governing mechanisms of propeller ventilation, the functioning of the marine Diesel engine, and the description of vessel-motions, their relation remains undescribed.

Missing links Figure 1.3 shows how *vessel-motion* and *engine-response* for marine Diesel engines has been treated so far: by connection A that describes both the still-water resistance and the added resistance from waves. However, it misses a description of propeller ventilation.

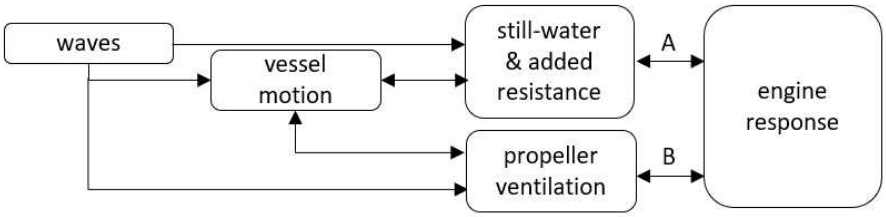

Figure 1.3: Engine response to: A) still-water and added resistance and B) propeller ventilation.

The combination of vessel-motion, engine response and propeller ventilation has theoretical relevance based on *a yet undescribed relation*, *unknown response characteristics* and the *impossibility to compare response characteristics*.

- Previous research efforts such as those by Koushan (2007) [21] and Dang and Brouwer (2013) [1] have established the variation of propeller loads and their connected gears and bearings. Although much is known about governing mechanisms of propeller ventilation, the functioning of the marine Diesel engine, and the description of vessel-motions, the *relation* between these three *remains undescribed* in the public domain to date.
- Secondly, theoretical relevance is found in the fact that methods such as Smogeli's (2006) [13] are able to reduce the influence of ventilation for electric drive systems, it remains unclear how a propeller subjected to ventilation-enabling boundary conditions, interact with a conventional propulsion system. As no method has yet been developed to link ventilation loads to a marine Diesel engine, it's *response characteristics* to these loads *remain unknown*.
- A third theoretical gap lies in the fact that there is no reasonable method to compare alternative propulsion system components and control strategies. A reduction of engine size as motivated by a reduction of EEDI, posed by IMO-MEPC (2009) [44], can not yet be made based on parameters describing the propulsion system's response to ventilation. In other words, a propulsion system designer does not yet have a theoretical method to make a significant comparison between the ventilation-response capabilities of alternative solutions, such as a naturally aspirated- and a turbocharged alternative.

  The relevance of this theoretical *impossibility to compare*, boarders on the practical relevance of a method to describe the engine's response to ventilation.

In summary: There is no description of engine response to wave-induced ventilation loads in the public domain to date, although it has theoretical relevance based on a yet *undescribed relation*, *unknown response characteristics* and the *inability to compare*.

1.4. Goal and scope of research

Section 1.2 indicated multiple significant problems resulting from propeller ventilation: *operational problems*, *damages* and *design problems*. Section 1.3 also found a missing theoretical description of the influence of wave-induced ventilation loads on the engine response. This work intends to address these problems and gaps by gathering information about the response of marine Diesel engines to wave-induced ventilation events. This intent is further specified in a specific goal:

Goal: *Increased understanding of the relation between wave properties, -height and -frequency, and the response of a marine Diesel engine, -speed and -torque, subjected to wave-induced ventilation.*

The research effort in hand focuses on the engine response (rotational engine speed n_e and -torque Q_e) to input-variations of both *waves* and engine speed setpoints $n_{e,set}[s^{-1}]$. Resulting insight in response of the engine to these different loads will contribute to our understanding of this propulsion system. It may further help the future improvements of this system for different stakeholders by focusing on other dependent parameters such as the hull-speed or propeller thrust:

- Ship designers can optimise the design of propulsion systems.
- Ship operators can predict and reduce speed reduction and operational losses.
- Engine designers can improve control strategies.

Scope of this research The scope of this research effort focuses on the effects that both *engine speed setpoint* $n_{e,set}[s^{-1}]$ and *wave properties -height* $\zeta[m]$ *and frequency* $\omega[rads^{-1}]$.
The engine speed setpoint $n_{e,set}$ will be varied in the higher end of its domain. The particular waves studied in this work will be long-crested head waves and -seas. Linear wave theory will be applied and the influences of wind and current will be neglected. Validation is not included in the scope.
This thesis will focus on a system with the following properties:

- A monohull coaster...
- with a medium-speed marine Diesel engine and...
- a reduction gearbox and a single FPP

A more detailed description of this scope is provided in section 2.6, after chapter 2 has given insight in the wide background of ventilation.

1.5. Research questions

Three research questions are posed below to reach the goal in section 1.4 and thereby address the *problems regarding ventilation* and the *missing theoretical description*.

Question 1. *Main research question: How does a marine Diesel engine respond to off-design loads, and in particular to frequently varying loads resulting from propeller ventilation?*

Question 1 covers all relations in figure 1.3, but in particular the links to- and from the propeller ventilation block: The wave-induced propeller-ventilation on the left side and the engine response to propeller ventilation on the right side, as indicated by B in figure 1.3.
Answering this question can help increase understanding of the working of a widespread vessel propulsion technology. Two sub-questions are posed to help answer it.

Question 2 investigates the hydrodynamics relating waves and vessel motions to propeller ventilation:

Question 2. *Sub-question: How do vessel motions in a seaway induce propeller ventilation?*

Experimental research such as that by Koushan (2007) [21] as well as theoretical research such as that by Minsaas *et al.* (1983) [32] has shown that propeller immersion is a characteristic parameter in the subject of ventilation. Question 2 can help explain how vessel motions can vary the immersion of a propeller and how variations of immersion induce load variations as a result of propeller ventilation.

The flow of water around a ventilating marine propeller is governed by a number of parameters following from effects such as the developed sea around the vessel, the vessel's hull shape and loading characteristics and the propeller loading as a result of previous input from the propulsion system. The vessels motions that are induced by the different loads to which the hull is subjected are to be investigated to determine their precise influence on the instantaneous immersion of the propeller.

Question 3 treats the link between propeller ventilation and engine response: B in figure 1.3.

Question 3. *Sub-question: Can static-immersion propeller-ventilation data be used to accurately describe ventilation under varying immersion conditions?*

Experimental research on ventilating propellers can be divided in two categories: static immersion research providing insight in propeller loading characteristics under ventilating conditions and dynamic immersion research capturing propeller loads of ventilation induced by one specific propeller motion. Given the multitude of conditions that can result in the occurrence of ventilation, a well structured method to describe these influences on propeller functioning is to be found. Question 3 can help construct an accurate description mechanism.

Answers to the posed research questions can provide critical steps in a generic method to estimate and predict engine response characteristics to wave-induced ventilation events. Thereby, they can be used to reach the goal of this research effort.

1.6. Research approach

This section proposes a research approach. The methodology applied in this research consists of simulation based research. Davis and Bingham (2007) [3] provide a clear description regarding the development of theory by using simulation. Their seven steps, linked to the research at hand in table 1.5, serve as a roadmap for this research.
Having introduced a relevant problem and research question, chapter 2 continues the identification of theory governing the problem of *ventilation response*.

Nr.	Point	Addresses
1	Research question	A relevant problem is introduced in sections 1.1-1.3. Section 1.4-1.6 discuss how this problem will be addressed.
2	Identification of theory	Chapter 2 discusses the theoretical background governing the posed problem and connects these different theoretical subjects.
3	Simulation approach	It is followed by chapter 3 that discusses literature sources proposing descriptions of characteristic system-components and theoretical methods that can be used to create a usable simulation approach.
4	Computational representation	Chapter 4 discuss the structure of the model describing the behaviour of a vessel and it's propulsion system as well as the casus-specific data that is going to be used as a representation of a specific vessel and it's propulsion system.
5	Verification of the computational representation	Chapter 5 verifies the behaviour of all the components of the model proposed in chapter 4. This model connects known theory with simulation to develop new theory.
6	Experiment to build novel theory	Hypotheses precede the experiment in chapter 6. It consists of simulations and results that are used to gain insight in the engine-response to different ventilation-induced load variations.
7	Validation	Validation of the theory that is constructed with the model simulations will not be performed within the frame of this thesis, but section 7.3 does list a number of methods and handles that can help validating the developed theory regarding load-variations and engine response.

Table 1.5: Steps in the development of theory by using simulation. Source: [3]

2

Theoretical background

This chapter discusses a number of theoretical subjects related to the problem that the modelling of ventilation induced load changes poses. Section 2.1 elaborates on theory regarding the complete propulsion system that, as a whole, is subjected to ventilation loads. An elaboration on previous research regarding damages to, and legislative requirements regarding the propulsion system provides a theoretical basis for propulsion system design under ventilating conditions. Section 2.2 discusses theory regarding the description of vessel-motion. It is followed by section 2.3 that discusses how ventilation imposes an unusual loading condition as the propeller doesn't function under ideal conditions and why this is a problem. Section 2.4 discusses partial problems of a propulsion system in the context of ventilation. Section 2.5 investigates how the subjects of previous sections can be connected in a single model. The scope of this research will be treated with more detail in the final section of this chapter.

2.1. Ventilation and the marine propulsion system

This section describes the marine propulsion and the theoretical problems regarding the ventilation to which it can be subjected. After a description of the propulsion system itself, the possible occurrence of damage is studied and legislation regarding the propulsion system discussed before a theoretical problem is stated. The function of the propulsion system lies in the transformation from potential energy that is stored on board of of a vessel, to the effective propulsion of that vessel. Klein Woud and Stapersma (2002) [11] describe a number of possible design layouts with different characteristics that all consist of at least four components: A propulsor, a connecting element, a prime-mover and a reservoir of potential energy.

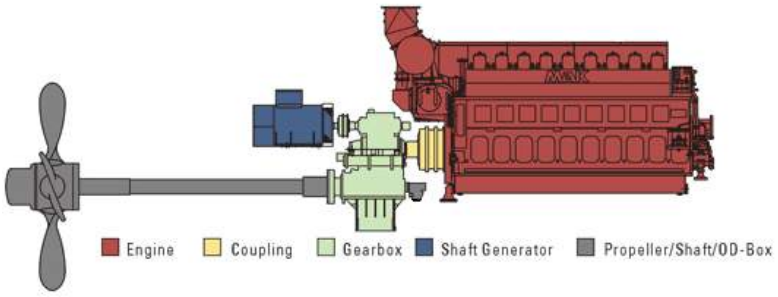

Figure 2.1: Schematic layout of a geared medium-speed propulsion system. Source: [14]

The most commonly used propulsors are the fixed pitch propeller(FPP), the controlable pitch propeller (CPP) and the waterjet. A direct connection, geared connection or electrical connection transports energy to the different system components. The prime-mover transfers potential energy to kinetic energy in the form of a rotating propulsor. That impels the surrounding water flow and thereby propels the vessel. The prime mover can consist of a marine Diesel-engine that is usually

turbocharged, a gas turbine or an electrical machine. These are connected to a supply of fuel, an electrical generator or a battery pack. Figure 2.1 shows an example conventional propulsion system consisting of medium-speed geared drivetrain.
The propulsion system components discussed above, function in different physical domains. The propulsor connects the field of dynamics with fluid dynamics and the prime mover connects either chemistry and thermodynamics or electrics with dynamics. A description of the functioning of such a subsystem is governed by certain assumptions regarding the specific physical domain. As operation in ventilating conditions breaches the common assumption of a continuous and incompressible flow of water that loads the propulsor, the regular description of the functioning of the propulsion system is no longer valid.
Resulting off-design loading conditions influence the behaviour of different system components. Dang *et al.* (2013) [1] describe how characteristic properties of a specific system component may, under such loading conditions, influence the catastrophic behaviour of the whole system. It is therefore that understanding of the behaviour of one limiting link in a system can help to understand the behaviour of the whole system. To improve our understanding of the behaviour of a system subjected to unique loading conditions as described above, present information regarding both component functioning, subsystem interaction and governing boundary conditions must be organised in a structured way.

Damages

As van Beek and van Terwisga (2006) [29] state "*Not much is known about the conditions for limited ventilation and its effect on propeller loading*". These load-variations can be categorised as destructive and non-destructive loads. Koushan (2007) [21] describes that "*there have been incidents of mechanical failure of power transmission components of thrusters that are believed to be related to ventilation*". Although a governing mechanism leading to such failures, Tooth Interior Fatigue Fracture (TIFF), is presented by Dang *et al.* (2013) [1], the loads on different power transmission components remain unknown. Different propeller-load measurements are available and will be discussed in sections 2.3 and 3.2.

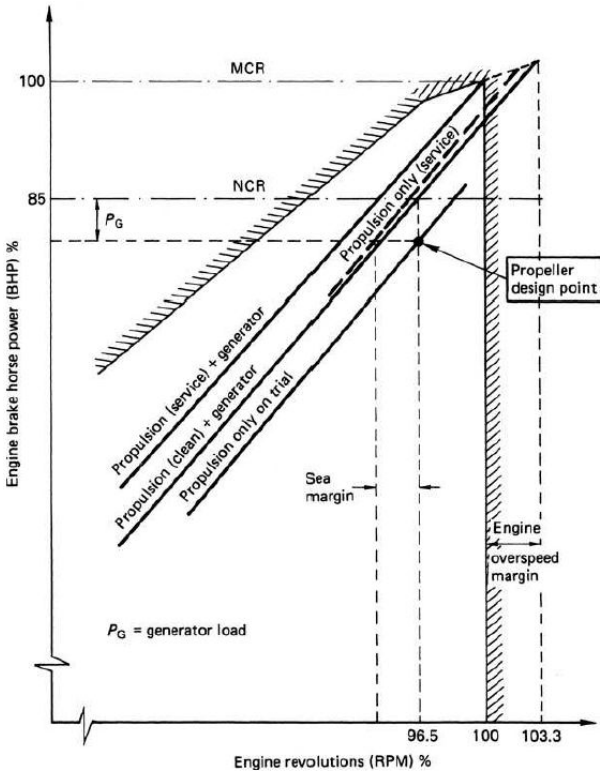

Figure 2.2: Typical propeller design point. Source: [15]

The non-destructive or not directly destructive load fluctuations that occur as a result of ventilation load, and thereby influence the behaviour of, different components of the propulsion system as discussed in section 2.1. Dang *et al.* (2013) [1] discuss how safety factors for pitting damage, sub-surface fatigue, tooth root damage, loss of lubrication film thickness, tooth interior fatigue fracture, TIFF henceforth and other ventilation-related mechanisms are included in the design stage of a propulsion system. The sea margin, as discussed in section 1.3, is another example of such a safety factor. Figure 2.2 shows how the sea margin functions as a safety margin for the installed engine power in the design of a propulsion system to ensure safe operation and prevent damages.

In summary, such margins are incorporated as a buffer to minimise the influence of unknown effects on the functioning of a system component and the functioning of the complete system. Increasing a margin results in increased capabilities under uncertain conditions, but may be costly. On the other hand decreasing a margin based on new knowledge about governing boundary conditions may be profitable. Knowledge regarding propeller blade loading under ventilating conditions has, as far as the

author is aware, not yet been coupled to engine loading descriptions, in the public domain at least.

Legislation

Implementing legislation regarding a required EEDI value, as done in IMO (2011) [46], and summarised in equation 2.1 improves the energy efficiency of the world fleet in time and thereby helps reducing the emission of greenhouse gasses such as carbon dioxide (CO_2 henceforth).

$$AttainedEEDI \leq RequiredEEDI = (1 - X/100)\ x\ Reference\ line\ value \tag{2.1}$$

However, as IMO (2016) [45] discusses, the lower boundary condition of providing minimal propulsion power to maintain the manoeuvrability of ships in adverse conditions is characterised by special characteristics for smaller ships of less than 20,000 [DWT]. It is found "*that the ability to recover the relative safety of head seas, clearly requires a minimum installed power (or more precisely: a minimum effective bollard pull, EBP)*" and that "*prescribing power requires further essential information on for instance the type of propeller, the presence of a duct and the occurrence of ventilation of the propeller*". Finally, this study also concludes that "*the direct loss of thrust due to ventilation of the propeller is substantial and should be accounted for in the assessment of the required thrust for a given installed power in relevant cases*". As there is no definitive method to account for this thrust loss other than an assumed margin, it is questionable if a further reduction of the required EEDI for these vessels is possible under an assumed set of boundary conditions.

Theoretical problem

It is unknown how ventilation induced load variations load a prime mover. This problem is solved in practice by including safety margins regarding the characteristics of propulsion system components. As it is unknown precisely how large these need to be to cope with certain loading conditions, it poses a potential to further reduce the amount of installed power and thereby reduce the value of the required EEDI. An improved understanding of the behaviour of a prime mover under ventilation thereby provides a potential to reduce costs and emission. This poses the theoretical problem that it is unknown how these loads are imposed on components of the propulsion system.

2.2. Vessel-motion theory

Vessel-motion presents the designer of a marine propulsion system with a number of theoretical problems. As Sørensen (2013) [35] describes, environmental loads can be organised in three categories: waves, winds and currents. These loads will be addressed in that order below before the theoretical problems are summarised. As a result of these loads, a vessel will move in six degrees of freedom.

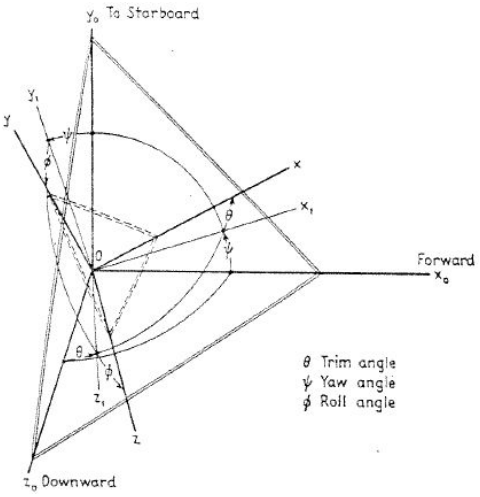

Figure 2.3: Orientation of body axes relative to fixed axes in terms of ϑ, ψ, φ. Viewed from below xy plane. Source: [16]

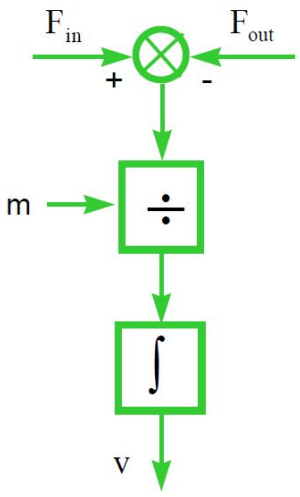

Figure 2.4: Block diagram of translational dynamics. Source: [17]

Sname (1950) [16] provides a broadly accepted description of displacement and motion of a vessel submerged in a fluid. The core of this work is shown in figure 2.3. The description provided by Sname provides a useful description of forces in three orthogonal directions and moments around these principle axes. Studying the behaviour of the marine propulsion system, this description is used by, among others, Stapersma (2000) [17] to describe the interaction between a propulsion system and a hull subjected to wave-loads as it moves forward in one (X) direction. This method requires the use of a relation between the vessels resistance and velocity and between velocity and propulsive force. However, this description focuses on an accurate description of the propulsion system dynamics and briefly describes the vessel-motions as one translating motion, summarised with the block diagram in figure 2.4. On the other hand, a more complete description of the forces and moments in all six directions can also be used to describe the functioning of a vessel.

The motion behaviour of a vessel can be described in the time-domain or in the frequency domain. By analysing the sinusoid wave components that form a developed seastate in the time domain, the wave loads to which a vessel is subjected can be determined per wave component and thereby for the whole wave. This is possible in both the time- and frequency domain. The relation between these two domains that describe the same develloped seastate and vessel-response is shown in figure 2.5. Traditionally, information regarding seastates is gathered in the time-domain such as for example by Haver (2004) [27], whereas research regarding the control of the marine propulsion system usually studies phenomena in the frequency domain.

A clear example is provided by Vrijdag and Stapersma (2017) [47]. The possibility to study the behaviour of the propulsion system response provides the model-designer with the theoretical question in which domain the problem at hand should be studied. Another question in the subject of vessel-motion, is how vessel speed is addressed. For a dynamic positioned (henceforth DP) system of a vessel, Sørensen (2013) [35] describes that there are two separate subsystems used to control a vessel dependent on its intended speed: A DP-system "*for automatic station keeping and low speed manoeuvring of free floating vessels or thruster assisted position mooring (PM) system for anchored vessels*". And an "*automatic sailing system and nautical system ... for automatic course keeping and course changing for transit operations*".

Theoretical hydrodynamics, as explained by Faltinsen (1993) [18], use a comparable differentiation between forward-speed and zero forward-speed effect to describe the loads of waves and currents on a vessel: "*A current or the forward speed of a structure will influence the added mass and damping coefficients*." This poses the question which speed regime shall be studied? A zero-speed stationkeeping regime or a manoeuvring regime at some forward speed, and how the governing hydrodynamics are to be described for that regime.

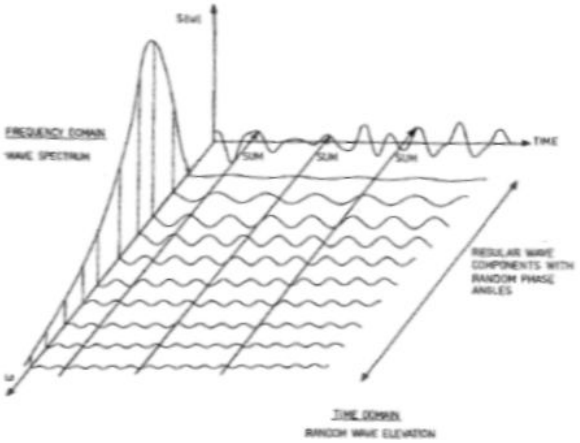

Figure 2.5: Figure illustrating the connection between a frequency domain and time domain representation of waves in a long crested short term sea state. Source: [18]

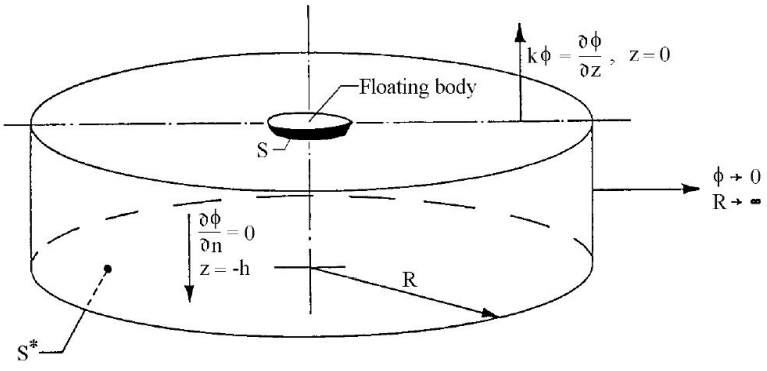

Figure 2.6: Boundary conditions. Source: [19]

Description of vessel loads - Waves

There are different methods to describe how waves impose a load on a vessel's hull. A classical approach lies in the application of a scale model that has the same shape as the intended vessel. By subjecting this model to different motions in a towing tank and exposing it to different waves, information about wave loads can be gathered and scaled. Once this is done, the expected loads for the prototype (real vessel) can be predicted. This method scales both viscous and non-viscous effects, but these are not scaled correctly simultaneously. Inviscid effects can therefore better be scaled with other methods.
Another widely used method is called strip-theory. It divides a hull in some 20-30 sections, or strips, along the length of the hull. These strips have a continuous cross-section. Journée (1992) [48] describes how these strips can be used to determine the wave-frequency dependent added mass and damping terms can be determined for each of these strips and thereby the vessel as a whole. This method, however uses potential theory to estimate the wave-loads on the vessel. It assumes an inviscid fluid and therefore neglects viscous loads on the hull.
First developed to predict wave loads for vessels without forward speed, adaptations for forward speed regimes have since been implemented in different software-packages that use potential-flow methods. Figure 2.6 depicts boundary conditions imposed on the flow in a potential-flow problem. The different methods to determine the added mass and damping coefficients pose the theoretical question which method is preferred and if this method is accurate enough to describe the required wave loads.

Description of vessel loads - Currents

To estimate the forces a current imposes on the hull of a vessel, either empirical data or experimental data have to be used. As current velocities are relatively small, the wave-making influence of currents can be neglected according to Faltinsen (1993) [18]. Laminair flow effects however load the vessel with forces in three directions: Surge, sway and yaw.
To describe the effects of currents on a vessels hull Faltinsen (1993) [18] proposes a description in three directions: surge, sway and yaw. The influence of the yaw movement is governed by the Munk-moment and a viscous yaw-moment as described in equation 2.2 (from [18]). Both these forces and both moments are described as a function of the current velocity (U_c) and relative direction β.

$$F_6^c = \frac{1}{2}\rho\left[\int_L dx C_D(x)D(x)x\right]U_c^2 sin\beta|\beta| + \frac{1}{2}U_c^2(A_{22}-A_{11})sin2\beta \qquad (2.2)$$

$$S(f) = \frac{4\kappa L\overline{U}_{10}}{(2+\tilde{f}^2)^{\frac{5}{6}}} \quad | \quad \tilde{f} = \frac{Lf}{\overline{U}_{10}} \qquad (2.3)$$

Description of vessel loads - Winds

Wind provides a vessel with a complexly varying and time-dependent three dimensional phenomenon. Sørensen (2013) [35] describes how it is usually modelled as a two-dimensional flow of air over a plane of the undisturbed water surface. The flow of air can than be described as a function of the velocity of the air, the height above the undisturbed horizontal plane and the direction. A final assumption that is made is that the airflow has two components: a mean component with a constant speed and a wind gust that varies in time. The gusts are characterised by a spectrum such as the Harris wind spectrum as provided by Sørensen (2013) [35] and described in equation 2.3: Such a wind spectrum can also be combined in a wind and wave spectrum. These different possibilities to model the influence of the wind on a vessel raise the theoretical question if this influence must be included in a model that describes loads on a vessel, and if so, how it can be modelled with enough accuracy?

In summary, this section described a number of theoretical problems that arise when describing environmental loads on a ships hull:
- Which specific motions are of interest to the study at hand?
- In which (time- or frequency-)domain should the motions of the vessel be described?
- Which speed-regimes should the description of motion cover in the chosen directions of motion?

- Should current loads be included? And if so, how should they be modelled?
- Should wind loads be included? And if so, how should they be modelled?
- Should wave loads be included? And if so, how should they be modelled?

The accurate description of loads to which a vessels hull is subjected as well as the description of resulting vessel-motions poses a theoretical problem that can be solved in different ways, dependent on the requirements a research question imposes.

2.3. Propeller theory

This section explains the functioning of a propeller and a number of disturbances in the description of propeller functioning. It continues with a description of the mechanism of ventilation and the characteristic role of propeller-immersion as a parameter.

A marine propeller propels a vessel by transforming a torque Q to a thrust force T by increasing the momentum of a flow of water. The functioning of a propeller that operates with a certain rotational speed n and velocity of advance v_a is traditionally described with the three coefficients in equations 2.4 to 2.6. For a certain propeller design, this information is gathered in towing-tank tests and shown in open-water diagram such as that in figure 2.7. This information characterises a propeller under controlled experimental conditions that inhibit the influence of disturbances. Under operational conditions such as installed on a vessel, such disturbances occur and need to be accounted for to accurately predict propeller loads.

$$K_T = \frac{T}{\rho n^2 D^4} \tag{2.4}$$

$$K_Q = \frac{Q}{\rho n^2 D^5} \tag{2.5}$$

$$J = \frac{v_a}{nD} \tag{2.6}$$

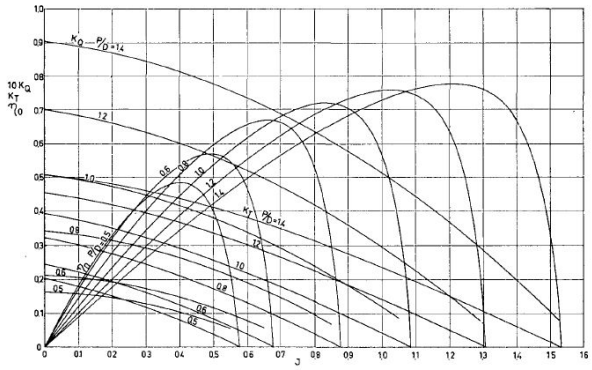

Figure 2.7: Open-water test results of B4-40 screw series. Source: [20]

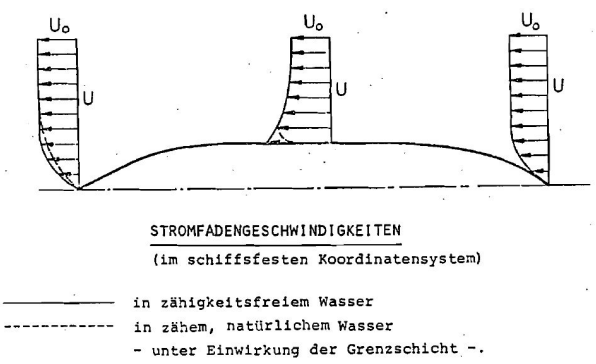

Figure 2.8: Flow thread speeds (in body-bound coordinate system)[1]. Source: [49]

Disturbances

The presence of the hull in the vicinity of the propeller influences the flow-field of the medium that enters the propeller. In figure 2.8, Brandt (1999) [49] shows an example of a disturbed flow-field as a result of the presence of the hull that generates a primary wave field. The influence of this disturbance can be described with three components: the wake factor, the thrust deduction factor and the relative rotative efficiency.

The wake factor w describes a the relation between the vessels velocity and the average velocity the propeller experiences in its propeller plane: $w = (1 - \frac{u_p}{u})$. The thrust deduction factor describes the relation between the towed hull resistance R_t and the self-propelled resistance R_{sp}, which includes the resistance that is added due to the presence of the propeller and its influence on the flow-field

[1] In German: Stromfadengeschwindigkeiten (im schiffsfesten Koordinatensystem).

surrounding the hull. Finally, the relative rotative efficiency describes the difference of efficiency between a propeller subjected to a non-uniform flow with a rotating component and and a uniform flow such as in a towing tank.

Other sources of disturbance in the prediction of propeller functioning are the propeller condition, the distribution of the inflow field and the occurrence of cavitation and ventilation. As the propeller condition deteriorates as a result of occurring cavitation or fowling on the propeller surface, its efficiency may deteriorate. Secondly the size of a marine propeller is in the order of magnitude of meters. During a rotation, a propeller blade can experience different inflow-speeds that vary significantly. This distribution of the flow velocity introduces another source of uncertainty regarding the functioning of the propeller. Finally, as discussed by, among others, van Beek and van Terwisga (2006) [29], the load variation during a single revolution *...is affected by the occurrence of cavitation and sometimes ventilation*.
In summary, the velocity distribution of the non-homogenous inflow-field of the propeller is not known in detail. In summary, these disturbances of the inflow of a propeller limit a correct prediction of the environment in which ventilation takes place.

The mechanism of ventilation

Section 1.1 defined and described marine propeller ventilation. Minsaas (1983) [50] discussed the role of a reduced immersion on the occurrence of ventilation. The influence of ventilation on the propulsion of a vessel can be described in two parts. First the ventilation of a bare propeller, as for example van Beek and van Terwisga (2006) [29] also found that "*An important effect of propeller immersion on blade spindle torque for both non-cavitating and the cavitating could be observed*", for a CPP. Secondly, the ventilation of a propeller in the wake a vessel's hull. As the dimensionless propeller shaft immersion ratio h/R decreases, the boundary effects introduced by the water surface on the bare propeller increase (see figure 2.9).

Koushan (2007) [21] demonstrated the leading role of immersion variation on the occurrence of ventilation and stated that "*when a thruster undergoes heave motion, it is the ventilation which is the primary cause of loading fluctuations rather than the heave motion. Of course, the heave motion acts as a generator and transporter of ventilation*". Secondly, the presence of the hull introduces two characteristic factors in the ventilation problem: The imposition of its movement as well as a diversion of the water surface that may change the trajectory of the air displacements. Experimental research efforts so far have neglected the influence of the hull and focused on the characteristic influence of the propeller's immersion ratio.
It shows how K_T varies non-linearly with J for a fixed immersion. This means that as a result of ventilation, it can no longer be assumed that a propeller operates with a thrust coefficient K_T for a characteristic value of J but that different values of J can result in the same thrust coefficient K_T.

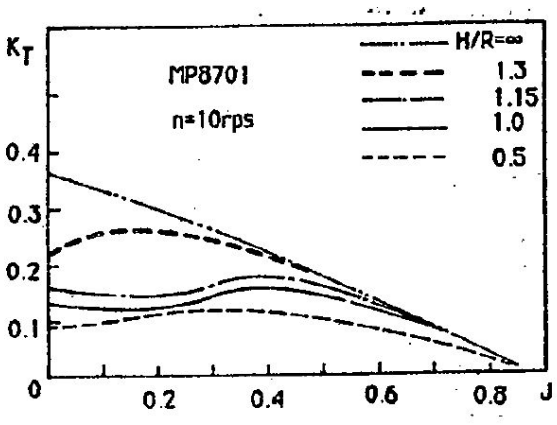

Figure 2.9: Influence of submerged depth on open water characteristics (MP8701). Source [7]

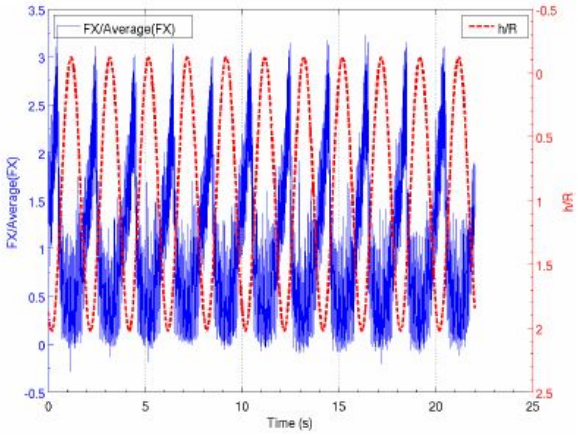

Figure 2.10: Relative blade thrust of open thruster and relative propeller shaft immersion; propeller shaft at highest position h/R=-0.15; amplitude/R=2.15; period=2 s. Source [21]

The parameter of propeller-immersion

The graph in figure 2.9 shows an example of an open water diagram subjected to different static propeller immersions and thereby to different ventilation regimes such as described in figure 1.2. This introduces the theoretical problem that the description of the functioning of a ventilating propeller, as for example shown in figure 2.10, can no longer be accurately be described by J alone.
In summary, immersion plays a characteristic role in the ventilation problem and there are two common methods to describe the characteristic functioning of a ventilating propeller. Either the propellers thrust- and torque-coefficients are given as a function of immersion and advance ratio, such as in figure 2.9, describing $K_T = f(h/R, J)$. Or the propellers normalised loads are given for a specific immersion in the time domain such as in figure 2.10, describing $F/F_{avg} = f(h/R, t)$. This introduces the theoretical problem that an accurate and effective description of propeller functioning under ventilating operational conditions must be chosen and adapted.

Summary

As discussed in the section above, propeller ventilation provides a number of theoretical problems. The accurate description of disturbances in the inflow field to which a ventilating propeller is subjected, poses the first of those problems. How can the non-homogenous and rotational inflow speed of the medium be described accurately enough? How can the influence of waves and non-constant immersion of the propeller be described? Secondly, the ventilation mechanism and its effects on a propulsion system can be described by different methods that have been applied with different intentions in earlier research. The description of the actual ventilation mechanism that is incorporated in this study, provides a significant theoretical problem.

2.4. Prime-mover theory

Prime-mover behaviour poses two theoretical questions in relation to the research at hand. The first one is about the description of the prime mover and the second about the variation of the load to which it is subjected. This section poses and explains the nature of these two questions.

Describing a prime-mover

The functioning of one prime-mover such as a marine Diesel engine, electrical machine or gas turbine, can be described in different ways. Power curves can be plotted in a graph such as the one displayed in figure 2.11, or the torque-speed curve in figure 2.12 to provide a description of the functioning of a prime-mover by linking the power-output to its rotational speed. Using a second parameter such as the amount of fuel injection or an armament(stator)-current, a unique power output from the prime-mover can be described. If the power-characteristic from an engine are known from for example factory acceptance tests, this method requires relatively little computation time to describe the effect the prime mover has on the system and uses data that can easily be verified and validated.

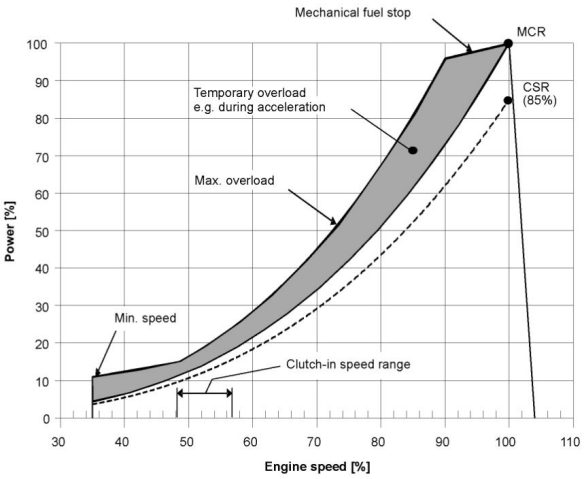

Figure 2.11: Operating field for FP propeller. Source: [22]

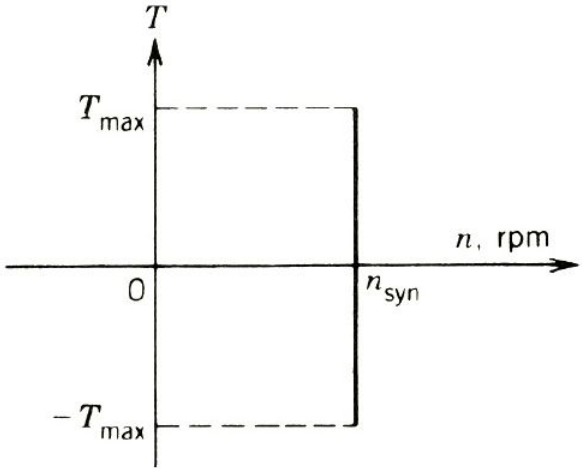

Figure 2.12: Torque-speed characteristics. (Of a synchronous machine). Source: [23]

Alternatively, the functioning of a prime-mover can be described with more detail by describing or modelling the behaviour and functioning of its specific components and their interaction. Shi (2013) [4] summarises a number of detailed engine core models for marine Diesel engines:

- Lookup-table approach This method is described above.
- CFD models Used for the investigation of combustion phenomena and the formation of exhaust emissions such as soot and nitrogen oxides (henceforth NO_x).
- Filling and emptying (or crank angle) model Models the cylinder volume as a single zone and solves differential equations for heat-release, mass distribution and the energy balance numerically. The heat release can be determined as a function of the crank angle with a Vibe-model.
- Mean value first principle models Either a simplified model that describes the cylinder process in a finite number of thermodynamic stages and uses mean values as an approximation, or a complete MVFP model that simulates both gas exchange and the closed cylinder process in a finite number of stages.
- Analytic model Describing the torque the engine produces as a function of engine speed and the amount of injected fuel and five engine-specific coefficients.
- Specific emission models The emission of CO_2 and sulphur dioxide (henceforth SO_2) can be modelled by describing it as a direct relation to the fuel combustion. The emission of NO_x requires a slightly more elaborate description, but can under steady-state assumptions also be modelled in a compact, lookup based approach, although all methods mentioned above can also be implemented to describe the formation and emission of NO_x in more detail.

In summary, there are different methods to model the behaviour of different prime-movers. This poses the theoretical question which of these methods is ideal to describe engine behaviour in relation to the propulsive capabilities of a ventilating propeller.

Load variation

Load variations that occur as a result of ventilation impose a unique loading condition on prime mover. Not all of the models described above provide reliable results under such conditions. Koushan (2007) [21] shows characteristic examples of the occurrence of a ventilation event in figure 2.13. This figure depicts a repeating pattern of thrust-loss and -recovery in a 2 [s] time-frame with propeller blade thrust forces that vary significantly compared to the average blade thrust. Koushan (2007) [21] describes that: *"This sudden drop happens just within a single revolution"*.

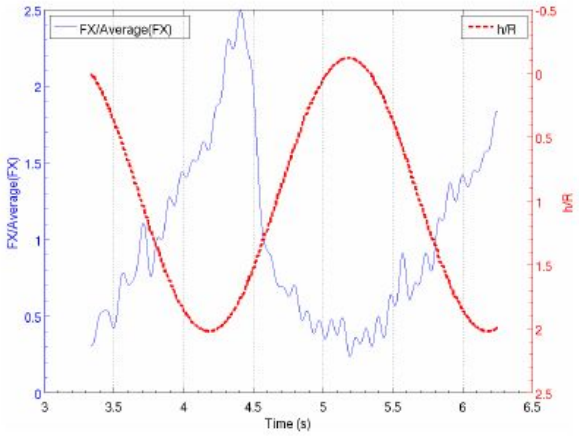

Figure 2.13: Low-pass(12 Hz) filtered relative blade thrust of open thruster and relative propeller shaft immersion; propeller shaft at highest position h/R=-0.15; amplitude h/R=2.15; period=2 s. Source: [21]

The load a prime-mover experiences under influence of ventilation is not constant, as will be discussed further in section 2.3, but varies significantly in a [ms] to [s] time-frame. This imposes significant requirements on a prime-mover model, to describe its functioning accurately in the same time-frame, as it may experience significant load changes and resulting accelerations and decelerations. As the prime-mover's capabilities to respond to load changes in this time-frame, influence the propulsion systems capability to propel the vessel.

Turbocharging limits In case of acceleration or deceleration, the functioning of a critical component such as a turbocharger or governor may become critical as it can intentionally or unintentionally limit the engines response capabilities. As summarised briefly by Hoornaert [42], a turbocharged marine diesel engine, consists of two main components: A cylinder block and a turbocharger. Figure 2.14a shows how these two components are controlled and connected while figure 2.14b shows in detail how the turbochargers turbine receives hot exhaust gasses (coloured red) which release internal energy by expanding and thereby moving the turbine blades. These blades are connected to a rotational compressor on the other side of the turbocharger, that compresses air that is fed to the engine block. Such a turbocharger system allows an engine to

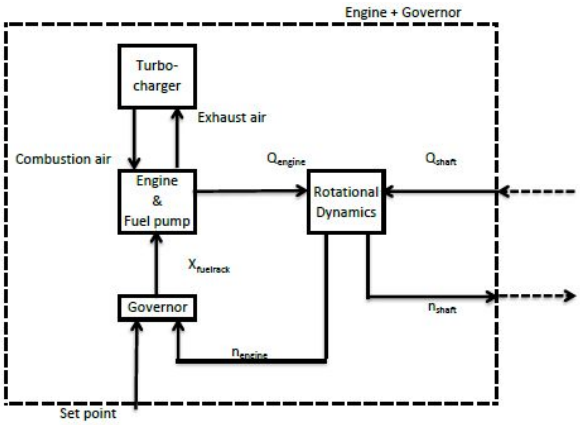

(a) The mechanical sub-system of a ships propulsion system. Source [42]

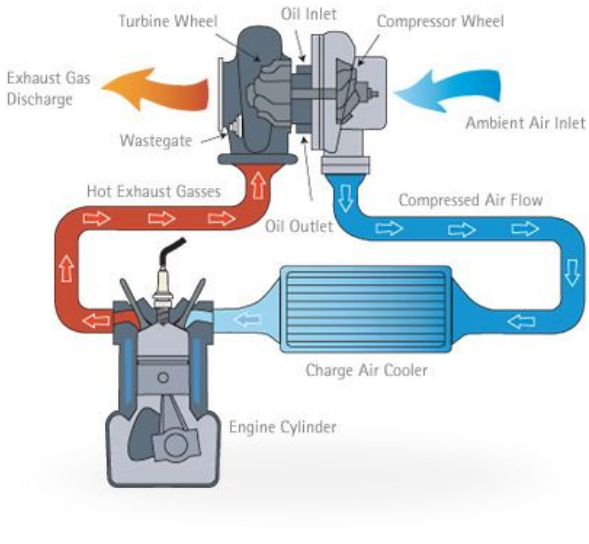

(b) Schematic of an engine turbocharger system. Source [42]

Figure 2.14: Turbocharger in the propulsion system.

combust more fuel, combust fuel more efficiently and deliver more power without the requirement for a significantly larger engine block. The downside to the implementation of a turbocharger system is that its performance is dependent on the flow of exhaust gasses. As a result, a turbocharged engine operating at low speed, may not be able to quickly increase the amount of generated propulsive power as there is a limit to the amount of available exhaust gas. This system-characteristic limits the turbocharged marine Diesel engine to respond to quick and significant increases in required power. And this in term limits the propulsion systems capability to respond to large load fluctuations.

Governor limits The governor can limit the injection of fuel to prevent different effects in different sections of the envelope:

- knocking and malfunctioning around minimal engine speed
- incomplete combustion of superfluous fuel resulting in black smoke by the air limit
- overloading engine components with torque-, power-, engine speed or thermally.

Dependent on the specific conditions, it is expected that the air-, torque- and power limits will affect operation during a single ventilation event the most. Smogeli (2006) [13] developed a number of control mechanisms that consist of combinations of traditional (engine)speed control and torque- or power control in response to the occurrence of ventilation.

Model limits Shi (2013) [4] summarises the dynamic- (and other) qualities of the different model-types in table 2.1. This poses the theoretical problem of the prime-mover response description: How can a prime-mover and its components best be modelled to describe a vessels propulsive capabilities under ventilating conditions?

	Model requirements	Dynamics	Time scale time steps	Capability	Accuracy
CFD model	-	-	-	-	+
Filling and emptying model	+/-	+	-	+	+
Complete MVFP model	+/-	+	+	+	+/-
Simplified MVFP model	+/-	-	+	+/-	+/-
Analytical model	+	-	+	-	+/-
Lookup table	-	+/-	+	+/-	+

Table 2.1: Evaluation and comparison of model technologies: engine core model. Source [4]

2.5. Connecting components

The occurrence of propeller ventilation connects a number of components functioning in different physical domains. Those connections will be discussed below, from the main propulsor to the flow surrounding the propeller, as this poses theoretical problems when describing the propulsion system.

Different connections

The combustion engine connects the domains of chemistry and thermodynamics with mechanics. A description of the composition of fuel allows for an accurate description of the release of energy in mean value first principle models as discussed in section 2.4. These models also require a correct description of the composition of air to model the transfer of heat by the fuel accurately. As a result of the combustion of fuel and the transfer of heat to the working medium of air, a combustion engine transforms stored energy to the rotation of a shaft with a certain amount of torque.

Dependent on the vessels propulsion system layout, medium- or high speed Diesel engines are connected to a reduction gearbox that transforms an amount of toque with the engines rotational speed to a larger amount of torque at a reduced rotational speed. Klein Woud and Stapersma (2002) [11] describe that most gearbox have a constant efficiency in the order of 98 %. This implies a 2% loss of energy by friction as a flow of heat to the gearbox-environment. Godjevac (2009) [51] describes a more elaborate model that includes the hydraulic control mechanism for CPP's.

	cc	el	fm	hm	hy	me	th
cc	GT, DE					GT, DE	GT, DE
el		EM		EM, FPP		EM	
fm				CPP, FPP			
hm		EM, FPP	CPP, FPP	CPP, FPP	CPP	CPP, FPP, HU	
hy				CPP		CPP	
me	GT, DE	EM		CPP, FPP, HU		GB	GB
th	GT, DE					GB	

Table 2.2: Components connecting different domains related to propeller ventilation. (Abbreviations in nomenclature).

The electrical machine connects the field of mechanics in the form of a rotating shaft with a certain amount of torque, to the field of electrics. Although different applications, require different specific machine designs, this transformation can take place in two directions as Sen (2012) [23] describes: Either as a generator that is connected to a Diesel engine or gas turbine and delivers electrical power to a grid, or by transforming electrical power to a torque on a rotating axle.
Assuming a rigid bodied hull and thereby neglecting the field of structural mechanics of the vessel, the hull connects the subjects of hydromechanics and fluid mechanics as both waves, wind an current load the hull as discussed in section 2.2.

Pitch actuation on CPP's is controlled by a hydraulic system. Godjevac (2009) [51] discusses a contemporary system that *"...most of modern CPPs have..."*. This connects mechanics with the field of hydraulics. FPP's and other thrusters also connect the mechanics of a rotating axis with hydromechanics while axles and electric grids provide a connection between different system components in their respective domains.

Table 2.2 provides an overview of the different domains of physics and chemistry that are related to the occurrence of propeller ventilation. The fact that propeller ventilation connects so many domains, poses the theoretical question how the behaviour of these system components can be modelled correctly and with enough accuracy to describe the propulsion systems behaviour under these unique loading condition.

Describing different mechanisms

There are different methods to describe the interaction of system components that operate in different physical domains. One of those descriptions that covers multiple domains is the example set by Stapersma (2000) [17], of which a characteristic part is shown in figure 2.4. A great advantage of the method Stapersma proposes, is that it allows for detailed modelling of propulsion system components such as the prime mover, while limiting the efforts required to model other components. This allows for a description of the system that can provide information regarding the systems static and dynamic response to governing boundary conditions. A significant disadvantage in the modelling method proposed by Stapersma (2000) [17] is that this method only describes the vessels motion in one (x)-direction.

Pedersen and Engja (2010) [24] propose the bond-graph modelling method as a possibility to describe complex systems spanning multiple domains. Using bonds (arrows) that describe power-flows or signals between different systems and components. This method can be used to develop state equations and methods to systematically analyse the response characteristics of systems spanning different domains ranging from three degree of freedom rigid body motions such as shown in figure 2.15, to for example thermodynamic models. This modelling method may not be as widespread in the field of marine technology, but it could help in the modelling, the analysis and the simulation of complex systems spanning different domains.

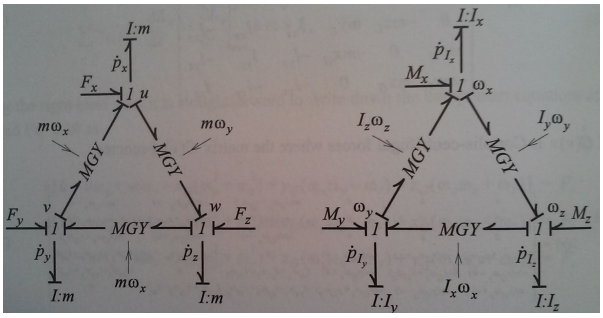

Figure 2.15: Bond graphs for 3D rigid body motion. Source [24]

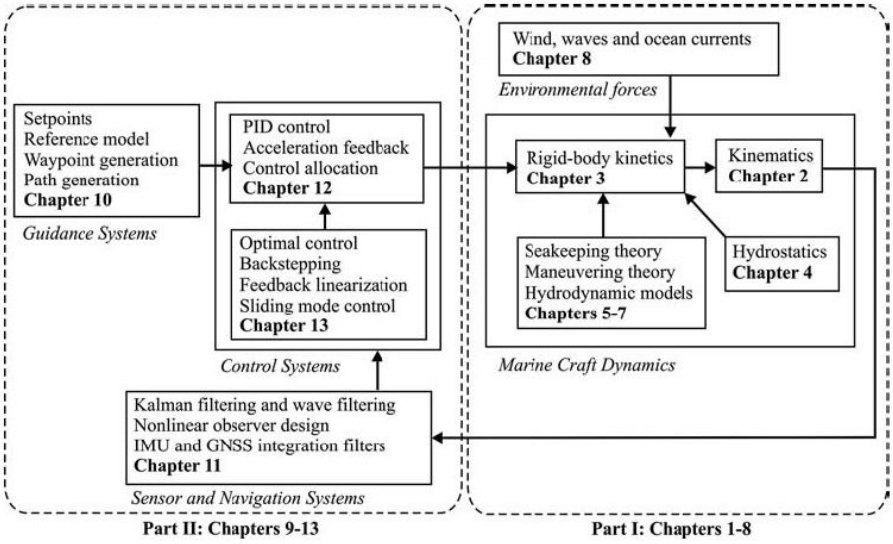

Figure 2.16: Arrangement of subject matters according to Fossen. Source: [25]

Fossen and Perez (2004) [8] provide a third method that can be used to describe the different mechanisms that influence a marine propulsion system subjected to ventilation. Figure 2.16 from Fossen (2011) [25] shows how this method can be used to combine a large number of subjects related to the control of motion of vessels. A number of these subjects may lie beyond the scope of the rest of this research, but the method does include a broader description of vessel-motions then

Stapersma as mentioned above. It also allows for a detailed modelling of certain system components such as by Pedersen and Engja (2010) [24]. Figure 2.16 shows a diagram that connects the different components regarding Fossen's control related studies in the different fields that can all be connected to propeller ventilation.
In conclusion, the different domains related directly or indirectly to the subject of marine propeller ventilation, are connected and these connections must be adequately modelled to properly describe the functioning of the marine propulsion system under ventilation-inducing boundary conditions.

2.6. Detailed scope of research

This section elaborates on the summarised scope in section 1.4, based on the findings regarding the theoretical background in this chapter. The research, answering the questions in section 1.5, covers the behaviour of a monohull coaster and the components of its conventional propulsion systems. An example is shown in figure 2.17.

Such ships traditionally have a marine Diesel engine installed as a prime mover on a propulsion line with a single FPP, as shown in figure 2.1. Finally, these ships are used in deep water and do encounter adverse conditions. The study at hand investigates rigid-body motions under adverse conditions that are encountered while sailing at low but positive transit speeds of less than 8 [kts]. The propulsion system at hand consists of a medium-speed engine, a reduction gearbox and a single FPP.

Figure 2.17: A coaster in head seas. Source: [26]

The propeller experiences the imposed motions of the rigid bodied and neutrally-trimmed hull to which it is attached, while enduring the environmental and propulsive loads to which it is subjected simultaneously. Loads imposed by wind and current shall be neglected as they are, in open seas under challenging conditions, the lesser to waves. This research effort shall be limited to the application of linear wave theory as discussed in section 2.2 which shall be used to describe loads imposed by both regular long crested waves and irregular seas.

The engine speed setpoint, seastate and resulting wave loads will be varied as described in chapter 6 to impose an explicit loading condition for the vessel, assuming an implicitly defined heading controlled by an auto-pilot as explained in Fossen (2011) [25]. It is expected that the vertical propeller motions are largest for head seas. Voluntary heading corrections are thereby not included. The vessels speed is limited by the explicitly defined seastate and the research shall neglect possible voluntary speed and motion reduction measures.

The resulting behaviour of the vessel and its propulsion system in response to these loads and control actions shall be used to gain insight in the propulsion systems capabilities to respond to load fluctuations as a result of ventilation. Although out-of-water ventilation events may occur, the focus of this work shall lie with submerged-ventilation events for values of $h/R \geq 1[-]$ and be limited to values $h/R \geq 0.5[-]$.

Study of the thermal loads of the prime-mover and validation efforts are not included in the scope of this research effort. Section 7.3 describes and gathers a number of parameters that are required for a successful validation effort.

3

Literature research

Chapter 2 discussed the theoretical background of the goal posed in section 1.4: *"Increased understanding of the relation between wave properties, -height and -frequency, and the response of a marine Diesel engine, -speed and -torque, subjected to wave-induced ventilation."*. This chapter gathers sources that can be used to help attain this goal with the scope of research posed in section 2.6. These can be used in the construction of a complete ventilation model in chapter 4.
Section 3.1 treats alternatives found in literature to describe vessel-motions and is followed by a section treating different research efforts that can be used to describe propeller functioning under ventilation conditions. It is followed by a section 3.3 treating on alternative descriptions of prime-mover components. The last section of this chapter treats how these different alternatives can be brought together.

3.1. Vessel-motion literature

This section treats different literature sources that provide alternative descriptions of *a. Reference frames and speeds*, *b. Linear waves* and *c. Resistance*. These can be used to construct a model in chapter 4. Wind- and current- loads are neglected following the scope in section 2.6.

a. Reference frame- and speed alternatives

a1. Vessel-bound {b} A reference frame attached to the hull at it's centre of gravity. It's motions can be described both in comparison with an inertial frame as under earthbound below, or with a constant moving seakeeping frame, following amongst others Fossen (2011) [25].

a2. Seakeeping {s} A reference frame moving with constant speed, fixed to this equilibrium state (Fossen (2011) [25]). In practise: a reference frame moving with the average forward speed.

a3. Earth-bound {e} A North-East-down inertial reference frame with a fixed position on the surface of the earth at still-water level. Following Fossen (2011) [25], the other vessel-bound and seakeeping reference frames can be coupled by kinematic transformations.

a4. Near zero- or transit-speed Sørensen (2013) [35] describes the application of *positioning systems* and *automatic sailing systems*in different speed-regimes: The first consists of dynamic positioning or position mooring systems. These are applied at near-zero speeds in the range to circa [kts]. The latter gather autopilot and *"GPS for automatic course keeping and ...changing for transit operations*" amongst other components such as radar and AIS (Sørensen (2013) [35]).

a5. Manoeuvring- or seakeeping theory Fossen (2011) [25] clearly sets apart how manoeuvring-theory describes *"ship motion in the abscence of wave excitation (calm water)*" whilst seakeeping *"is the study of motion when there is wave excitation and the craft keeps its heading ψ and its speed U constant (which includes the case of zero speed)."* The core difference between these two is the inclusion of dissipative forces, and the description of motion around a constantly

moving seakeeping-reference frame (Fossen (2011) [25]). A unified model is also described which can combine a seakeeping model with different linear- and non-linear forces to reach a complete description of non-linear motion in the time-domain.

Definition 2. *Speed is the rate at which an object moves or is able to move.*

Definition 3. *Velocity is the speed at which something moves in a particular direction.*

With definitions 2 and 3 following [52] in mind, it is noted that there is an overlap between the speed regimes to which manoeuvring- and seakeeping theory can be applied and the implicit description of speed in the scope in section 2.6.

a6. Time- or frequency domain As described by Boyce and DiPrima (2012) [53] and summarised in appendix B, differential equations can be transformed from the time- to the *frequency domain* and back. The same continuous parameter or signal can be described in both domains. As described by Fossen (2011) [25] *"the time-domain models are useful both for simulation and control systems design."*, whilst analysis of a system in the frequency-domain can be usefull to study it's particular response-characteristics.

b. Linear wave alternatives

b1. Regular waves A regular wave is a single long-crested sinusoid wave moving in direction ψ with characteristic amplitude ζ_a, frequency ω, wave-number k and phase-shift ϵ as equation 3.2. Faltinsen (1993) [18] describes that the hydrodynamic problem to describe a vessels response to regular waves, can be solved in two steps: Restrained vessel wave excitation and rigid-body motion without wave excitation.

Restrained vessel wave excitation Excitation loads from regular waves with different frequencies coming from different directions can in term be gathered in two groups: Froude-Kriloff forces and moments and diffraction forces and moments.

- Froude-Kriloff forces and moments describe the forces on the hull of a vessel that occur as a result of pressure variation resulting from a passing, undisturbed waves. In the idealised theoretical case of a vessel made of netting, subjected to excitation loads from a passing wave, the netting-vessel would only be subjected to Froude-Kriloff forces and moments, as the waves would pass undisturbed through the vessel.
- Diffraction forces and moments occur as a result of the deflection of a waves that meets an impermeable obstacle such as the hull of a vessel.

Rigid-body motion without wave excitation Forcing rigid body motion with the exciting wave frequency ω ($\overline{F}_{exc}(\omega)$ in equation 3.1), but without exciting waves, reveals the relation between a vessels motion $\dot{\overline{x}}$ in all six degrees of freedom and the added mass- (A), damping- (B) and restoring- (C) characteristics of the vessel, as described in equation 3.1.

$$(M + A)\ddot{\overline{x}} + B\dot{\overline{x}} + C\overline{x} = \overline{F}_{exc}(\omega) \tag{3.1}$$

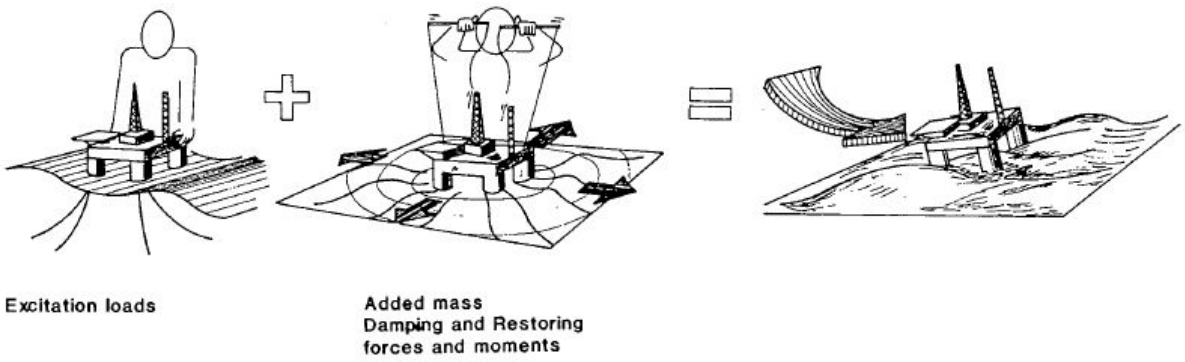

Figure 3.1: Superposition of wave excitation, added mass, damping and restoring loads. Source [18]

The added mass, damping- and restoring forces are induced by the forced motion of the vessel on the mass of water surrounding the vessel.

b2. Bichromatic and irregular waves Following the work of Journée and Massie (2001) [19] figure 3.2 shows an irregular wave constructed by adding two or more regular waves with different wave frequencies ω and related group velocities c.
Bichromatic waves consist of $N = 2[-]$ components with different frequencies.
Irregular waves: As Journée and Massie describe, "*the wave elevation (in the time domain) of a long-crested irregular sea, propagating along the positive x axis, can be written as the sum of a large number of regular wave components (in the frequency domain)*". This is described with equation 3.3 where k_n is the wavenumber and, $\epsilon_n[n]$ the random phase shift of component n. It is further remarked that this relation assumes deep water, thereby reducing the dispersion relation for water to $\omega^2 = k \cdot g$, fixing the value of the wave number for a certain wave frequency.

$$\zeta(x,t) = \zeta_a cos(kx - \omega t) \quad (3.2)$$

$$\zeta(x,t) = \Sigma_{n=1}^{N} \zeta_{a_n} cos(k_n x - \omega_n t + \epsilon_n) \quad (3.3)$$

$$c = \frac{\omega}{k} = \frac{\lambda}{T} \quad (3.4)$$

$$\omega_e = \omega - Vk \cdot cos(\mu) \quad (3.5)$$

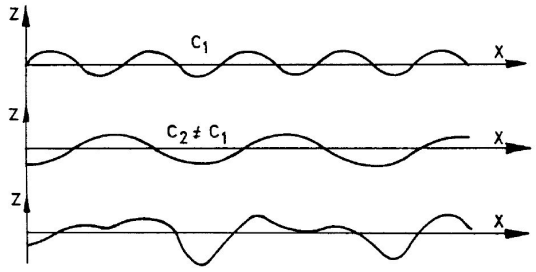

Figure 3.2: Supeposition of two uni-directional harmonic waves. Source: [19]

Frequencies of encounter in irregular waves:
Using the linear combination above in combination with figure 3.3a, the frequency of encounter can be described. Whereas the $\omega_n[rads^{-1}]$ is the circular frequency of wave component n, relating the wave components motion with respect to a fixed point, the frequency of encounter $\omega_e[rads^{-1}]$ relates it to the moving vessel. Using equation 3.4 and the definition that $\omega = 2\pi T$, we can deduce that the period of encounter $T_e[s^{-1}] = \frac{\lambda}{c+Vcos(\mu-\pi)} = \frac{\lambda}{c-Vcos(\mu)}$ as proved by (among others), Journée and Massie (2001) [19]. Combining this with the definition of c in equation 3.4, the frequency of encounter of a component is now defined by equation 3.5.

Figure 3.3: Different wave-properties.

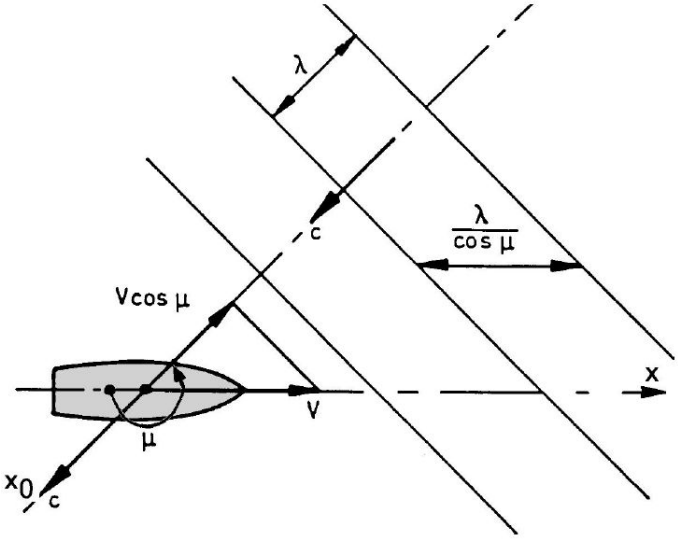

(a) Frequency of encounter. Source: [19]

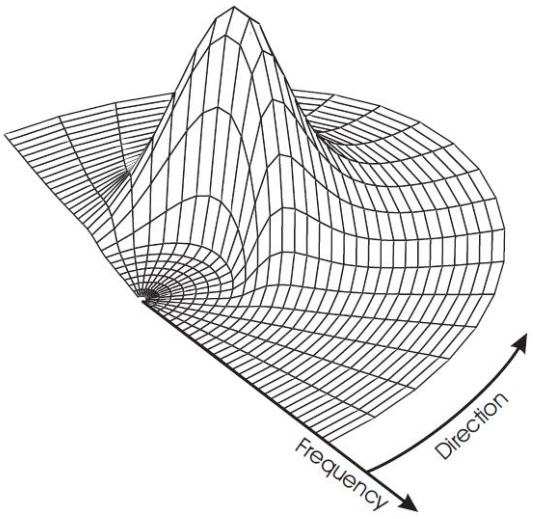

(b) Spectrum as function of frequency and direction. Source: [35]

b3. Fourier transformation and seastate A Fourier-transform can transform information regarding an irregular wave described as a function of time such as equation 3.3, to a description of the same irregular wave in the frequency domain. Equation 3.6 describes the basic Fourier transformation of a time-dependent and repeating signal $F(t)$. A brief elaboration on the method can be found in appendix B whilst a graphic application of the method is shown in figure 2.5.

$$F(t) = a_0 + \Sigma_{n=1}^{\infty} (a_n cos(n\omega t) + b_n sin(n\omega t)) \tag{3.6}$$

Such a frequency dependent wave spectrum $S(\omega)$ such as shown in figure 2.5 can be combined with a directional spectrum $D(\psi, \omega)$ as posed by Sørensen (2013) [35] in equations 3.7 and 3.8, to describe the amount of energy in a specific seastate, S_{tot}. Figure 3.3b provides an example of a graphical characterisation of such a spectrum. This characterises a specific irregular seastate. Equation 3.9 describes a realisation of this seastate as a function of x, y, t, ω_q and ψ_r, for a seastate $S(\omega, \psi)$ divided into N segments of frequency q and M segments of direction r. Sørensen's notation in the earth-bound inertial reference frame $\{e\}$ has waves with a zero-heading ($\psi_r = 0$) propagating north.

$$S(\omega, \psi) = S(\omega)D(\psi, \omega) \tag{3.7}$$

$$S_{tot} = \int_0^{\infty} \int_0^{2\pi} S(\omega, \psi) d\psi d\omega \tag{3.8}$$

$$\zeta(x, y, t) = \Sigma_{q=1}^{N} \Sigma_{r=1}^{M} \sqrt{2S(\omega_q, \psi_r)\Delta\omega\Delta\psi} \cdot sin(\omega_q t + \phi_{qr} - k_q(xcos(\psi_r + ysin(\psi_r))) \tag{3.9}$$

Different seastate's at different times and different places can be described with different spectra:

b4-1. Wave spectrum - Bretschneider Bretschneider (1964) [54] gathers a broad description of the generation of waves and the decay of swell as well as both deep- and shallow water effects. Using the frequency f instead of the radial frequency ω, he proposes the wave spectrum: $S(f) = af^{-m-2}e^{-bf^{-n}}$. This description is comparable to that of Pierson and Moskovitsz (1964) [55].

According to Sørensen (2013) [35], the international towing tank conference (henceforth ITTC) provides another two-parameter spectrum for open seas with $A = 0.31H_s^2\omega_p^4$ and $B = 1.25\omega_p^4$ as a function of the significant wave height H_s and radial peak frequency ω_p. For one and the same spectrum, these parameters are connected. The two-parameter spectrum is described as: $S(\omega) = \frac{A}{\omega^5}exp(-\frac{B}{\omega^4})$.

b4-2. Wave spectrum - Pierson and Moskovitz Pierson and Moskovitz (1964) [55] describe a widely used spectrum for fully developed seas with governing wind speeds from 20 to 40 [kts]: $S(\omega)d\omega = \frac{\alpha g^2}{\omega^5}e^{-\beta(\omega_0/\omega)^4}d\omega$. The quality of this description lies in it's validity for different wind speeds. It's main disadvantage lies in the fact that it uses wind-measurements from non-standard measurement heights on board of weather ships. The data can therefore not easily be transformed to standard wind measurements. Like the ITTC spectrum, the Pierson and Moskovitz spectrum depends on the value of both the significant wave height H_s and the radial peak frequency ω_p.

b4-3. Wave spectrum - Torsethaugen and Haver Torsethaugen and Haver (2004) [56] describe a simplified version of a principally different wave spectrum that incorporates a broad spectrum of both significant wave height H_s and radial peak frequency ω_p. Dependent on the governing sea state's character, either primary- and wind dominated, or secondary and swell dominated part of the spectrum dominates. I is compared with a double-peaked Ochi-Hubble model and data from three different locations on the Norwegian continental shelf. Torsethaugen and Haver (2004) [56] found only small deviations for the highest frequencies of the wind dominated spectrum.

b4-4. Wave spectrum - non-linear Draupner limit The seastates and spectra discussed above require observations to describe a realistic spectrum that can be used to describe realistic wave forces on a vessel. Haver (2004) [27] provides an upper limit to such observations with the well-documented

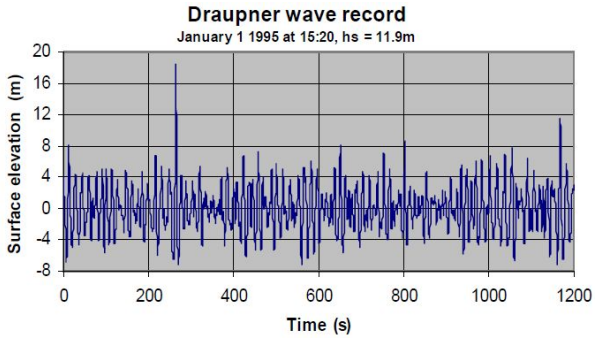

Figure 3.4: Time history including an possible freak wave event. Source [27]

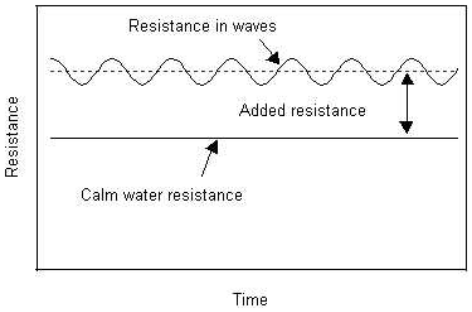

Figure 3.5: Resistance in waves. Source: [6]

observation of a possible freak wave event measured with a look-down laser observer on the Draupner platform on the 1^{th} of January 1995, in a storm with two low pressure fields.
A maximum wave height of almost 26 [m] was measured with a less unusual significant wave height of $H_s = 11.9[m]$. The local wave peak height with an annual probability of 10^{-2} (so a 1 in 100 year peak height) is around 27 [m]. However, this would be expected to occur with a significant wave height in the range of $H_s = 13 - 14[m]$, and not $11.9[m]$. Figure 3.4 shows a 20 minute wave record including an unexpectedly large wave. Haver's observations provide a well-documented upper limit.

c. Resistance alternatives

c1. Scaling Scaling of the resistance to which a vessel is subjected, comprises the scaling of two different types of occurring forces: The *friction-related* forces can be scaled using Reynolds-equality, and the *wave-related* forces that can be scaled using Froude-equality. These equality's are mutually exclusive. Traditionally, *friction-related* forces are predicted for the prototype based on it's known wetted area and Reynolds-equality. In practice, this means that the drag forces of a wetted plate can be used to determine the drag-forces to which the wetted surface of the hull will be subjected. In turn, the *wave-related* forces of the prototype are predicted with experimental scale-model tests in a towing tank at different speeds using Froude-equality. Appendix C treats the Reynolds number Re and Froude number Fr that govern these phenomena in detail.

c2. Potential-flow and strip-theory These methods divide the shape of a hull in a number of small panels, each subjected to a potential flow. Dependent on boundary conditions such as impenetrability and assumed inviscid flow properties, the forces on the hull panel and thereby the whole hull can be determined for a vessel sailing at a certain speed, subjected to certain waves. Journée and Massie (2001) [19] provide a broad introduction to the subject of potential methods in offshore applications. They also describe how irregular frequencies can impose numerical problems when determining loads on a vessel and how this can be solved by imposing another boundary condition on the hull: By imposing a potential-flow restriction on the free surface of the vessel's body (the inside of the hull). In practise, this is called "*putting a lid on free surface inside the body*" Journée and Massie (2001) [19]. These methods describe different forces on the hull, including it's resistance whilst moving at different speeds.

c3. Unified approach As potential methods assume in-viscid flows, the viscous effects that load a hull could be underestimated in some cases. Fossen (2011) [25] summarises a unified approach that combines manoeuvring- and seakeeping theory as discussed under **a5.**: Time-domain models are appended with "*nonlinear terms...to describe coupled maneuvers at high speed. Fluid memory effects and wave force terms are kept from the seakeeping theory.*"
The transformation of force terms between the vessel- or body-bound reference frame {b} and the seakeeping reference frame {s} lie at the core of this method and introduce terms describing *Coriolis and centipetel forces* (Fossen (2011) [25]). This approach also describes resistance of a vessel moving at different speeds.

c4. Comparison of applications Gourlay (2015) [57] compared different commercial software packages that applied the methods discussed under **c2.** and **c3.** to both Panamax and post-Panamax

container ships and a Panamax bulkcarier. In these tests "*the benchmarking showed in general good agreement of numerical predictions with model test results for three cargo ships studied over the entire range of wave frequencies*" Gourlay *et al.* (2015) [57]. Although this specific study focusses on slightly different ship-type's and boundary conditions, such software-packages can be used to predict the hydrodynamic loads with sufficient accuracy, by using potential code theory as discussed above. Bentley (2014) [5] applies the panel method to potential flow problems as treated in section 2.2 and indicated with figure 2.6, to describe the total resistance of the hull with equations 3.12-3.11 in it's Maxsurf software package.

$$R_{sw} = R_{wm} + R_{visc.} = f(\dot{x}) \tag{3.10}$$

$$R_{aw} = \quad = f(\omega_i, \psi_i, \dot{x}) \tag{3.11}$$

$$R_{tot} = R_{sw} + R_{aw} \tag{3.12}$$

Still-water resistance consists of wave-making resistance and viscous resistance (equation 3.10). Added resistance is the result of motions induced by encountered waves (equation 3.11). This differs from the wave-making resistance which is induced by the displacement of still water by the moving hull. The summation of these components in equation 3.12 is illustrated in figure 3.5. Table 3.1 lists different methods gathered by Bentley (2014) [5] to predict these resistance components.

R	Estimation method's	Intended for head seas, z- and ϑ (displacement mode-)
$R_{sw}[N]$	Wyman	planing and displacement hull-forms.
	Holtrop	tankers, gen. cargo-/fishing-/container-ships, tugs, frigates.
	Compton	transom stern, displacement and semi-planing powerboats.
	Fung	transom stern vessels larger than Compton.
	van Oortmerssen	small ships such as trawlers and tugs.
	Series 60	single screw cargo ships.
	KR-barge	box shaped vessels.
$R_{aw}[N]$	Gerritsma and Breukelman (1967, 1972), Salvesen (1978), Havelock (1942)	fast cargo hull-forms. wider range of hull-forms (theoretically also oblique waves).

Table 3.1: Resistance prediction methods according to Bentley (2014) [5] and [6].

3.2. Propeller literature

This section treats different literature sources that provide alternative descriptions of propeller functioning during ventilation events. Figure 3.6 divides these sources in three categories with the intent to describe ventilation for all vessel motion: *i. varying immersion*, *j. constant immersion* and *k. unknown loss*. These different strategies can be used to describe different propeller immersions and thereby all possible vessel motions in the scope in section 2.6 in a model in chapter 4.

i. Varying immersion alternatives

This category consists of experiments and simulations for propellers that focus on propeller- or blade loads for one specific vertical motion to which it is subjected. These efforts intend to identify peak loads on propulsion system components that occur as a result of ventilation. Figure 3.7 shows the definition of torque's and forces to which the propulsion system is subjected. An improved description of these peak loads allows designers to improve their design and prevent damages.

i1. Forced heave motion (1/2) Koushan (2007) [21] measured thrust loads on open- and ducted azimuthing propellers that were subjected to different constant as well as varying immersion ratio's. Koushan's most important conclusion is that "*when a thruster undergoes heave motion, it is the ventilation which is the primary cause of loading fluctuations rather than the heave motion. Of course, heave motion acts as a generator and transporter of ventilation.*"

A characteristic example of consists of the open thruster subjected to an imposed heave motion with an amplitude/R = 2.15 [-], a peak value of h/R = -0.15 [-] and a period of 2 [s] such as shown in

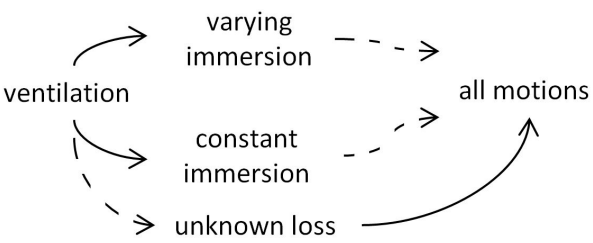

Figure 3.6: Ventilation addressing strategies and possibilities (dotted).

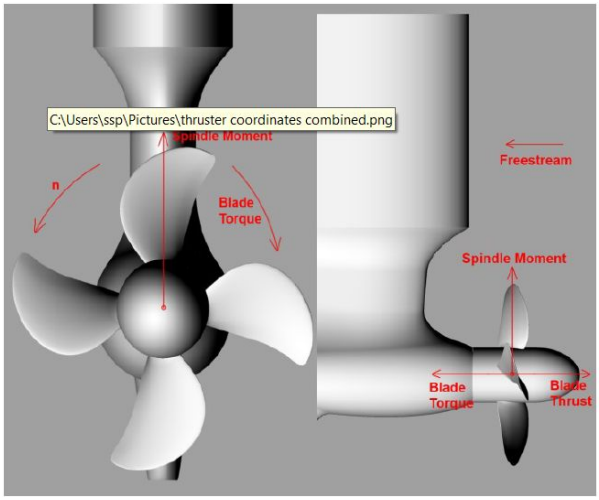

Figure 3.7: Coordinate system. Source: [28]

figure 2.10. It was found for this and other imposed propeller motions that "*variations in relative blade torque are almost identical to variations in relative blade thrust under ventilated conditions.*" Using measurements as those in figure 2.13, Koushan proves that the largest blade thrust fluctuations occur upon the inception of ventilation when the thrustforce is suddenly greatly reduced.

Koushan's data shows how a propeller subjected to a sinusoid-heave motion displays cyclic ventilation behaviour that consists of a sudden loss of thrust, a stabilisation period and a recovery of thrust, all dependent on the immersion. Koushan also finds that a ducted propeller limits the formation of a ventilation regime on the emerging side of the propeller and that open propellers therefore experience more violent ventilation events.

Koushan (2007) [21] only compares azimuthing thrusters and this raises the question whether or not the conclusions above are equally valid for regular propeller thrusters. As the wake and their will not be completely the same, results may vary.

i2. Forced heave motion (2/2) Van Beek and van Terwisga (2006) [29] researched two useful effects in the light of this study, as they can occur on CPP's under varying immersion: Propeller cavitation and -ventilation. Their experiments, performed in a depressurised towing tank, are performed with varying propeller immersion. It is assumed that this method of immersion-variation is comparable to the method applied by Koushan (2007) [21] who imposed a heave motion on the thruster without the presence of waves.

The most important finding for varying immersion was that the occurrence of cavitation under ventilating conditions diminishes the effects of ventilation on the blade spindle torque "*approximately a factor two.*" An important conclusion is therefore that pure-ventilation, and not cavitation-induced loads, characterise peak-loading situations.
Figure 3.8 shows the effect of varying immersion on blade spindle torque. Although figure 3.7 shows that blade spindle torque and propeller torque, this image confirms the cyclic load variation as a result of occurring ventilation.

i3. Imposed wave Dang *et al.* (2013) [1] measure propeller loads on a Wageningen B4-70 propeller installed on a generic pulling azimuththruster. Ventilation experiments with wave-induced variable immersion confirm the cyclic nature of ventilation behaviour as well as the significant presence of load peaks and the uncertainty in thrust prediction as a result of ventilation-induced hysteresis effects.
Figure 3.9 displays T_{Bx} the thrust force on a key-blade, equipped with 6 force transducers. The photo in figure 1.1 is taken at the screenshot-marking during the passing of a wave crest. Full scale

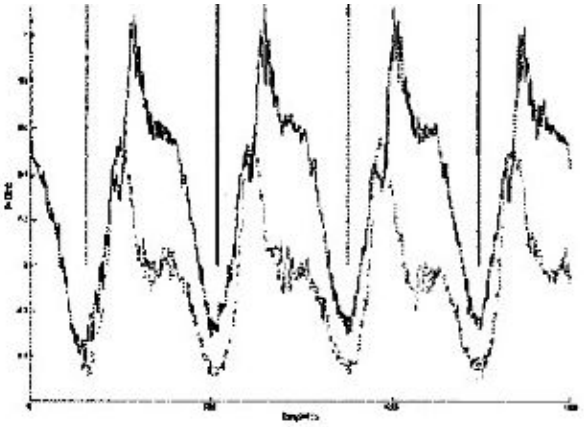

Figure 3.8: Effect of propeller immersion on blade spindle torque (atmospheric pressure). Source: [29] (Time horizontal, blade spindle torque vertical)

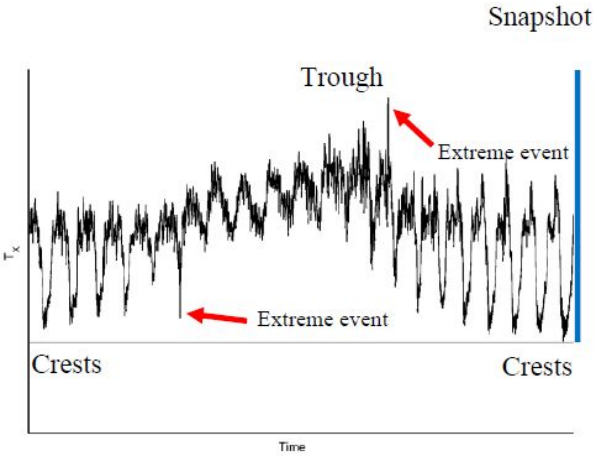

Figure 3.9: Time trace of T_{Bx} during approximately one wave period. Source: [1]

measurements on a ducted DP thruster show significant variations of shaft torque during an operation. The fluctuations around a certain speed setpoint can, at least in part, be explained by the occurrence of ventilation.

j. Constant immersion alternatives

This category groups research efforts that focus on the same loads for a propeller that is subjected to a constant immersion ratio.

j1. Out-of-water factor Koushan (2007) [21] also researched time-average loads on constantly immersed azimuth thrusters. These are shown in figure 3.10 and show how both ducted and open propellers experience significant thrust losses for constantly reduced immersions. This data confirms the different ventilation mechanisms for ducted- and open propellers that were found by Koushan for varying immersion and organised in figure 1.2. The propeller thrust measurement FX also confirms that for larger immersions ($h/R \geq 1.6[-]$), ventilation has a significant effect on thrust production. For this specific propeller design which is used in both the ducted- and open propeller, it amounts to a loss of $\pm 40[\%]$. Koushan thereby quantifies the influence of ventilation under static immersion.

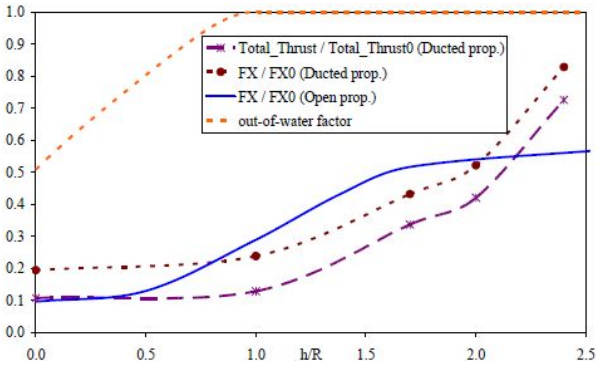

Figure 3.10: Comparison of time-averaged loadings of ducted and open thrusters. Source: [21]

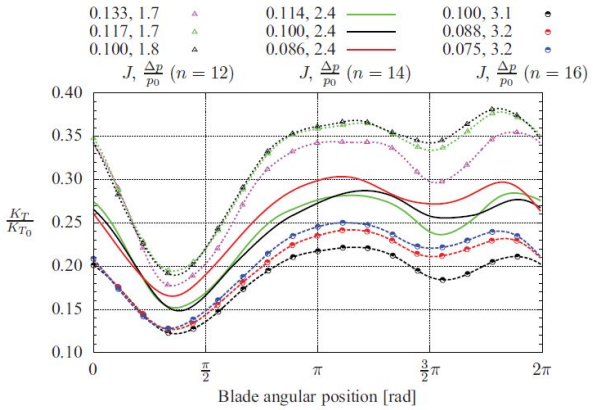

Figure 3.11: Thrust ratio for each blade angular position [–∘– = 16, — = 14, ...△... = 12 Hz]. h/R = 1. Source: [30]

j2. Blade loads For different immersion ratio's h/R, Califano (2010) [30] provides measurement data regarding the thrust variation for a blade that rotates 360 [∘]. This is shown in figure 3.11 and reveals the range of blade-thrust fluctuations as a function of rotational speed and immersion ratio for a propeller blade rotating at a constant immersion. These results show different behaviour for

different steady-state ventilation regimes dependent on the immersion ratio, with the blades moving downwards at $\pi/2$ [rad].
The results for open thrusters clearly show how different propeller blades are loaded simultaneously as the air pockets under these conditions are drawn towards the side of the propeller that is rotating downwards. Califano thereby answers the question how ventilation induces load differences between different blades on one propeller.

j3. Scaling FPP ventilation
Guoqiang *et al.* [7] present four significant contributions for FPP's of which the ventilation scaling laws in table 3.2 are the first: For accurate modelling, the experimental propeller and full scale model should adhere to these scaling laws. Guoqiang *et al.* (1989) [7] state that: "*condition e can also be expressed by Froude number due to the same H/R as follows:* $Fr = g/(n^2D)$". They further rewrite the cavitation number, as a product of immersion ratio and rotational Froude-number in equation 3.13.

a. Propellers with geometric identical shapes.
b. The Reynolds number of larger than critical value.
c. Same advance coefficient J.
d. Same dimensionless submerged propeller depth h/R.
e. Same dimensionless pressure coefficient.

Table 3.2: Ventilation scaling laws as posed by [7].

$$\sigma = 2\Delta p/\rho(nD)^2 = g(h/R)/n^2D = (h/R)\cdot Fr_p \tag{3.13}$$

If h/R and Fr_p are kept equal on full scale, this results in a *"test that is done under the condition that the model and full scale propeller are operated at the same cavitation number"*, (Guoqiang *et al.* (1989) [7]). Appendix C expands on these parameters.

Secondly, Guoqiang *et al.* contribute the description of thrust variation as a function of occurring propeller slip ratio S [-] that varies for different ventilation regimes, from partial ventilation with S_P to super-ventilation (fully developed ventilation) S_S. Equation 3.14 provides an example for occurring slip ratio values S $S_S \leq S \leq 1.0$, using a definition of a propeller-Froude number from scaling law e.

Thirdly, as Koushan (2007) [21] found that "*variations in relative blade torque are almost identical to variations in relative blade thrust under ventilated conditions* " for propellers ventilating under varying immersion, Guoqiang *et al.* found that "*all the results obtained in the test show that the variation tendency of* K_T *with* J *is similar to that of* K_Q" and that the variation of K_T alone can therefore be used to investigate a ventilating propeller.

$$K_T = K_{T1}(0.13 + 2.878(h/R)^{2.4})(0.16 + 6.48Fr - 2.41Fr^2)(1-S)(S-S_S)/(1-S_S)^2) \tag{3.14}$$

A fourth contribution by Guoqiang *et al.* is shown in figure 2.9 and comparable figures for other rotational speeds n. These images show results comparable to those of Califano (2010) [30] in figure 3.11 and display different thrust variations as a function of the dimensionless advance ratio J, the propeller rotational speed n and the immersion ratio h/R. The difference between these two lies in the fact that Califano describes thrust per propeller blade whereas Guoqiang *et al.* describe the thrust from the propeller as a whole. The open-water diagrams from Guoqiang describe the functioning of a propeller under steady state conditions for fixed immersion ratio's. This raises the question if they can be used to model ventilation-induced load fluctuations for all motions as discussed with figure 3.6 and if this data can be used to describe propeller condition under a vessels hull, instead of in open water.

j4. Influence of rudder angle on ventilation For constant immersion ratio's, van Beek and van Terwisga (2006) [29] found that "*an effect of rudder angle on ventilation or on blade torque could not be found, neither in the non-cavitating, nor in the cavitating condition.*" Test were conducted for rudder oscillations of 10 degrees and it is found that "*the dynamic effect of rudder angle is consequently neglegible.*" This is explained with the far smaller frequency of the rudder angle variation in comparison with the blade passing frequency which is of a significantly higher order and is a governing parameter in the occurrence of ventilation whilst variation of rudder angle has no significant effect on propeller-blade immersion. In conclusion, no relation between rudder angle and ventilation was found.

j5. On hysteresis, bistability and the Weber-number Van der Leij (2019) [31] describes hysteresis and bistability in propeller ventilation, before treating the influence of the Weber number We. The discrete character of ventilation results in *inception*- and *wash-out* regimes where more- and less air is transported through the propeller plane, instead of a continuous, stable flow of air. Hysteresis[1] results in two descriptions of propeller functioning: *before a changed passage of air* and *after a changed passage of air*. This results in two different description of thrust under *previously* and *newly* stable conditions. Bistability is an intermittent occurring of these two different equilibria.

As described by van der Leij (2019) [31]: "*The box around the critical advance ratio in fig. 3.12 is a bistable region. Depending on the origin (low or high J), the phenomenon behaves differently. This is known as hysteresis. Due to added resistance, e.g. in waves, loading of the propeller increases, which may incept ventilation. When thrust is then decreased, ventilation may wash out. Eventually this could lead to continuous inception and wash-out of (more severe) ventilation.*"
Van der Leij (2019) [31] also mentions it's influence on propulsion: "*In excessive situations, this can be problematic in heavy seas, where thrust loadings are continuously high and the propeller keeps ventilating. Especially when the propeller pitch is not controllable, a vessel could end up in a state when it no longer has enough thrust to even stay in position and loses control. In lesser severity, ship speed and efficiency decrease, which is neither favourable, although surmountable if in lesser demanding conditions overall efficiency is increased.*"

Van der Leij (2019) [31] also summarises the work of Shiba (1953) [59] who noted that influence of Weber number on ventilation inception "*dissapeared at We = 180*" (van der Leij (2019) [31]). Appendix C shows that this influence can be neglected as this occurs below the clutch-in-speed of engines in the scope of this work. *Finally*, van der Leij (2019) [31] remarks that "*It should be noted that propellers investigated are not always comparable to modern ship propellers anymore. Conclusions derived by Shiba should thus always be used with care.*"

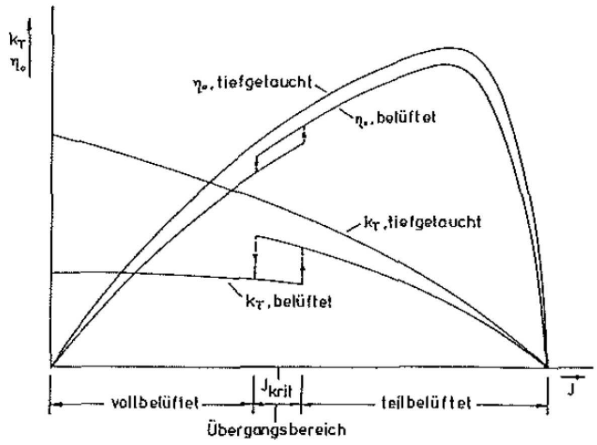

Figure 3.12: Influence of ventilation on open water propeller diagram. Adopted from Pohl. Source: [31].

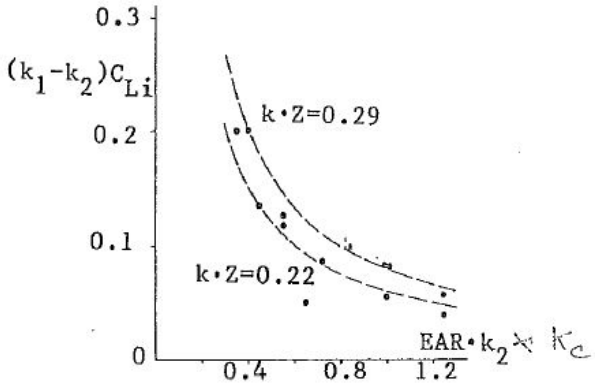

Figure 3.13: Ideal liftcoefficient estimated from incipient ventilation. Source: [32]

k. Unknown loss alternatives

This category focuses on the load variations that ventilation may induce. Guoqiang *et al.* (1989) [7] provided descriptions to estimate slip for different ventilation regimes, such as equation 3.14, but other research efforts have focused on other descriptions of this unknown loss.

k1. Lift coefficient of a propeller blade Minsaas *et al.* (1983) [32] provide descriptions for different effects occurring in the thrust-resistance equilibrium of a vessels hull and thereby study the flow-regime that leads to the occurrence of ventilation. Based on a theoretical analysis of the breakdown of lift on a propeller blade subjected to air pockets, they describe the occurrence of ventilation inception as a function of the ideal (theoretical) lift coefficient with the graph in figure

[1] From ancient Greek ὑστέρησις, lagging, late- or shortcoming. (Pape (1914) [58], from German)

3.13. This is used in turn to estimate the unknown thrust fluctuations with the parameter K_{Ti}^{**} in equation 3.15. This value of unknown thrust-loss is than compared with an empirically determined boundary value of K_T to determine if and to what degree ventilation will occur and thrust will be lost. This method is based on the assumed equilibrium at the point of ventilation inception between air pocket development and pressure drop at the edge of a propeller blade.

$$(k_1 - k_2)C_{Li} = \frac{K_{Ti}^{**}k_1}{1.5EAR} - (\sqrt{1+\sigma_V} - 1) \tag{3.15}$$

k2. Load torque observer As described in section 3.3, Smogeli (2006) [13] uses the term $\dot{\hat{Q}}_a$ in equation 3.21 to estimate the unknown loss of torque that occurs as a result of ventilation. The inertia I_s of the shaft and connected propulsion system are known and measures shaft torque and acceleration $\dot{\omega}$ are used to estimate torque lost to the entrained water $\dot{\hat{Q}}_a$.
This method to estimate an unknown loss by observing a varying load, replaces one unknown *loss of propeller load*, with an other unknown *variation of entrained water*. The goal of this method is not to provide a definite estimate of *what happens*, but the observation *that something happens*, which is especially useful for electrical propulsion systems that can respond quickly to significant load fluctuations.

k3. Entrained water MacPherson *et al.* (2007) [60] point out different flaws and possible corrections on both analytical and empirical methods to determine I_{ew}, the rotational inertia of water entrained in the the propeller. The lesser flawed, basic and analytical estimate of Schwanecke (1963), equation 3.16 only uses characteristic propeller-design parameters such as blade pitch ratio P/D [-] and expanded area ratio A_e/A_0 [-].

$$I_{ew,p} = m_{44,p} = 0.0703\frac{\rho D^5}{\pi Z}\left(\frac{P}{D}\right)^2\left(\frac{A_e}{A_0}\right)^2 [kgm^2] \tag{3.16}$$

Although non of these methods are expected to provide an accurate estimate under ventilating conditions, they can be used as a first-estimate.

Summary of section 3.2

Varying immersion research has provided insight in the scale and frequency of thrust and torque variations and confirm that, in the words of Koushan (2007) [21], "*variations in relative blade torque are almost identical to variations in relative blade thrust under ventilated conditions.*" These efforts however only describe the development of load fluctuations for varying immersion (see figure 3.6) and neglect the influence of the presence of the hull on the inflow conditions for both the medium (seawater) and the disturbances (air pockets). It was also found by van Beek and van Terwisga (2006) [29] that cavitation that occurs simultaneously with ventilation can dampen the load fluctuations that ventilation would incur. Dang *et al.* (2013) [1] show the scale of load variations and how hysteresis effects play a significant role in the occurrence of ventilation.
For constant immersion, van Beek and van Terwisga (2006) [29] show that, and explain why, rudder angle variation has no significant influence on ventilation behaviour. Koushan provides an example of the order of thrust loss for constantly immersed propellers. Califano (2010) [30] measured thrust variations experienced by a blade during it's rotation at a fixed propeller immersion as shown in figure 3.11. Guoqiang *et al.* [7] confirmed that the relation between propeller thrust and torque under ventilation conditions is valid for both constant and varying immersion as Koushan (2007) [21] determined.
Unknown loss is treated by other methods such as treated by Minsaas *et al.* (1983) [32], by assuming how ventilation inception takes place or as Smogeli (2006) [13], by measuring torque-variations empirically. MacPherson *et al.* (2007) [60] compared methods to estimate the inertia of entrained water in a propeller. Together, all these methods provide possibilities to describe specific aspects of the behaviour of a propeller subjected to ventilation or to verify model components that describe components of a propulsion system subjected to ventilation.
Table 3.3 gathers these research efforts and their varied parameters.

Source	Type	Propeller	J [-]	h/R [-]	Result
Varying immersion					
Koushan (2007) [21]	exp	Azi, D	u	$-1 \leq\leq 1$	$T_{avg} = f(h/R)$ $M_{avg} = f(h/R)$
	exp	Azi, O	u	$-1 \leq\leq 2.5$	$T_{avg} = f(h/R)$
	exp	Azi, O	u	(1,1.15)	$T = f(h/R)$
	exp	Azi, D	u	(0.98,0.9)	$T = f(h/R)$
van Beek and van Terwisga (2006) [29]	exp	CPP, O	u	u	$M_{bs} = f(h/R)$
Dang *et al.* (2013) [1]	exp	Azi, O	0.8	u	$T = f(\delta)$
	exp	Azi, O	0.6	u	$T = f(\delta, \delta_2)$ $M = f(\delta, \delta_2)$
	exp	Azi, O	0	(1,1)	$T = f(\delta)$
	exp	Azi, D	u	u	$M = f(n_{eng})$
Constant immersion					
Koushan (2007) [21]	exp	Azi, O, D	u	$0 \leq\leq 2.5$	$T_{avg} = f(h/R)$ $M_{avg} = f(h/R)$
Califano (2010) [30]	exp	Azi, O	$0.075 \leq\leq 1.133$	$1 \leq\leq 2.97$	$T = f(h/R, \frac{\Delta p}{p_0}, n, \dot{n})$
Guoqiang *et al.* [7]	exp	FPP, O	$0 \leq\leq 0.85$	$0.5 \leq\leq \infty$	$T = f(J, h/R)$
Unknown loss					
Minsaas (1983) [32]	the	FPP, O	u	u	$T = f(\sigma_v, C_{Li}, k_p)$
Smogeli (2006) [13]	the	FPP, O, D	∀	∀	$M = f(n, Q_a, Q_f)$
MacPherson *et al.* (2007) [60]	the	FPP, O	∀	$\geq 2[-]$	$I_{ew}[kgm^2]$

Table 3.3: Table summarising research efforts regarding propeller-ventilation. ≤≤is a range of static immersion ratio's, (eq,amp) is a sinusoidal immersion ratio with equilibrium eq and amplitude amp, u = unknown, ≤≤ = range of highest peaks, T = thrust, M = torque, avg = average, bs = blade spindle, exp = experimental, the = theoretical, Azi = azimuthing thruster, O = open, D = Ducted, ∀ = for all values, δ = steering angle [deg], σ_v = ventilation number, C_{Li} = lift coefficient for ideal angle of attack, k_p = propeller-characteristic coefficients, Q_a = added torque (bias) and Q_f = friction torque.

3.3. Prime-mover literature

This section treats sources discussing *d. engine size* and main components of the propulsion system: *e. Marine Diesel engine alternatives*, *f. turbo-charging*, *g. governor* and *h. gearbox*. These alternative sources can be used in section 4.4 to construct a sub-model of a prime-mover. Following the scope in section 2.6, two points are stipulated: *Firstly*, efforts are focused on a medium-speed marine Diesel engine. *Secondly* the goal and research questions in section 1.5 require a correct description of the engine's torque and rotational speed at a timescale in the order of [ms], as figure 2.13 shows significant load-variations under the influence of ventilation within a [s] timescale.

d. Engine size alternatives

The following sources pose two limits to engine size for shipowners and propulsion system designers to select smaller or larger engine designs. These limits oppose each other and are expected to become more stringent. A better description of engine-response to ventilation events as discussed in section 1.5, will ensure that such choices more often can be made based on knowledge about response, instead of estimated margins.

d1. Upper limit - EEDI The EEDI, as summarised in equation 1.1 and defined in equation A.1, has a number of different terms in the numerator of the fraction that are written in the standard form from $\Sigma_{i=1}^{n} P_i \cdot C_i \cdot SFC_i$. This is a sum of n engines and power sources that produce an amount of brake power P which is corrected with a fueltype-dependent CO_2-emission factor C and has a certain specific fuel consumption SFC. IMO-MEPC guidelines from (2009) [44] thereby shows how a reduction of installed engine power reduces CO_2 emissions.

d2. Lower limit - Minimum power requirement The IMO-MEPC interim guidelines (2013) [2] require the installation of a minimum amount of power, defined as "*total installed MCR, in kW*" with a power line value as a function of the vessels deadweight in metric tons, shown in equation 3.17. Parameters a and b are shown in table 3.14. In time, these values of a and b provide a lower limit to

$$Minimum\ Power\ Line\ Value = a\ x\ (DWT) + b \tag{3.17}$$

Ship type	a	b
Bulk Carriers	0.0687	2924.4
Tankers	0.0689	3253.0
Combination Carriers	see tankers above	

Figure 3.14: Parameters a and b for determination of the minimum power line values for the different ship types

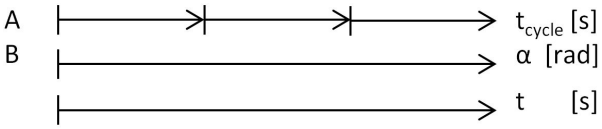

Figure 3.15: Alternative descriptions of time. A: cycle time scale. B: crank angle scale.

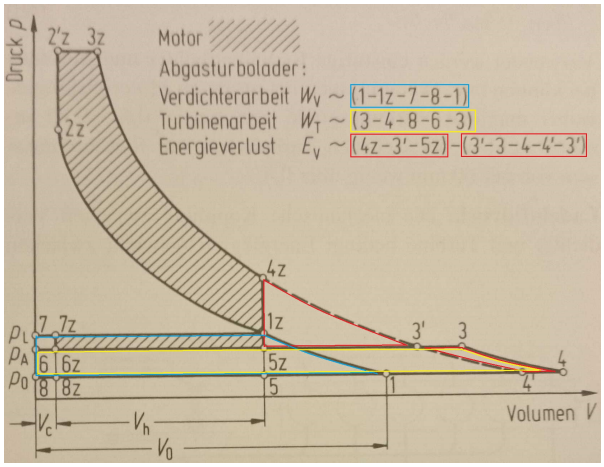

Figure 3.16: Use of: Comparison process of a turbocharged engine (shaded area, index z) with compressor-work (1-1 z-7-8-1) and turbine-work (3-4-8-6-3) for pure pressure-charging, in German.Colours adapted, from source: [33]

the required amount of installed engine power as a function of deadweight.

e. Marine Diesel engine alternatives

Different types of models can be used to describe the prime mover with more or less detail: Lookup-table based models are computationally efficient, but lack detail, whereas detailed CFD models are, amongst other purposes, applied to study the dispersion of fuel droplets after injection in the cylinder of marine Diesel engines. The following Mean Value First Principle models are more detailed than lookup-table models, but focus on a description of the whole engine, instead of the mentioned CFD models.

e1. Diesel A model As Stapersma (2009) [41] describes, the Diesel A engine model is an ongoing research effort at Delft University of Technology which focuses on an accurate description of the functioning of the engine. It can easily be adapted to describe different engines based on the principle particulars in the manufacturers product sheet.
Different Mean Value-estimated processes are described dependent on the engine crank-angle [°] such as the opening and closing of valves and ports, the entry and exit of air masses and the transfer of heat through the combustion of fuel. The crank-angle is coupled to simulation time following B in figure 3.15.

These processes are described with the First Principle description of a Seiliger process by a assumption of principles such as the conservation of mass or -energy or isochoric, -baric, -thermal processes. The air-to-fuel ratio λ_{afr} is used as a governing parameter that characterises the three stages of the combustion process. Figure 3.16 shows an example of a PV-diagram for a turbocharged marine Diesel engine. The blue area indicates compressor work, the yellow area turbine-work and red areas energy losses.
The model can easily be applied to describe the functioning of different engines based on the principle particulars in the manufacturers product sheet. The resulting Diesel-A model provides a detailed description of engine-functioning and can be used with different purposes:

Firstly, to analyse engine functioning in different operational regimes and propulsion systems. An example of such variations lies in the description of different engine responses during pitch-control and acceleration tests by Geertsma *et al.* (2017) [61].
Secondly, to analyse the functioning of an engine with different fueltypes and -properties or with different engine components (Klein-Woud and Stapersma (2002) [11]). Airborne emissions are another example of such characteristics.

e2. Diesel B model The Diesel B engine model is a second continuous research effort at Delft University of Technology in cooperation with the NLDA (former Royal Netherlands Naval College). Since it's development in 1988, components of the model have been adapted by a number of authors.

As with the Diesel-A model, the Diesel-B model describes the closed-cylinder and heat-release processes based on a 6-point Seiliger cycle, as summarised by Ding (2011) [62]. The heat release varies with the an air-to-fuel ratio λ_{afr} [-] that in term depends on the turbo-charger functioning. In addition, the Diesel-B model is supplemented with a description of gas-exchange processes:
- inlet- and outlet receivers with heat-exchange and influence on pressure of charged air.
- compressor and turbine functioning based on characteristic rotational dynamics of the turbo-charger.
- inter-cooler reducing temperature of the compressed charge-air.

Schulten (2005) [63] describes this model in more detail. The accurate application of this model for a specific engine gives a more detailed description of it's functioning. Ding (2011) [62] shows an application of the Diesel-B model that does just that: It studies the functioning of the engine as both a power-source for both a vessels propulsion system and it's pumping system in a dredging vessel. However, this model also requires significantly more information than the principle particulars shared in a manufacturers product sheet.

In summary, the Diesel-A and Diesel-B models are Mean Value First Principle models that can be used to describe the functioning of the same marine Diesel engine. They both use a Seiliger-cycle description of the closed-cylinder process. The Diesel-B model requires more detail in the description of it's components, and provides more details about the functioning of the prime-mover. In general, the Diesel-A model can be used to efficiently describe the functioning of the engine in a larger propulsion system, whereas the Diesel-B model can be used to study the precise functioning of the engine and it's components.

f. Turbo-charging alternatives

f1. Static approach As explained in section 2.4, turbo-charging increases the pressure and the amount of fresh air in the cylinder with a rotating compressor that is powered by a turbine wheel subjected to expanding exhaust gasses. Grote *et al.* (2007) [33] describe how all types of engines (2-stroke, medium speed and high speed) can use turbocharging to increase charge pressure.

$$\begin{aligned}\pi_V &= p_L/p_0 \\ &= \left(1 + \eta_{ATL}\frac{\dot{m}_A c_{pA} T_A}{\dot{m}_{Lges} c_{pL} T_0}\left(1 - \pi_T^{(1-\chi_A)/\chi_A}\right)\right)^{\chi_L/(\chi_L - 1)}\end{aligned} \tag{3.18}$$

The functioning of the turbo-charger as shown in figure 2.14b can be modelled with the following three steps: *Firstly* a mass flow of air from the cylinder $\dot{m}_A = \dot{m}_{Lges} + \dot{m}_B$ (with $\dot{m}_B$ the mass of injected fuel), expands in the turbine. *Secondly*, this expansion exerts an amount of work on the connected compressor. Grote *et al.* (2007) [33] use the turbocharger efficiency η_{ATL} to characterise the turbocharger. *Thirdly* the compressor charges an increased flow of air $\dot{m}_{Lges}$ into the cylinder, assuming isentropic compression. The air is compressed with a ratio of π_V as defined in equation 3.18

f2. First-principle approach Miedema and Lu (2002) [34] describe an alternative method to describe the functioning of a turbo-charger. A simplified first-principle turbine-compressor model relates the amount of work which is fed through the turbine to the charge air pressure $p_1[Pa]$. It is based on the heat-transfer that occurs from the exhaust-gas with temperature $T_6[^\circ]$ according to equations 3.19 and 3.20. This results in an idealised first-order model that describes the functioning of the non-ideal turbine and compressor and estimates $p_1[Pa]$ based on matching at nominal operation.

Figure 3.18 summarises the relations between the components of this rotating turbine- and charger-model. According to Miedema and Lu (2002) [34], the time-constant $\tau[s]$ of this first-order system is it's *most important parameter*. It is related to the engine size and *"the time constant for*

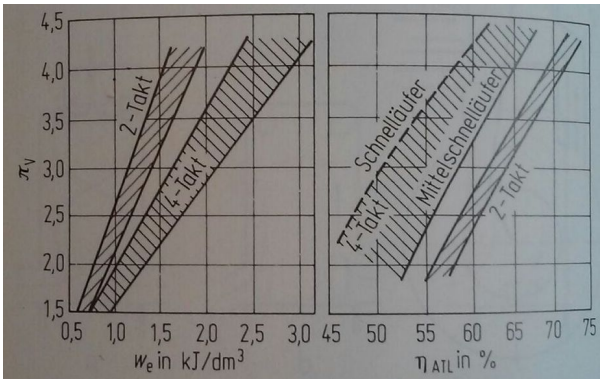

Figure 3.17: Relation between pressure ratio π_V and specific effective work w_e, respectively the required turbocharger efficiency η_{ATL} for Diesel engines, translated from German. Source: [33]

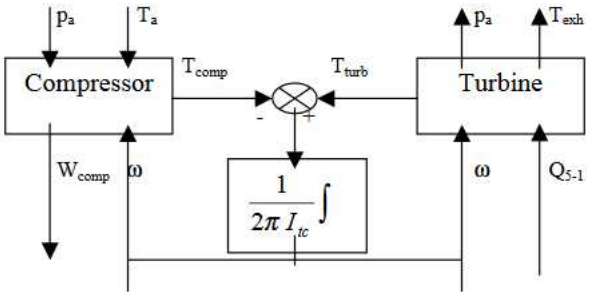

Figure 3.18: Ideal first-order model of turbine-compressor system. Source: [34]

turbine and compressor system normally range from 1 to 2 seconds."

$$p_1[Pa] = p_{atm}[Pa]\left(\frac{\eta_{com}[-]\cdot q_{61}[Jkg^{-1}]}{c_{p,a}[Jkg^{-1}K]\cdot T_{amb}[°K]}+1\right)^{\frac{n_{tc}}{n_{tc}-1}} \tag{3.19}$$

$$q_{61}[Jkg^{-1}] = \frac{T_6[K]-T_1[K]}{c_{v,a}[Jkg^{-1}K^{-1}]\cdot T_{amb}[K]} \tag{3.20}$$

In summary, the functioning of the turbo-charger can be described with different levels of detail. More detailed descriptions such as those of Grote *et al.* (2007) [33] describe more detail while the description proposed by Miedema and Lu (2002) [34] provides a more idealised version.

g. Governor alternatives

Definition 4 simplifies complexer control theory in the scope of this research:

Definition 4:

A governor is a limited PI-controller that governs the fuel-pump.

g1. Diesel engine control strategies Sørensen (2013) [35] describes how a marine propulsion systems has the objective to control the amount of thrust force the system generates. As this cannot be measured directly, FPP systems use rotational speed as a control objective instead while CPP systems use either propeller blade pitch or both speed and pitch (called consolidated) control objectives. Figure 3.19 shows how governors using traditional speed-droop control function and can be used to share loads isochronously (equally shared in time), Sørensen (2013) [35].

g2. Improvements with a load torque observer As discussed in section 2.4, Smogeli (2006) [13] presents *two significant improvements* to the speed-based control that Sørensen posed above and in figure 3.19. Both Smogeli's control methods use a propeller load torque observer to recognise the occurrence of ventilation based on a control plant model for torque balance on the propeller shaft that incorporates the effects of motor torque, propeller torque including hydrodynamic added mass and frequency dependent friction torque. The resulting propeller load torque observer is shown with $\dot{\hat{Q}}_a$ in equation 3.21.

$$\begin{aligned}\dot{\hat{\omega}} &= \frac{1}{I_s}(u-\hat{Q}_a-Q_{f1}\hat{\omega})+k_a(y-\hat{y})\\ \dot{\hat{Q}}_a &= k_b(y-\hat{y})\end{aligned} \tag{3.21}$$

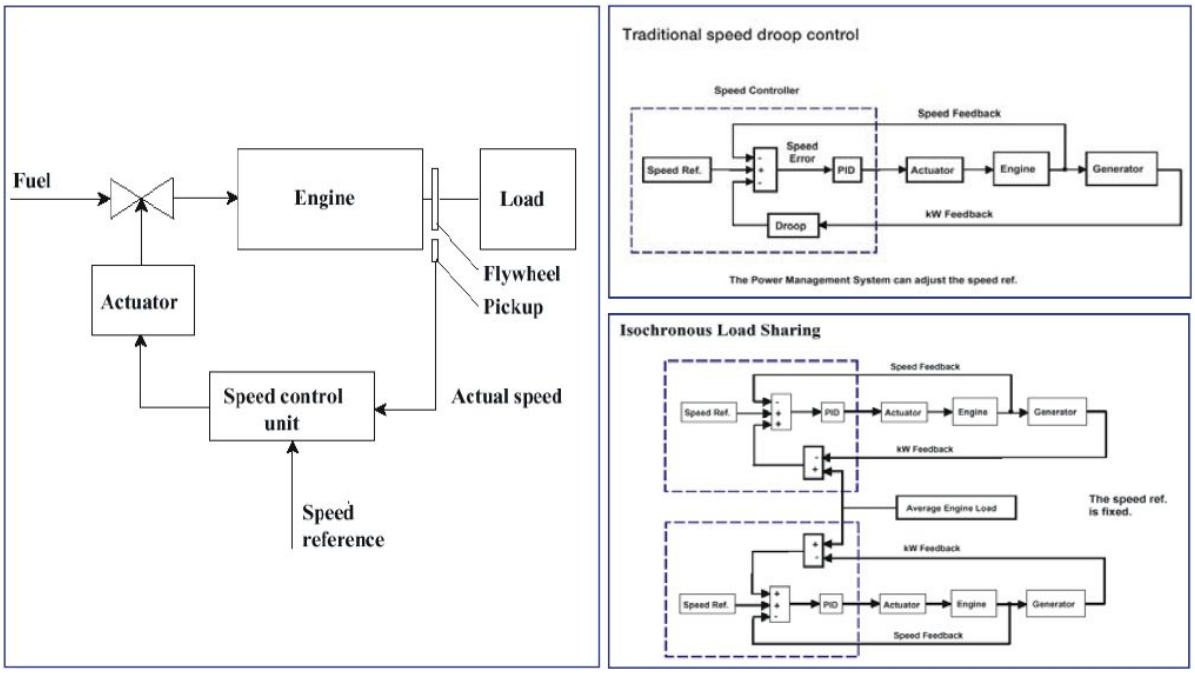

Figure 3.19: Governor for a diesel engine, schematics of speed droop and isochronous control modes. Source: [35]

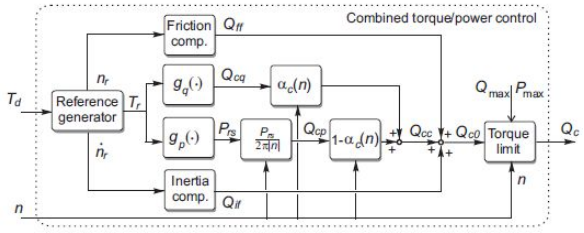

Figure 3.20: Combined torque/power control scheme. Source: [13].

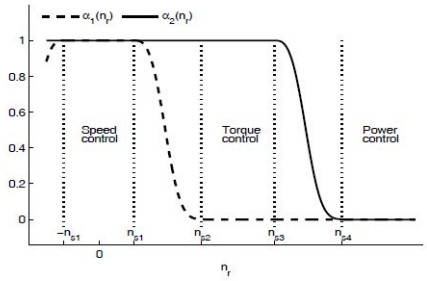

Figure 3.21: Example weighting functions $\alpha_1(n_r)$ and $\alpha_2(n_r)$ used in the combined speed/torque/power controller. Source: [13].

Smogeli's *first* alternative engine control strategy is a combined Torque/Power based control strategy. This is summarised in figure 3.20. His *second* alternative elaborates on this method by including the speed-dependent weighing functions such as shown in figure 3.21. These weighing functions shift the equilibrium between torque- and power- control strategies as a function of the rotational speed n.

g3. Limits Klein Woud and Stapersma (2002) [11] describe different limits to the functioning of a marine Diesel engine. As indicated in the envelope in figure E.1:
These primary limits are imposed by different physical phenomena. The minimum *clutch-in speed* is limited by the fact that a certain load cannot be provided if the amount of fuel combusted does not suffice because the engine speed is too low. The *maximum speed* is governed by inertial forces of the piston and connecting elements that accelerate and decelerate during a revolution.
Secondary limits resulting from transient phenomena limit the engine indirectly: The previously mentioned limits can be neglected temporarily without damaging the engine, for example during emergency manoeuvres. Operation outside the engine envelope can be accepted temporarily. However, two notes are made: *Firstly*, this is only accepted temporarily. The inability of the cooling system to maintain an acceptable temperature of components does not directly damage the engine, but it will damage them eventually. *Secondly*, dependent on specific agreement, warranty may be broken if an engine is overloaded. In a worst-case scenario, an engine can fail catastrophically

These primary or secondary limits can be imposed by limiting the fuelrack setting $X[mm]$ as a function of engine speed. A more elaborate limiter includes transient limits as defined in appendix E.

$$Q_e[Nm] = \frac{P_b[W]}{2\pi[radr^{-1}]n_e[rs^{-1}]} \quad (3.22)$$

$$Q_p[Nm] = Q_{eng}[Nm] \cdot \eta_T \quad (3.23)$$

$$\eta_T = \eta_S \cdot \eta_{GB} \quad (3.24)$$

$$\dot{q}_{loss}[W] = (1 - \eta_T) \cdot Q_{eng}[-] \quad (3.25)$$

Limit	Phenomenon
minimum speed n_e	fuel-injection
air-limit	charge air $m_1[kgcycle^{-1}]$
thermal limit	heat-flow Q to components
maximum torque	torque $Q_e[Nm]$
maximum power	power $P_b[W]$
maximum speed n_e	inertial forces

Table 3.4: Engine limits.

h. Gearbox alternatives

h1. Constant functioning The one step reduction gearbox for medium speed engines, as mentioned by Klein Woud and Stapersma (2002) [11], is characterised with a reduction ratio defined with the engine's- and propeller-rotational speed: $i\ [-] = \frac{n_e}{n_p}$. It can be modelled using the definitions of torque exerted on the gearbox, in equations 3.22 and 3.23. Assuming that torque is transformed with a constant transmission efficiency $\eta_T[-]$ in equation 3.24, a certain amount of power is lost to the environment of the gearbox and shaft bearings as a flow of heat, described in equation 3.25. Klein Woud and Stapersma mention η_{GB} in the range of $1 - 2[\%]$ and η_s in the range of $0.5 - 1[\%]$.

3.4. Modelling interaction in literature

This section briefly lists proposed possibilities to model and describe interacting subsystems related to the propulsion system of a vessel in section 2.6.

l. Approaches to combined descriptions

l1. Immersion and a quasi-static assumption Journée and Massie (2001) [19] discuss the effects that immersion, free surface and in particular waves under a quasi-static assumption have on propeller thrust and torque.
For a transient ventilating condition, Journée and Massie (2001) [19] note "*a frequency connected with the development of the ventilated area on the propeller blades. This wave-induced effect can not be simulated by means of results in calm water.*"
They continue with the quasi-steady assumption to "*interpret h_p as the submergence of the instantaneous position of the wave surface, see figure 3.22*", before they state that time-average thrust and torque data "*can find the effect of the wave induced motions of the ship on the thruster characteristics*".

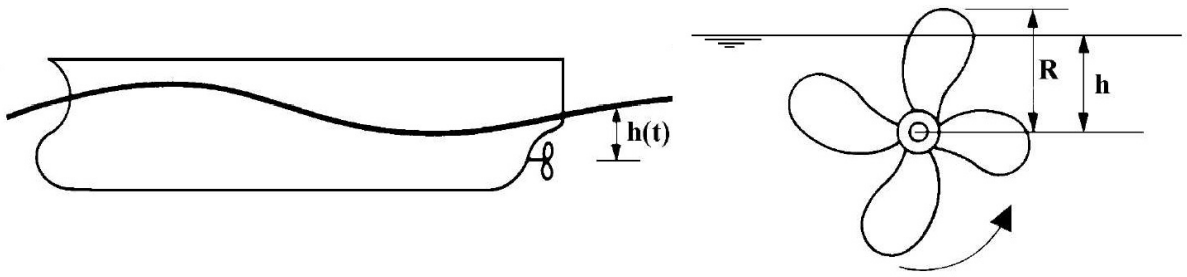

Figure 3.22: Effect of Waves on a Propeller, a Quasi-Steady Approximation. Source: [19]. Adapted by author.

In summary, Journée and Massie (2001) [19] provide a combination of a quasi-static approach, the use of varying propeller-immersion h_p and a description of propeller thrust and torque.

I2. Propulsion system Section 2.2 used figure 3.23 to summarise the block diagram proposed by Stapersma (2000) [17] that can be used to model the interaction between different propulsion system components. Figure 3.23 shows this complete block diagram. The model connects two equilibria, those of (shaft)torque and (vessel)translation, but does not include vessel motion in other directions than the single x-dimension.

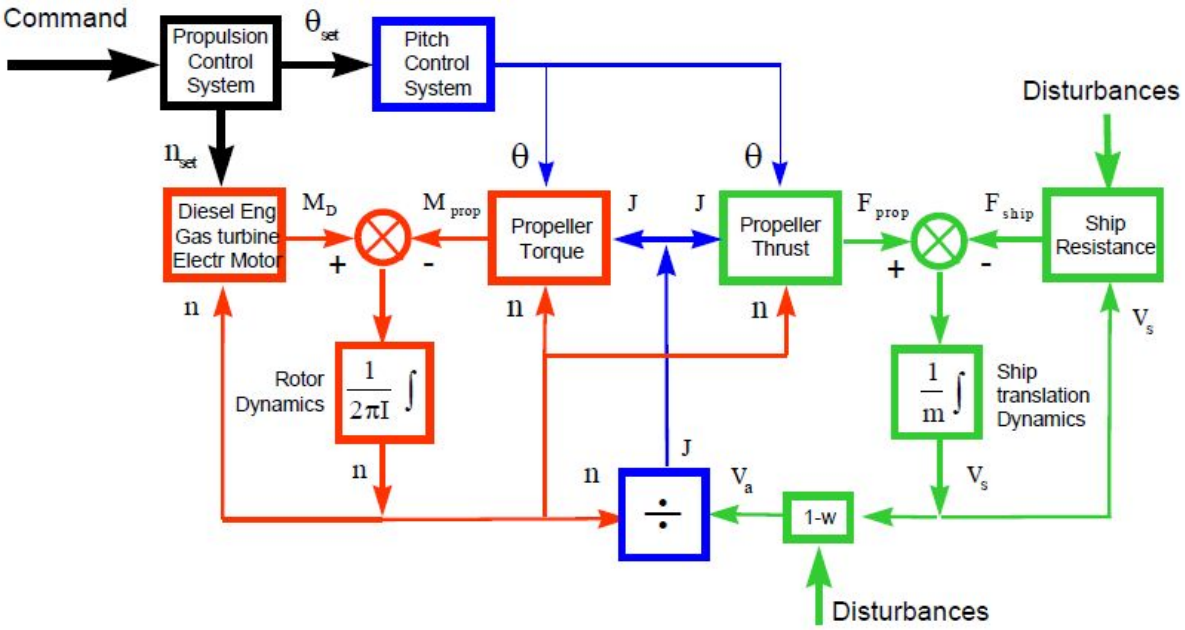

Figure 3.23: Block diagram of ship dynamics. Source: [17]

I3. Control As discussed in section 2.5, Fossen and Perez (2004) [25] propose another modelling method that can be used to describe ship dynamics. It is shown if figure 2.16 and it provides a more elaborate description of the hydrodynamic loads on a vessel as it moves with six degrees of freedom. Although the model may appear to be a more complex alternative, different components such as the sensor and navigation system or the guidance system can be limited or neglected dependent if preferred.

3.5. Summary

The previous sections listed and summarised different sources describing effects related to the scope of this research. These can serve as alternative building-blocks to a model constructed in chapter 4. *Firstly*, vessel-motions and related hydromechanics were treated. *Secondly*, various approaches to the description of ventilation and its components were gathered. *Thirdly*, alternative descriptions of a prime-mover and it's components were gathered. *Finally*, three alternative descriptions that focus on a combination of multiple parts were discussed in the scope of research.

4

A quasi-static ventilation model

The previous chapter gathered alternative approaches and relations that can be used to reach the goal of this work, as posed in section 1.4: *Increased understanding of the relation between wave properties, -height and -frequency, and the response of a marine Diesel engine, -speed and -torque, subjected to wave-induced ventilation.*. This chapter intends to use a number of these alternatives to propose a model that can describe how different inputs, consisting of *waves* and *engine-speed setpoint* $n_{e,set}[s^{-1}]$, load the propulsion system as it experiences these events, resulting in a specific output engine torque $Q_e[Nm]$ and -speed $n_e[s^{-1}]$. The model is built as an adaptation of the

Figure 4.1: (Selection of) Effect of Waves on a Propeller, a Quasi-Steady Approximation. Source: [19]. Adapted by author.

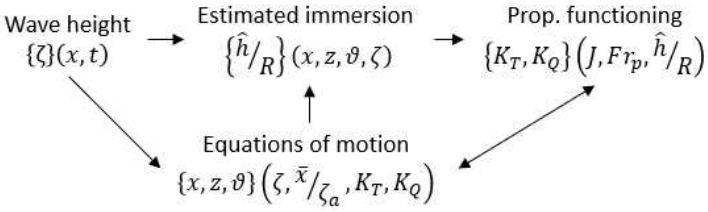

Figure 4.2: Steps, {functions}, (parameters) and relations → in the model.

description by Journée and Massie (2001) [19] as shown in figure 4.1: A vessel subjected to waves, moving in three dimensions, resulting in a time-variant propeller immersion $h(t)$. The propeller, subjected to ventilation, interacts with the functioning of a Diesel engine DE. Figure 4.3 describes the core of this model.
Section 4.1 treats the quasi-static approach at the heart of this model. The following sections 4.2 - 4.4 discuss the vessel-motion-, propeller- and prime-mover sub-models that implement the quasi-static approach, before section 4.5 covers the selection of a suitable vessel-design for the model. Verification of this computational representation, point 4 in table 1.5, takes place in chapter 5.

4.1. The quasi-static approach

This section poses a quasi-static approach to describe the functioning of the propulsion system as it ventilates. Firstly, *characteristic parameters* are selected and applied in a model. These are followed by a brief analysis of the mechanism at the core of this model: *dynamic ventilation based on static data*. This builds on an estimated immersion, an estimated thrust coefficient and further details.

Characteristic parameters

Selection Based on the sources in section 3.2 and a detailed analysis of dimensionless parameters in appendix C, four promising parameters are treated: J, h/R, Fr_p and We.

- J as defined in equation 2.6, following Klein Woud and Stapersma (2002) [11] characterises the relation between the *advance velocity* and the *circumferential speed* of a propeller, and thereby

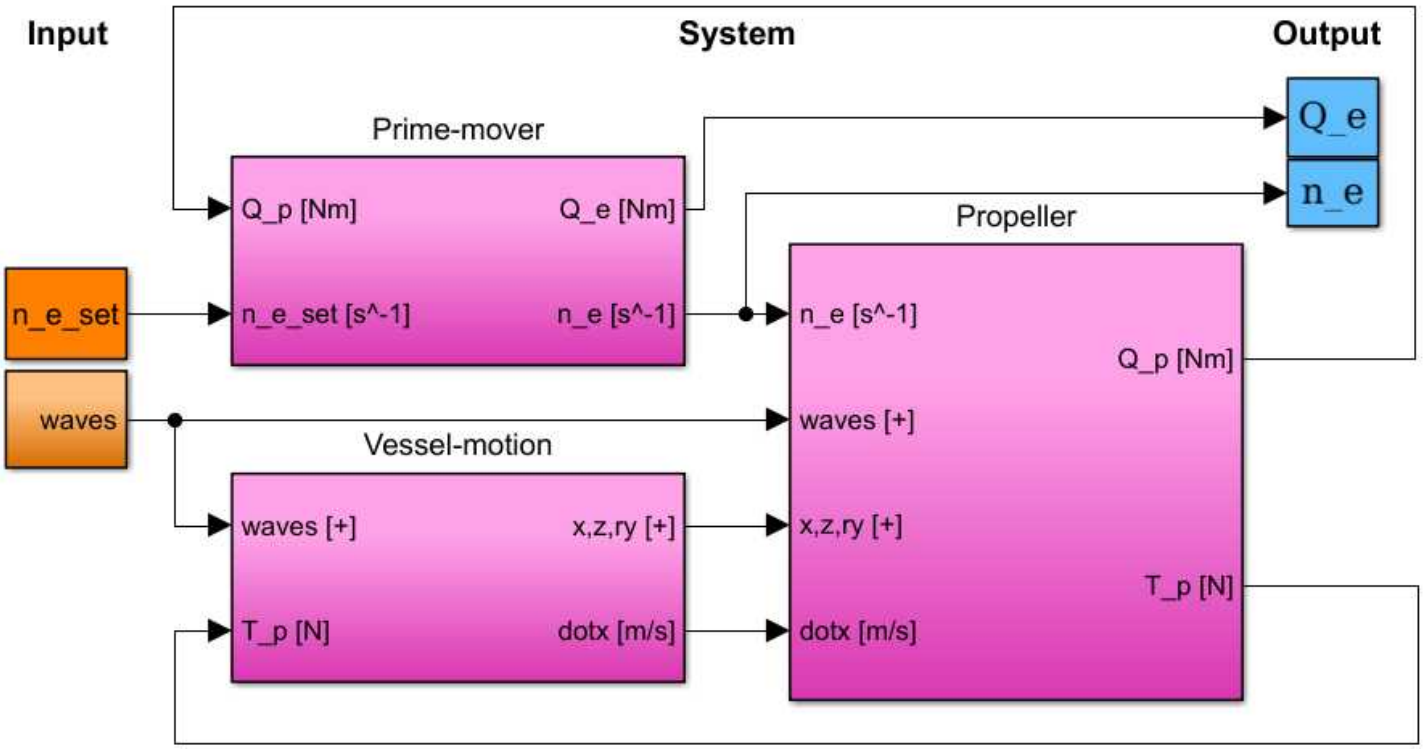

Figure 4.3: Structure of the model with input (orange) sub-models (magenta) and output (blue).

the inflow-conditions of the propeller. It is therefore widely used to characterise the functioning of propellers.

- h/R as defined in equation 4.4 characterises the relation between the *shaft centerline immersion* and *diameter* of a propeller. Following **i2.**, multiple sources amongst which Koushan (2007) [21] and van Beek and van Terwisga (2006) [29] confirm its characteristic role in ventilation.
- Fr_p as defined in equation 4.1 characterises the relation between the *gravitational-* and *inertial*-forces in the flow around a propeller. Different sources amongst which Guoqiang *et al.* (1989) [7] in **j3.** confirm its role in ventilation as it describes how a flow around a propeller can deform the fluid-surface above.
- We as defined in equation 4.2 characterises the relation between the *intertial-* and *surface tension-forces* in the flow around a propeller. Following **j5.**, Shiba (1953) [59] and van der Leij (2019) [31] describe its role in the inception stage development of cavities and air-pockets in a flow. As Carlton (2007) [15] summarised Shiba (1953) [59]: *"...if the Weber number is greater than 180 then its effect is probably insignificant"*. As this occurs at speeds below the clutch-in speed of a marine Diesel engine, the effect of We on propeller ventilation is deemed insignificant, especially as this work does not focus on the lowest rotational-speeds.

Other parameters amongst which the Reynolds number Re and the cavitation number σ are treated in appendix C and deemed to be insignificant parameters in the scope of this work.
In conclusion: the advance ratio J, propeller-Froude number Fr_p and immersion ratio h/R are selected as characteristic parameters in the proposed model.

Application in model Selecting 3 degrees of freedom (x,z,ϑ) from the work of Fossen and Perez (2004) in **i3.**, the model describes 3 equations of motion in the earth-bound reference frame from **a3.** This is done to describe motions of the hull at both lower and transit speeds as per **a4.** and include the influence of waves, thereby resulting in a seakeeping model from **a5.**, to describe engine response in the time-domain from **a6.** Figure 4.2 describes how the characteristic parameters (J, Fr_p, h/R) interact in this model.

Dynamic ventilation based on static data

Different sources such as Koushan (2007) [21] in **i.** treated experimental data for a specific dynamic immersion. As propeller-loading data for all possible dynamic immersion is *not available* and would be a *large* data-set, an approach based on *static ventilation data* or constant-immersion as in **j.** is proposed here. An *estimated immersion* is used to *estimate thrust coefficient* K_T and propeller functioning, before *further details* are treated.

$$Fr_p[-] = \frac{g[ms^{-2}]}{(n_p[s^{-1}])^2 \cdot D[m]} \tag{4.1}$$

$$We = n[s^{-1}] \cdot D[m] \sqrt{\frac{\rho[kgm^{-3}] \cdot D[m]}{S[kgs^{-2}]}} \tag{4.2}$$

$$z_p(\eta, t) = z_{p0} + z(t) + x_{p0} \cdot sin(\vartheta(t)) \tag{4.3}$$

$$\hat{h}/R(t) = (z_p(\eta, t) + \zeta(x, t))/R \mid \{x = x_p\} \tag{4.4}$$

Estimated immersion $\hat{h}/R$ A detailed treaty by Califano (2010) [30] summarised in **j2.** treats the relation between sink length l_s, and ventilating blade- and propeller loads. Figure 4.4 indicates how different sink lengths can result in different types of ventilation, as previously indicated in figure 1.2.

- Experimental research efforts mostly vary the sink length by imposing waves, indicated by ζ in figure 4.5 A, or by varying immersion of the propeller z_p in figure 4.5 A.
- Parameters ζ and z_p can be used to estimate the immersion of a propeller immersed below a hull with equations 4.3 and 4.4. Figure 4.5 B shows that this introduces a systematic error as there is no waterline directly above the propeller.
- Equation 4.4 is applied although it under-estimates the sink length l_s. This is done as it is a *known systematic error* which can easily be addressed once a specific hull-geometry is known, experiments are done or full-scale ventilation measurements are used. Secondly, this known systematic error can be compared with experimental data as summarised by figure 4.5 A

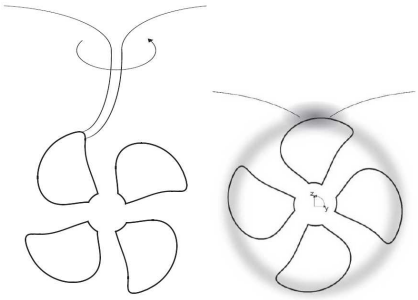

Figure 4.4: Sketch of different types of propeller ventilation. (Left) By formation of a free-surface vortex. (Right) Surface-piercing. Source: [30].

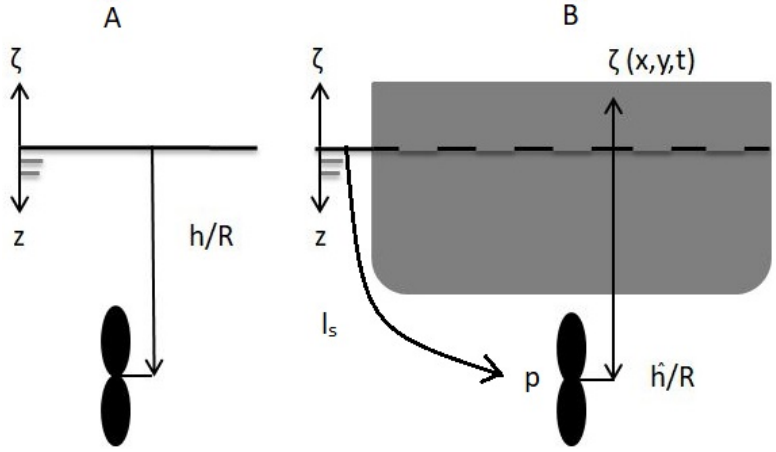

Figure 4.5: Conceptual model of: A experimental setup, B estimated immersion $\hat{h}/R$.

Estimate thrust coefficient K_T The previously estimated immersion $\hat{h}/R$ is used to estimate thrust production and propeller functioning. Appendix I elaborates on this estimation. This estimate introduces a second *known systematic error*. This error is reduced by:
Firstly, continuously interpolating in the domain of measurement, in other words: by not extrapolating beyond the domain of measured h/R-values.
Secondly, by ensuring that the domain of measured propeller thrust K_T covers all occurring ventilation- and transition regimes, in other words, all regimes shown in figure 1.2.

Further details The output of the complete quasi-static ventilation model consists of engine speed and -torque $(n_e[s^{-1}], Q_e[Nm])$-data. The input of the model consists of engine speed setpoint and waves-data $(n_{e,set}[s^{-1}], waves[+])$, the latter summarised in table 4.1. The $waves[+]$ data consists of a list of wave-parameters $\left[\overline{\zeta_{a,i}}, \overline{\omega_i}, \overline{k_i}, \overline{\epsilon_i}, \overline{\psi_i}\right]$ per wave-component. This is implemented as a block from the Marine systems simulator (mss) <http://www.marinecontrol.org>, by Fossen and Perez (2004) [8].

in		relation	out
user-input	[+]	$[\zeta_a, \omega, k, \epsilon, \psi]$ ∈ eq. 3.2 & **b1.**	waves [+]
user-input	[+]	$\left[\overline{\zeta_{a,i}}, \overline{\omega_i}, \overline{k_i}, \overline{\epsilon_i}, \overline{\psi_i}\right]$ ∈ eq. 3.3 & **b2.**	
user-input	[+]	$\left[\overline{\zeta_{a,i}}, \overline{\omega_i}, \overline{k_i}, \overline{\epsilon_i}, \overline{\psi_i}\right]$ ∈ eq. 3.7 & **b3.**	

Table 4.1: Relations waves-block MSS. source: [8]

In summary, this section describes a model that can describe the response of a marine Diesel engine to wave-induced ventilation events. This is done estimating the sink-length based on immersion $\hat{h}/R$ and estimating thrust and propeller-functioning with a *quasi-static approach*.

4.2. Vessel-motion sub-model

This section describes how propeller- and wave-loads ($T_p[N], waves[+]$) on a hull result in displacements $[x, z, \vartheta]$ and forward speed $\dot{x}$. Figure 4.6 shows how this can be done in four blocks describing: *wave-loads*, *motion in* $x - direction$ and *coupled motions in* z- *and* ϑ-*directions*.

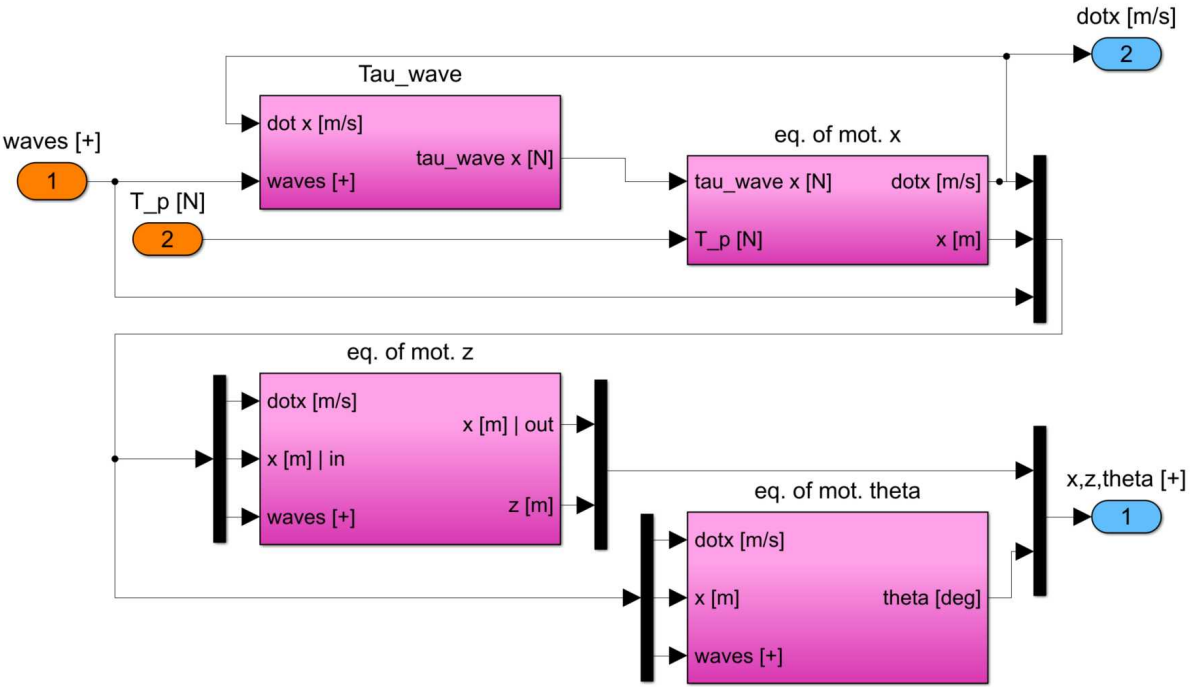

Figure 4.6: Vessel-motion sub-model.

Wave loads $\tau_{wave,x}$ This block determines the generalised added wave forces $\tau_{wave,x}$. Specifically in x-direction, this is the added wave resistance R_{aw}, as explained in **c5.**, summarised in figure 3.5. This done following equation 3.11, with the application of potential-flow and strip-theory as elaborated in **c2.**, and summarised in table 4.3. The description of $\tau_{wave,x}$ is used in equation 4.5 and can be determined for the wave-types in table 4.2.

Wave types for adverse-condition head-seas			
Linear			Non-linear
Regular waves	Irregular waves		
Long crested	Long crested	Wave spectrum	
equation 3.2	equation 3.3	equation 3.8	not
figure 3.2	figure 3.2	figure 3.3b	considered

Table 4.2: Organisation of different wave-types in the waves-block.

in		relation	out
$\dot{x}$	$[ms^{-1}]$	eq. 3.11 ∈**c2.**	$\tau_{wave,x}$ $[N]$
waves	$[+]$	Maxsurf [5]	

Table 4.3: Relations added wave force $\tau_{wave,x}$.

Motion in x**-direction** Following the now-determined forces on the hull, equation 4.5 can now be solved for x to determine displacement x, speed $\dot{x}$[1] and acceleration $\ddot{x}$. This is done with the

[1]Velocity v_s $[ms^{-1}]$ refers to the velocity (vector unit) of a ship as a whole, possibly with components in both {e} x- and y-dimensions whereas speed $\dot{x}$ $[ms^{-1}]$ refers to the (scalar) displacement of a ships COG in the x{e} dimension only. These terms are used intermittently in this research effort as the ships heading is assumed to be fixed.

characteristic hull properties, amongst which the mass and still-water resistance, that are estimated with the Maxsurf software package by Bentley (2014) [5] & [6]. Table 4.4 lists the parameters and causal relations in this block as well as the z and ϑ blocks.

$$m \cdot \ddot{x} = T_p - R_{sw}(\dot{x}) - \tau_{wave,x} \quad |\{\tau_{wave} = R_{aw} = f(\dot{x}, \omega_i, \psi_i)\} \tag{4.5}$$

$$(m + a_{33}) \cdot \ddot{z} + b_{33} \cdot \dot{z} + c_{33} \cdot z + a_{35} \cdot \ddot{\vartheta} + b_{35} \cdot \dot{\vartheta} + c_{35} \cdot \vartheta = -\tau_{wave,z} \quad |\{a, b, c = f(\dot{x}, \omega_i, \omega_i)\} \tag{4.6}$$

$$(I_{yy} + a_{55}) \cdot \ddot{\vartheta} + b_{55} \cdot \dot{\vartheta} + c_{55} \cdot \vartheta + a_{53} \cdot \ddot{z} + b_{53} \cdot \dot{z} + c_{53} \cdot z = -\tau_{wave,\vartheta} \quad |\{a, b, c = f(\dot{x}, \omega_i, \omega_i)\} \tag{4.7}$$

in		relation	out	
T_p	$[N]$	eq. 4.5	$\dot{x}$	$[ms^{-1}]$
$\tau_{wave,x}$	$[N]$		x	$[m]$
$waves$	$[+]$	eq. 4.6	z	$[m]$
$\dot{x}$	$[ms^{-1}]$	eq. 4.7	ϑ	$[^\circ]$
x	$[m]$			

Table 4.4: Relations equations of motion in x, z, ϑ-direction.

Coupled motions in z- and ϑ-directions The imposed waves result in heave- and pitch-motions. The coupled system of equations 4.6 and 4.7, is solved for (z, ϑ), by imposing separate wave components following linear wave-theory as treated in **b.**, for wave types in table 4.2. This is done with the Maxsurf-software package, but can be done analytically per wave-component as shown in appendix K.
The ship's heading is assumed to be fixed, resulting in head-seas, which has two effects on the the proposed model: *Firstly*, hydrodynamic calculations are simplified as μ, the relative angle between a ship's heading and the incoming wave component, is only dependent on ψ_i [°]. *Secondly*, the proposed quasi-static ventilation model can be used in a worst-case scenario analysis regarding the influence of ventilation, as this heading results in the largest fluctuation of the propeller-shaft immersion ratio h/R [-]. Table 4.5 lists four further assumptions pertaining to the vessel-motion sub-model.

Linear waves (**b.**)	are assumed to provide an sufficiently accurate description of waves and wave-loads to which the modelled hull is subjected.
Potential flow (**c2.**)	as described in section 2.2, is assumed to describe hydrodynamic excitation forces (τ_{wave}) and characteristic rigid-body motion parameters (m, I, a, b, c) as described in section 3.1 sufficiently accurate. Shallow-water effects are neglected in the Maxsurf-implementation of the dispersion relation as shown in equation F.7.
Viscous forces (**c3.**)	are neglected by potential-flow solutions. It is assumed that resistance ($R = f(\dot{x})$) can be estimated sufficiently accurate by scaling empirical data (**c1.**) for use in equation 4.5), and that the application of Maxsurf to describe the $\dot{z}$ and $\dot{\vartheta}$ is sufficiently accurate.
Entrained water (**k3.**)	by the propeller adds mass and inertia to the system. This is neglected completely with the exception of rotational inertia by equation 3.16 from Schwanecke (1963) for the prime-mover sub-model.

Table 4.5: Further hydromechanic assumptions.

In summary, this section described a sub-model of causal-relations that link imposed waves and thrust to the displacement and speed of the vessel selected in section 4.5.

4.3. Propeller sub-model

This section describes how *vessel-motion-*, *prime-mover-* parameters a description of imposed waves can be used to describe a propellers *thrust- and torque production* (T_p,Q_p). Figure 4.7 shows how this can be done in six blocks describing: The *characteristic parameters* selected in section 4.1, *open-water data* determined with the quasi-static approach from section 4.1, and *thrust and torque*-production by the propeller as selected in section 4.5. Table 4.6 lists the different causal relations that are used in the different blocks in this sub-model.

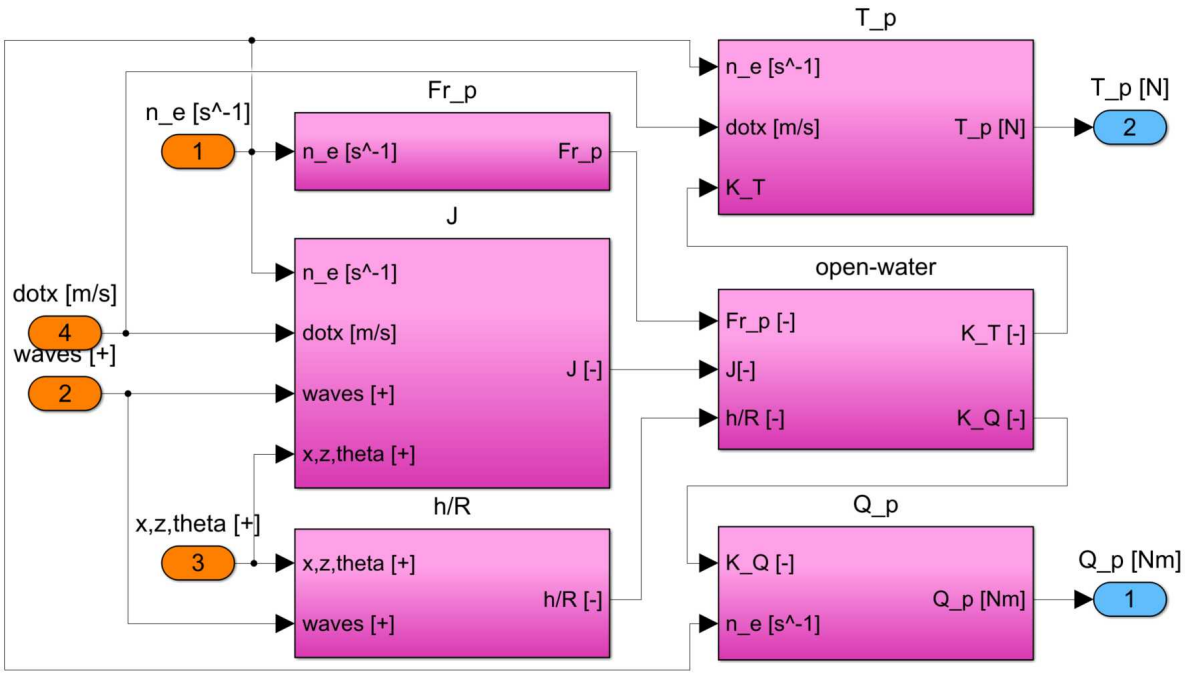

Figure 4.7: Sub-model of a possibly ventilating propeller.

Characteristic parameters Three separate blocks determine J, Fr_p and h/R, about which two remarks are made here: *Firstly*, advance ratio J is determined with the horizontal component of orbital wave-disturbances at shaft-immersion as a propeller-plane average. This is done with equations F.10-F.12. *Secondly*, variation of $Fr_p = f(n_p) = f(n_e)$, induces the use of different open-water diagrams such as figure 4.8 and figures I.1a-I.1c. The variation Fr_p is interpolated to cover a domain of Fr_p spanning multiple ventilation regimes, as show in figure 1.2.

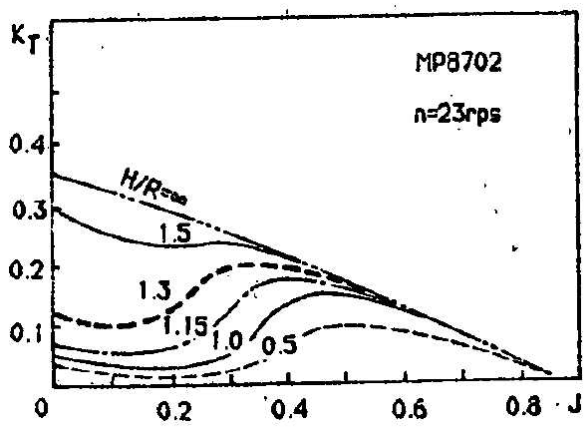

Figure 4.8: Influence of submerged depth on open water characteristics (MP8701). Source: [7]

Open-water data A principle assumption lies in the description of torque-variation, based on thrust-variation: Propeller thrust and -torque losses as a result of occurring ventilation events are comparable in size ([-]) and occur simultaneously. This assumption is based on **i2.** and Koushan's (2007) [21] finding that "*variations in relative blade torque are almost identical to variations in relative blade thrust under ventilated conditions*". For propellers ventilating under varying immersion, Guoqiang *et al.* (1989) [7] found that "*all the results obtained in the test show that the variation tendency of K_T with J is similar to that of K_Q*" and that the variation of K_T alone can therefore be used to investigate a ventilating propeller, as discussed in section 3.2.

Thrust and torque With the estimation of K_T and K_Q as a function of (J,Fr_p,h/R), the thrust- and torque (T_P,Q_p) that the propeller exerts on the hull and the propulsion system are determined conventionally with equations 2.4 and 2.5. The thrust deduction factor $t[-]$ is varied with speed. It is further remarked that the border between non-ventilating deep water and reduced-immersion conditions that may induce ventilation is placed at $h/R \geq 2[-]$ or ∞ in figure 4.8, as confirmed by multiple experimental sources including Guoqiang *et al.* (1989) [7].

in		relation	out	
$\dot{x}$	$[ms^{-1}]$	eq. 2.6 & F.12	J	$[-]$
$waves$	$[+]$	eq. 4.1	Fr_p	$[-]$
n_e	$[s^{-1}]$	eq. 4.4	h/R	$[-]$
$[x,z,\vartheta]$	$[+]$	$w(\dot{x})[-] = (1-u_p/u_0) \in p.14$		
J	$[-]$	fig. 4.8 & I.1a - I.1c	K_T	$[-]$
h/R	$[-]$		K_Q	$[-]$
Fr_p	$[-]$			
$\dot{x}$	$[ms^{-1}]$	$t(\dot{x})[-] = (T-R)/T$	T_p	$[N]$
n_e	$[s^{-1}]$	eq. 2.4	Q_p	$[Nm]$
K_T	$[-]$	eq. 2.5		
K_Q	$[-]$			

Table 4.6: Relations of the propeller sub-model.

In summary, this section described a sub-model of causal-relations that link rotational engine speed, hull speed, displacements and imposed waves to the thrust and torque produced by the propeller of the vessel selected in section 4.5.

4.4. Prime-mover sub-model

This section describes how the engine speed setpoint and propeller torque ($n_{e,set}[s^{-1}], Q_p[Nm]$) are used to determine an engine speed and -torque ($n_e[s^{-1}], Q_e[Nm]$). Figure 4.9 shows how this can be done in four blocks describing: the *governor*, *cylinder process*, *turbo-charger* and *shaft*.

Governor The governor is modelled with the causal-relations in table 4.7, and consists of three parts: A limiter with five different speed-dependent limits from table 3.4 and figure E.1.
A PI-controller tuned with the Good Gain method by Haugen (2010) [64].
A fuel-pump modelled as a negative feedback-loop with an integrator, from **e1**, scaled for nominal fuel-rack- and fuel-consumption settings following [10].

in		relation	out	
n_e	$[s^{-1}]$	$X_{lim}[-] = f(n_e[s^{-1}]) \in$ **g3.** & fig. E.1	X_{lim}	$[-]$
X_{lim}	$[-]$	PI-controller ∈ [25], [35], fig. 2.16	X_{req}	$[mm]$
n_e	$[s^{-1}]$			
$n_{e,set}$	$[s^{-1}]$			
X_{req}	$[mm]$	negative feedback with integrator ∈ **e1.**	m_f	$[kgcycle^{-1}]$

Table 4.7: Relations governor consisting of limited PI-controller & fuelpump.

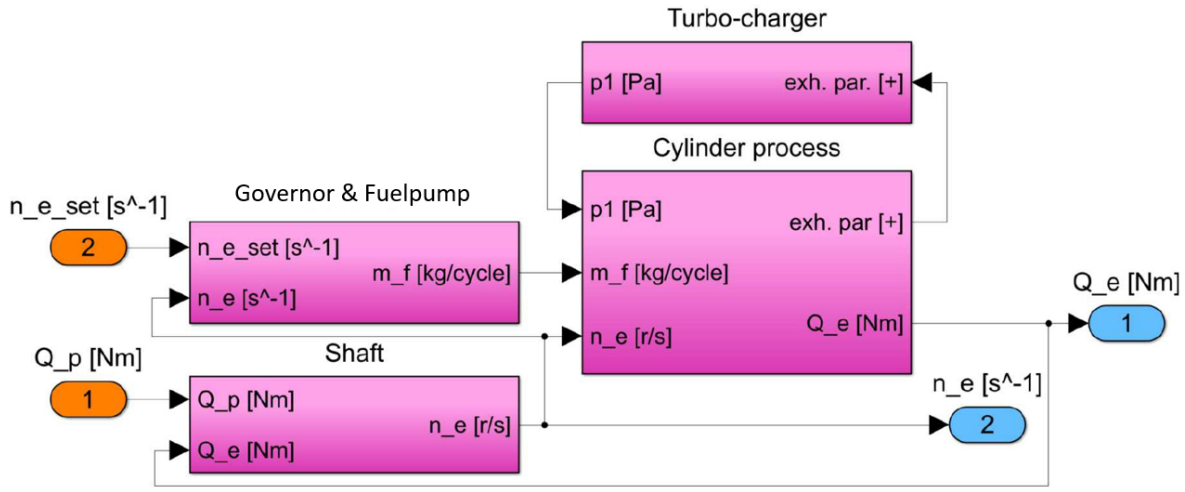

Figure 4.9: Prime-mover sub-model.

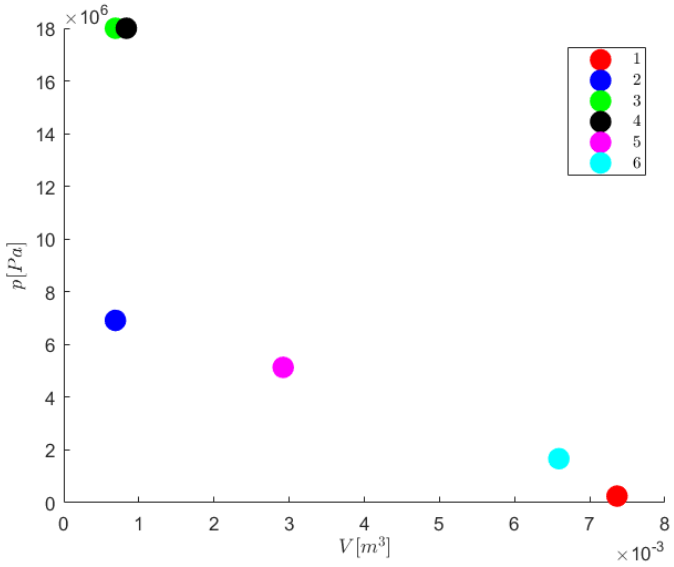

Figure 4.10: Nominal pV-diagram of Seiliger-cycle as used in Diesel A model.

in		relation	out	
p_1	$[Pa]$	Heat-release ∈ **e1.**	q_{cv}	$[Jkg^{-1}]$
m_f	$[kgcycle^{-1}]$		q_{cp}	$[Jkg^{-1}]$
n_e	$[s^{-1}]$		q_{ct}	$[Jkg^{-1}]$
p_1	$[Pa]$	Seiliger-cycle ∈ **e1.** & fig. 4.10	w_{cycle}	$[Jkg^{-1}]$
q_{cv}	$[Jkg^{-1}]$		m_1	$[kg/cycle]$
q_{cp}	$[Jkg^{-1}]$		T_6	$[K]$
q_{ct}	$[Jkg^{-1}]$			
n_e	$[s^{-1}]$	Engine-design ∈ **e1.** & [10]	Q_e	$[Nm]$
m_1	$[kgcycle^{-1}]$			
m_f	$[kgcycle^{-1}]$			
w_{cycle}	$[Jkg^{-1}]$			

Table 4.8: Relations in the cylinder process.

Cylinder process The process described in figure 3.16 is modelled with the Diesel-A model from **e1.**. For the engine selected in section 4.5, this results in the nominal pV-diagram in figure 4.10. The

description of the cylinder process can be divided in three parts, as shown in table 4.8, that describes the causal-relations between the different input- and output-parameters of the block:
The heat-release by combustion of injected fuel is modelled as a three-phase process with constant volume, -pressure and -temperature, following the Seiliger-cycle on which the Diesel-A in **e1.** is built. The Seiliger-cycle is used to describe the cylinder process, based on these heat-releases. It results in the cycle-work w_{cycle} and the exhaust parameters [+], of which m_1 and T_6, mass and temperature at cylinder-opening, are used as input for the turbo-charger sub-model.
Finally, engine design parameters covering amongst others torque-loss and fuel-consumption are used to determine *engine* torque Q_e and other resulting parameters such as brake power P_B and fuel-consumption sfc, based on the *cylinder process*. Following the scope of this work, the description of heat-flows is limited to the cylinder process and the description of the turbo-charger.

in		relation	out
m_1	$[kgcycle^{-1}]$	eq. 3.19-3.20 ∈ **f2.**	p_1 $[Pa]$
T_6	$[K]$	$atm. \leq p_1[Pa] \leq limit$	

Table 4.9: Relations limited heat-to-pressure estimator.

Turbo-charger The functioning of the turbo-charger is modelled and described as a *heat-to-pressure estimator* as discussed in **f2.**, with the relations in table 4.9. It uses a first-order system with time-constant $\tau_{TC} = 2[s]$ to model the turbocharger system and it's characteristic rotational inertia. To ensure stability of the prime-mover sub-model, it is limited with an upper and lower limit, that describe the functioning of an ideal bypass-valve and result in a charge-pressure p_1 between atmospheric- and maximum pressure.

in		relation	out
Q_e	$[Nm]$	$Q[Nm] = I[kgm^2] \cdot \dot{\omega}[rads^{-2}]$	
Q_p	$[Nm]$	eq. 3.22-3.25 ∈ **h1.**	n_e $[s^{-1}]$
		η_T ∈ **h1.**	

Table 4.10: Relations shaft.

Shaft The shaft is modelled with the relations in table 4.10. Two further remarks that can be made lie in the *rotational inertia* and *power equilibrium*: Inertia of the rotating shaft is estimated based on the Damen (2017) [9] general arrangement, and equations 3.22-3.25 are based on an equilibrium of power for the gearbox: $P_P[kW] = P_B[kW](1 - \eta_{gb}[-])$.

In summary, this section described a sub-model of causal-relations that link engine speed setpoint and propeller torque to the engine torque and -speed of the vessel selected in section 4.5.

4.5. Selecting a suitable vessel-design

This section narrows the scope in section 2.6 down to a specific vessel design in *four* steps: *Firstly*, the global goal from section 1.4 is linked to a specific vessel design, before the details of this design regarding *vessel-motion*, the *prime-mover* and it's *propeller* are treated.

Intending to study representative ventilation events for a contemporary design for unrestricted navigation, a relatively slow sailing, low powered traditional cargo ship that meets EEDI regulations with a marine Diesel engine is selected. This ensures that possible results are applicable to a larger part of the world fleet. A length less than 100 [m], speed less than 12 [kts], a Froude number of ± 0.2 [-] and less than 3 [MW] installed P_e, results in the same adverse conditions as ships twice as long. This follows from IMO-MEPC (2015) [2] and table 1.4 that define adverse conditions discretely as a function of L_{pp} [m], instead of installed engine power as used for EEDI-regulations.

Hoornaert (2014) [42] describes that these smaller vessel designs encounter a relatively large added resistance and load fluctuations in comparison to their installed propulsive engine power P_e in adverse

conditions. Further selection of a ballast- or trial-loading condition ensures that: characteristic data for said loading condition is available and the loading condition is relatively susceptible to ventilation events for head seas in adverse conditions. Based on these characteristics, a ship design by Damen (2017) [9] is selected. Appendix D, published with permission, consists of the vessels product sheet. The model will be used to describe the functioning of a vessel's propulsion system in a timeframe up to 15 minutes as this is considered large enough to capture all related effects. The data is valid for positive speeds up to 7 [m/s].

Vessel motion Using the design's principle particulars, a standard hull design is scaled in the Maxsurf software package to fit the selected design. Hydrodynamic properties of the design, following **b.** and **c2.**, are matched with the properties described by Damen (2017) [9]. In turn, this scaled design is used to estimate three sets of data for a range of different vessel speeds v_s [m/s], occurring wave frequencies ω [rad/s] and -directions ψ [°], thereby implementing equation 3.5:
Firstly, it is used in the Maxsurf Resistance package to estimate a relation between the hulls speed v_s and still-water resistance R_{sw}. The Holtrop-algorithm is selected based on it's suitability for "*predicting the resistance of ... general cargo ships...*" Bentley Systems (2014) [5].
Secondly, the added wave resistance $R_{a,w}$ is determined as the sum of Froude-Krylov- and diffraction forces. These are gathered in the generalised wave force τ_{wave} [+].
Thirdly, the Maxsurf Motions package is used to determine, force response amplitude operator F_i/ζ_a and displacement response amplitude operator η_i/ζ_a in z- and ϑ-directions with potential-flow calculations.

Propeller Head-seas resulting in significant fluctuations of the propeller-shaft immersion ratio and thereby shortens the sink length l_s. Propeller design and -performance under these conditions will be, described and simulated based on the Damen (2017) [9] design with a number of blades and a diameter. Other details are based on a conventional Wageningen-B series design as described by van Lammeren *et al.* (1969) [20] and ventilation-related characteristics provided by Guoqiang *et al.* (1989) [7] as treated in appendices H & I.

Prime-mover Based on the product sheet from Damen (2017) [9], the Wärtsilä 8L20 engine is selected. It's characteristic properties are described in Wärtsilä (2017) [10] and shown in appendix E. It is a conventional turbocharged 4-stroke engine and it is operated on fuel oil with a lower calorific value of $h^L = 42.7[MJkg^{-1}]$. The amount of installed engine power is less than the 3 [MW], which Hoornaert (2014) [42] calls "*vessels more likely to encounter too heavy engine loading in adverse conditions...*", which makes it relatively susceptible to problems regarding load-fluctuations. An engine of this type is used by a significant part of the world fleet.

4.6. Summary

This section summarises characteristic properties of the model described in this chapter. The model described in this chapter revolves around multiple loops:

- A *thrust-loop* describing motion in x-direction.
- A *torque-loop* describing rotation of the engine and stiffly-coupled propeller with rotational speed n_e- or n_p. This loop also contains:
  - A *charge-pressure loop* describing charge-pressure p_1 based on exhaust parameters from the cylinder-process which varies with p_1.
  - Two *speed-loops* in the PI-controller and limiter of the governor block:
    The PI-controller that use the rotational engine speed n_e to determine the required fuel-rack setpoint X_{req}, which in turn influences n_e. The limiter uses n_e to determine the fuel-rack setpoint limit X_{lim} based on the air-, torque- and power limits from table 3.4. This can also influence n_e.

The torque-, charge-pressure and speed-loops are related to rotational motions. Table 4.11 lists the characteristic properties of these motions.

Characteristic	propeller	shaft	engine total	entrained water **k3.**	**f2.** turbo-charger
$I_i[kgm^2]$ or $\tau_{TC}[s]$	4332	494	135	132	2
source / method	[15] & [20]	est.	[10]	[60] & [65]	[34]

Table 4.11: Applied characteristic rotational intertia (left) and 1^{th} order time-constant (right).

Figure 4.11 summarises the thrust- and torque loops of the model of the vessel selected in section 4.5, that is built on the quasi-static approach described in section 4.1. The model will be verified in chapter 5. The model has three significant limitations:

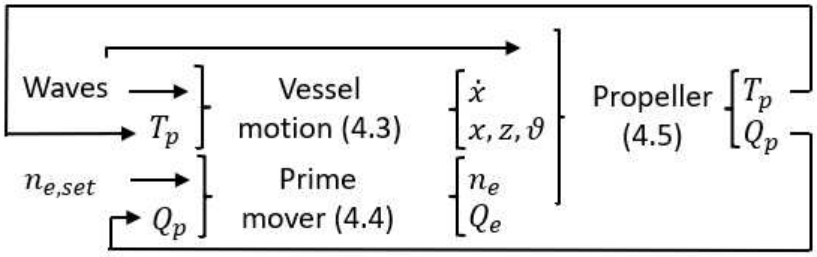

Figure 4.11: Thrust- and torque loop of the model.

- The applied vessel-motion data only covers positive vessel speeds up to 7 $[ms^{-1}]$.
- The propeller functioning is described with an open-water diagram for the first-quadrant, covering positive J, positive K_T and -K_Q values for immersion ratio's up h/R = 0.5 [-].
- The operational envelope of the prime-mover only describes functioning in the range of 5.8-17.1 $[s^{-}1]$.

.

5

Model verification

Point 5 in table 1.5 describes the goal of this chapter: Verification of the functioning of all the components of the model proposed in chapter 4. This model connects known theory from chapters 1-3. Verification of the model allows for the development of new theory with experiments by simulation in chapter 6. This chapter thereby enables the completion of the goal from section 1.4:"*Increased understanding of the relation between wave properties, -height and -frequency, and the response of a marine Diesel engine, -speed and -torque, subjected to wave-induced ventilation.*". This chapter is divided in seven sections. The first two sections briefly describe the verification process and the input-signals of the model. Sections 5.3-5.5 treat verification of the most-important parts of the three sub-models. The final sections 5.6 and 5.7 conclude the verification of the model.

5.1. Introduction

This section introduces the concepts of verification and functioning of the model. Verification ensures that the model from chapter 4, a computational representation, properly represents the causal relations of the *in-relation-out*-tables in that chapter. In particular, that the model provides a true, accurate and valid description of the modelled system and its functioning.

This is checked with three steps per component, sub-model and the complete model:
Input-variations, both static and dynamic, are applied. *Resulting output* is generated and finally *compared with expected outcomes*.
All components and sub-models are verified and found to describe the causal relations which they were intended to represent. The rest of this chapter describes several verification steps with respect to the *quasi-static method* to describe propeller ventilation and *engine response* to wave-induced ventilation events.
In conclusion, the functioning of the model and its sub-models must be true, accurate and valid.

5.2. Input-signals

This section discusses valid values of the engine-speed setpoint and shows that the waves-block accurately describes different types of waves.
Engine-speed setpoint $n_{e,set}[s^{-1}]$ Although a signal, and not a block or sub-model, the engine-speed setpoint is compared and checked. The accurate realisation of any correct engine-speed setpoint $n_{e,set}[s^{-1}]$ should describe a single, continuous signal that:

- Lies between the minimum and maximum engine speed n_e in figure E.1.
- Does not increase the engine load more than defined in figure E.2.

Waves-block The waves-block by Fossen and Perez (2004) [8] produces a waves-signal $waves[+]$. This describes the characteristic properties of wave-components for different wave-types as listed in table 4.2. It is verified for long-crested regular wave components, a bichromatic wave and Torsethaugen wave-spectra as listed in table 5.1.

	$\omega_p[rads^{-1}]$	$\psi_0[^\circ]$	s [-]	M [-]	$\kappa[-]$	ω_i and ψ_j selected	compare figures
Regular wave, component 1	0.94	180	-	1	1	non-random	3.2 - 5.1
Regular wave, component 2	0.54	180	-	1	1	″	3.2 - 5.1
Bichromatic, long crested	[0.54 0.94]	180	-	1	2	″	3.2 - 5.1
Torsethaugen spectrum - [35]	1	-30	4	10	200	random	see app. J
Torsethaugen spectrum - [35]	1	-30	4	10	100	″	see app. J
Torsethaugen spectrum - [35]	1	-30	4	10	50	″	see app. J
Adverse Torsethaugen, long-crested	0.57	-180	1.5	1	50	″	**??**

Table 5.1: Waves-block verification.

The input-variations in table 5.1, result in the output $\zeta(x,t)$ of figures 5.1 and J.1-**??** in appendix J. A comparison of figures as listed in table 5.1 and appendix J, shows that the waves-block accurately realises output data $\zeta(x,t)$, that describes the expected outcome for all listed wave-types. Journée and Massie (2001) [19] do not describe a scale, but the components describe a bichromatic wave of equal-shape. The spectral-realisations match the expected outcome equally well.

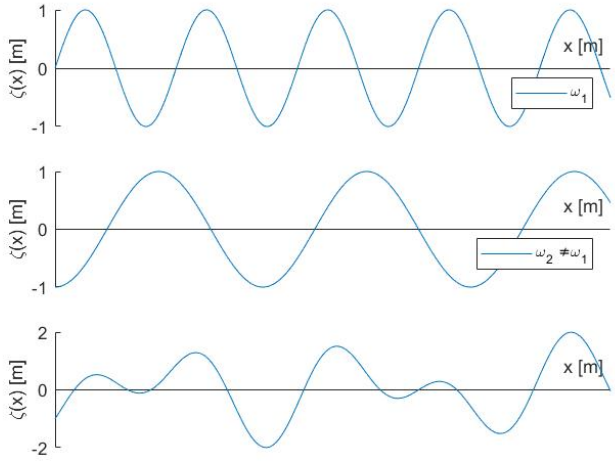

Figure 5.1: Superposition of two uni-directional harmonic waves with the MSS-toolbox from [8].

In conclusion, the input signals are described accurately and realistically by the model.

5.3. Verification of the vessel-motion

It is the goal of this section to show that the vessel-motion sub-model produces valid descriptions of vessel-motions. Having verified the functioning of the four blocks in the vessel-motion sub-model, this section highlights the verification of two significant parts:

- Firstly the causal relation between hull-forces and hull-speed x.
- Secondly, the causal relation between imposed waves and heave- and pitch-displacements z and ϑ.

The input to these relations as shown in figure 4.6, is varied dynamically to compare the resulting outcome with the expected outcome.

How thrust influences speed Figure 5.2 shows the verification of the motion in x-direction.

- This figure shows how a constant propeller thrust T_p of 23.3 [kN] results in a speed of 4 $[ms^{-1}]$ in the absence of waves. It further shows the response of the block to two sinusoidal variations of T_p with $\pm$ 50 [%] implemented with a phase shift. This results in three different responses of the vessel-motion sub-model. In other words, the response of three equal vessels to different variations of propeller thrust T_p.

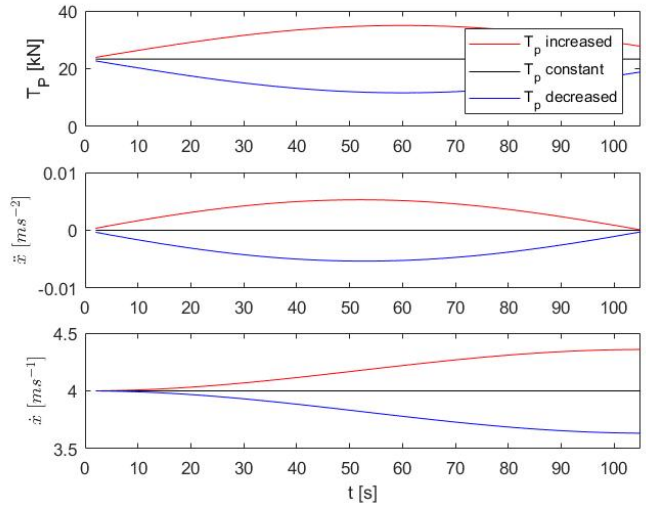

Figure 5.2: Resultant force $F_{x,res}$, acceleration $\dot{x}$ and speed $\dot{x}$ for a sinusoidal variations of thrust T_p in the absence of waves.

- With the still-water resistance $R_{sw} = f(\dot{x})$ and in the absence of waves, the resultant force in x-direction on the hull is positive, neutral and negative. Following Newton's second law of motion, $F_{res} = m \cdot \ddot{x}$, these resultant forces result in positive, neutral- or negative hull-accelerations.
- Figure 5.2 finally shows that the initial speed of 4 $[ms^{-1}]$, increases, remains constant or decreases for these different accelerations. It can furthermore be seen that larger positive and negative accelerations $\ddot{x}$ result in steeper lines in the $\dot{x}$ graph, than the smaller accelerations.

In summary, the relations between force and acceleration and between acceleration and speed are found in the output of the block as it is varied dynamically. These causal relations are shown as expected based on the relations that the block is supposed to describe. It is found that the block accurately describes these relations and the resulting equation of motion in x-direction.

How waves result in heave- and pitch-displacement The verification of the blocks describing the coupled equations 4.6 and 4.7 is shown in figure 5.3. This figure shows the response of the blocks describing heave- and pitch-displacements z and ϑ for different imposed head-waves.

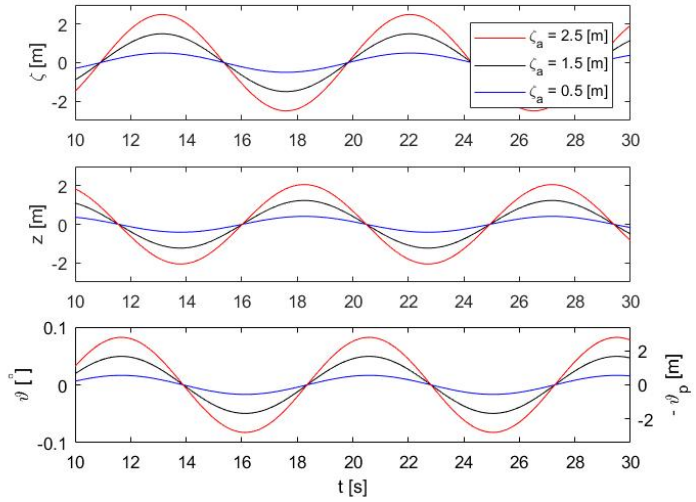

Figure 5.3: Wave-height, heave- and pitch motions for three amplitudes ζ_a with $\omega = 2\pi/11[rads^{-1}]$ at $\dot{x} = 0[ms^{-1}]$.

- Verification at zero-speed is done for three waves with different amplitudes ζ_a and a realistic period of 11 [s], corresponding with table 1.4 following IMO-MEPC (2015) [2].
- As a result of these imposed waves, the blocks display both heave- and pitch displacements increasing with wave amplitude ζ_a, with the same encounter-frequency. The values of response amplitude operators z/ζ_a and ϑ/ζ_a are found to be portrayed in the expected range, as is the difference between heave- and pitch- phase-shift $\epsilon_{z\zeta_a}$ and $\epsilon_{\vartheta\zeta_a}$. This phase-shift expresses that a wave does not simultaneously impose heave and pitch motions.
- Rotation pitch ϑ results in a vertical displacements of points along the hull. The lower, right axis in figure 5.3 displays the same pitch as occurring on the centre of gravity, shown on the left axis, but as experienced by the propeller: $\vartheta_p[m]$. It's negative definition as the propeller is mounted behind the centre of gravity.

In summary, the shown displacements for heave- and pitch- display motions in the expected ranges and with the expected phase-shifts ϵ. The blocks are deemed to provide an accurate description of the coupled-responses z and ϑ of the hull to imposed wave-components.
In conclusion, the wave-force, as well as the equations of motion verified here, in x-direction and for coupled heave- and pitch-motions, describe their causal relations realistically. The vessel-motion sub-model is found to describe the parameters shown in section 4.2 accurately.

5.4. Verification of the propeller

It is the goal of this section to show that the propeller sub-model provides an accurate and valid description of the functioning of a propeller under non-ventilating and ventilating conditions.
As shown in figure 4.7, there are six blocks describing three input-parameters, open-water data and the torque- and thrust produced by a ventilating propeller.
Having verified the functioning of all these blocks, this section focuses on two significant parts of the verification of the propeller sub-model:
- Firstly, the causal relations between imposed waves and propeller-shaft immersion.
- Secondly, the causal relation between immersion and thrust-variations.

How waves result in varying immersion The verification of the block describing the immersion of the propeller-shaft centre-line h/R, is summarised in figure 5.4.

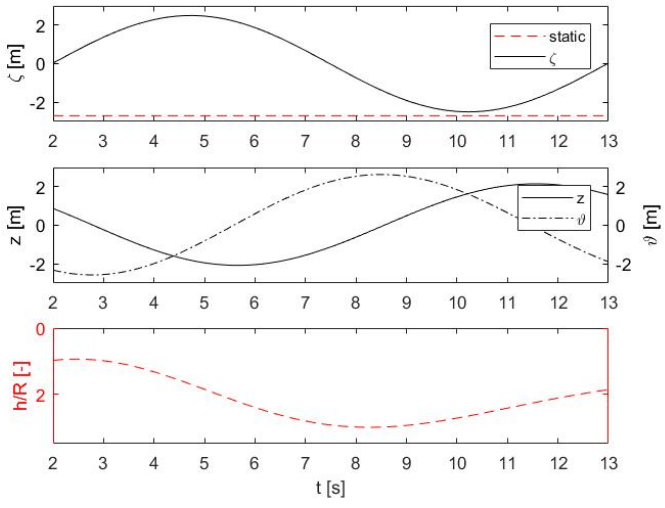

Figure 5.4: Immersion-related parameters wave-height ζ, static immersion of 2.5 [m] and motions z and ϑ vary the propeller-shaft immersion h/R. Wave period $T = 11[s]$.

- Firstly, it shows both the static immersion of the propeller in still-water, as well as the imposed wave with an amplitude ζ_a. This imposed wave is the $\zeta_a = 2.5[m]$ wave used in figure 5.3.

- Secondly, it shows the same heave- and pitch- displacements of the propeller on the hull displaced by this wave.
- Finally, the aforementioned parameters are added up non-dimensional as immersion ratio h/R in equations 4.3 and 4.4.

In summary, the immersion block accurately describes variation of the propeller immersion.

How waves result in thrust-variations Figure 5.5 shows the open-water diagram for the propeller experiencing the same wave and resulting immersion h/R as shown in figure 5.4.

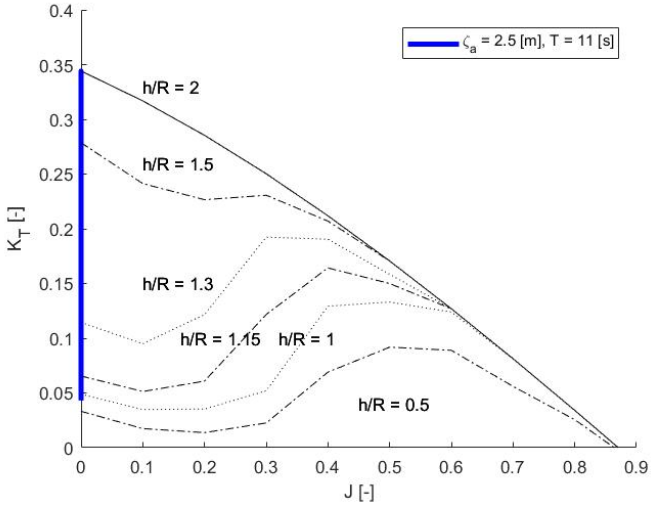

Figure 5.5: Thrust variation for $J = 0[-]$ and $Fr_p = 0.2[-]$ with h/R [-] varying as in figure 5.4

- The propeller is functioning in bollard-condition with a constant rotational speed n_p that results in the propeller Froude number $Fr_p = 0.2[-]$.
- With (J,Fr_p) constant, the operational point of the propeller only varies with h/R.
- For all values of $h/R \geq 2[-]$, the propeller is considered to be submerged so deeply that it does not ventilate. As $h/R < 2[-]$, the thrust coefficient K_T can diminish significantly in time frames less than 3.5 [s].

Figure 5.5 shows variations of the thrust coefficient K_T in the range of 0.35 [-], to 0.05 [-] for the smallest immersion h/R in figure 5.4. This is within the range shown in figure 4.8 as published by Guoqiang *et al.* (1989) [7] and verifies that the open-water block accurately describes the variation of K_T with h/R.
Further verification of the influence of Fr_p on the thrust- and torque coefficients showed that the block also accurately describes different ventilation regimes: The iso-immersion lines of constant h/R as a function of J, as shown in figure 5.5, vary with Fr_p.

In conclusion, the propeller sub-model accurately describes the causal relations from table 4.6.

5.5. Verification of the prime-mover

It is the goal of this section to show that the prime-mover sub-model produces an accurate and valid description of the functioning of the prime-mover. All four blocks in the prime-mover sub-model in figure 4.9 are verified. This section treats the verification of:

- the turbo-charger block, as this is a significant simplification.
- the governor block, as it is specific to the selected engine design and
- the complete prime-mover sub-model, by mapping its operational envelope.

How exhaust-parameters influence charge-pressure Although part of a loop and thereby dependent on it's own output, the turbo-charger block is verified separately. This is done to verify if the simplified *heat-to-pressure estimator* based on equation **??** functions in the same manner a turbo-charger would.
Figure 5.6 shows how (m_1, T_6), two of the exhaust parameters from the cylinder model, are used to estimate the charge-pressure p_1 with equation **??** as proposed by Miedema and Lu (2002) [34]. These parameters are varied sinusoidal with a range of 25[%] below- and up to nominal values. This is done with a characteristic period of 3 [s] which is slightly longer than the selected time constant of $\tau_{TC} = 2[s]$ of the first-order model.

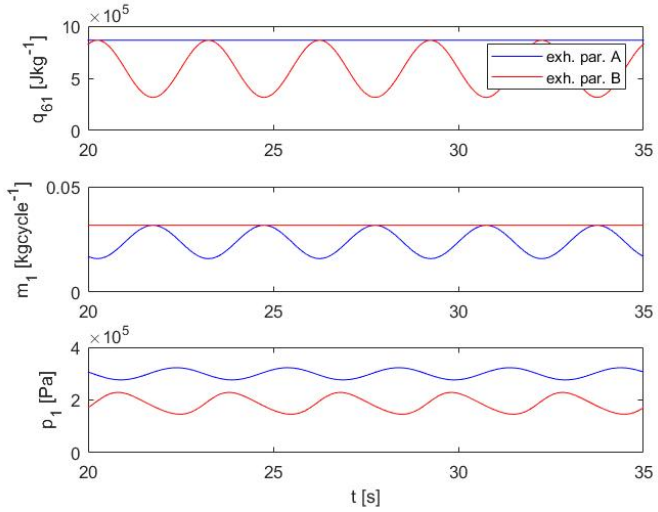

Figure 5.6: Characteristic turbine-compressor parameters for sinusoidal 25[%] nominal variations with periods of 3 [s].

- By varying T_6 in exhaust parameters B, $q_{61}[Jkg^{-1}]$ is varied. It represents the specific heat of the mass of combustion air entering the turbine-compressor system.
- Exhaust parameters A varies the charged mass per cycle m_1. This also varies the amount of energy entering the turbine-compressor system.
- The resulting estimations of charge-pressures p_1 vary sinusoidal and show that:
  - Reductions by percentage of T_6 have a larger influence on p_1 than reductions of m_1.
  - The setting of time-constant $\tau_{TC} = 2[s]$ results in a delay in the rang of 0.6-0.8 [s] between the variations of input and resulting output.

It is thereby verified that both m_1 and T_6 increase and decrease the estimated value of p_1 as expected, *and* that the turbo-charger system introduces a brief delay. The turbo-charger block is therefore considered to be a sufficiently accurate description of a turbo-charger for this application.

How the governor controls engine speed n_e Figure 5.7 shows the response of the Diesel engines governor to a step-function in- and decrease in engine speed setpoint. This illustrates the settings of the PI-controller listed in table 4.7 and the ability of the governor to control the engine speed for varying loads.

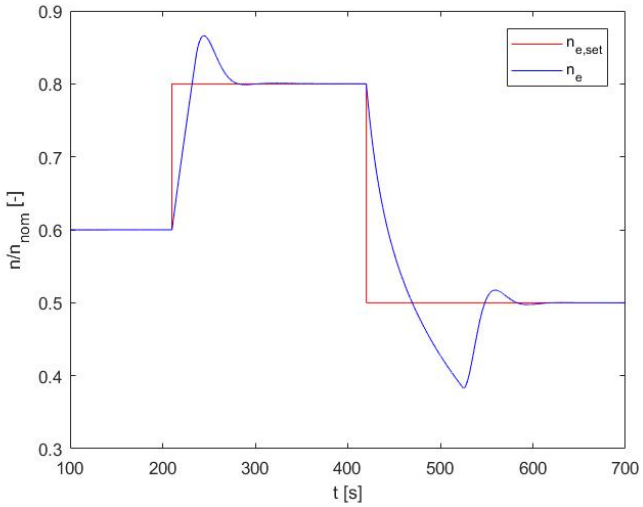

Figure 5.7: Response to 20 [%] increase and 30 [%] decrease of engine speed setpoint $n_{e,set}$.

- With the governor in place in the torque-/speed-loop with the rest of the prime-mover sub-model and the propeller load, the engine speed setpoint $n_{e,set}$ is varied.
- The increase of engine speed n_e is followed by an overshoot of 6.5 [%] n_e/n_{nom} with negligible undershoot.
- The slightly larger decrease of engine speed results in 11.7 [%] n_e/n_{nom} undershoot and minor overshoot with a *time between under- and overshoot* $T_{uo} = 32.4[s]$. Although not directly comparable with the maximum recommended load increase time for a load of 65 [%] as shown in figure E.2, the response of the system to the governor is considered to take place in a realistic time frame.

Figure 5.7 shows that the governor-block accurately describes a governor based on a PI-controller as described in table 4.7.

How the prime-mover functions in different conditions By varying engine load and speed-setpoint within the nominal range, the engine envelope can be mapped as shown in figure 5.8.

- Static variations of load torque and engine-speed setpoint, dotted blue lines, covering the nominal domain. The response of the sub-model is limited by the five limits in table 3.4.
- The static envelope of the model, dashed blue line, is drawn around these static operating points.
- The envelope by Wärtsilä (2017) [10], red dashed line, is nearly the same and has the same maximum continuous rating. It is slightly larger but based on the same limits.
- A dynamic limit, black line, drawn around the transient response. This indicates that brief operation beyond the static limit can be expected in response to variations of the engine-speed setpoint and/or transient loads. The transient responses shown are within the maximum load-increases defined in figure E.2.

The response, (n_e,P_b), of the prime-mover sub-model differs slightly from the envelope by Wärtsilä (2017) [10]. This difference results from slightly different parameters of the in-cylinder process as well as the description of the turbo-charger. These vary slightly but are sufficiently equal as they follow the same limits, relations and have the same nominal operation point.

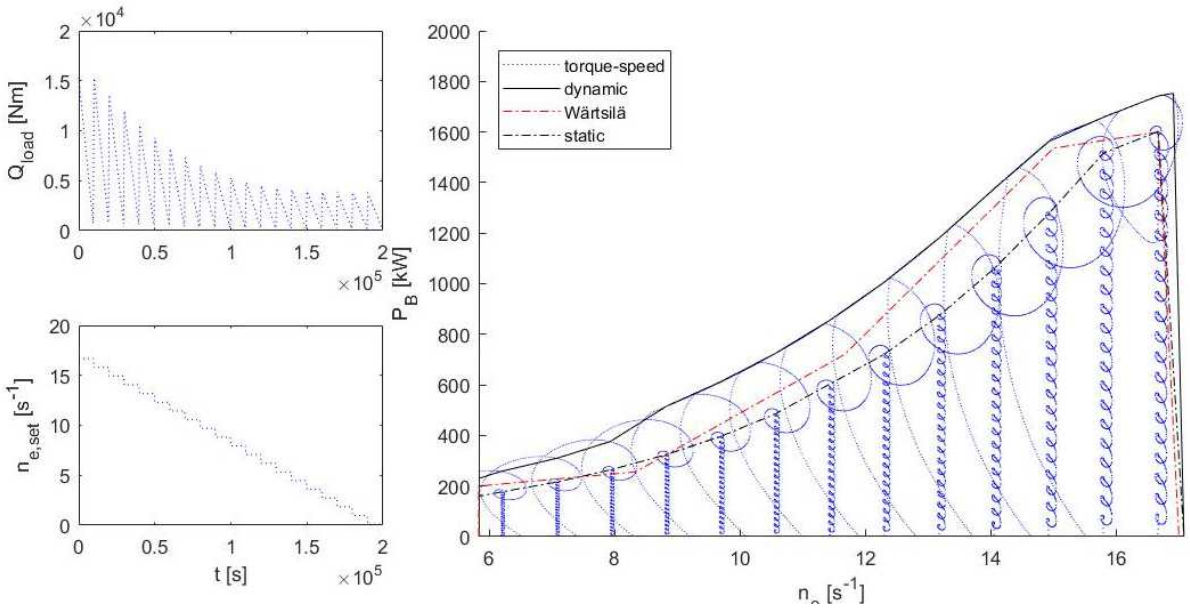

Figure 5.8: Envelope of the prime-mover sub-model.

Two further remarks are made:

- Firstly that, dependent on variations of the speed setpoint $n_{e,set}$ and load torque Q_{load}, the engine can intermittently function beyond its static envelope, as shown in figure 5.8.
- Secondly, that this model is controlled by a governor and setpoint as described in section 4.4. It does not implement advanced control strategies as this is not included in the scope. This introduces uncertainty regarding the prime-movers dynamic response.

In conclusion, the different blocks of the prime-mover sub-model as well as the prime-mover as a whole describe sufficiently accurate and valid results for both static loads and brief, transient responses to variations of load and setpoint.

5.6. Verification of the model

It is the goal of this section to show that the model produces sufficiently accurate and valid description of the functioning of a propulsion system subjected to ventilation-inducing waves. This is done in three steps: Firstly, a standardised analysis is proposed. Secondly the model is subjected to a wave load that is not equal, but comparable to that of the experiments by Koushan (2007) [21]. Finally a comparison of results can show how well the model functions in it's description of engine response to ventilation events.

Standardised analysis The thrust-loop as well as the torque-loop containing a charge-pressure loop and two speed-loops were listed in section 4.6. The relations in these loops can be analysed starting at every point in the loop. The following analyses are ordered from a start with governing input leading to a resulting functioning of the studied system. These seven summarising steps will be applied in the following sections of this report.

Propeller thrust T_p is normalised with it's average value, to focus on variations within a specific simulation. As the engine speed setpoints are constant, they are described as a relative error $e[s^{-1}] = n_{e,set} - n_e$. It is further remarked that the values of engine speed torque Q_e are normalised with their nominal values to compare the experiment with nominal engine operation.

description	step	variable	[unit]
Imposed waves	1	$\zeta(x,t)\|x = x_p$	$[m]$
From immersion to ventilation	2	$h/R(t)$	$[-]$
	3	$T_p/T_{avg}(t)$	$[-]$
From ventilation to engine functioning	4	$e(t)$	$[s^{-1}]$
	5	$m_f(t)$	$[kgcycle^{-1}]$
	6	$p_1(t)$	$[Pa]$
From engine functioning to engine response	7	$Q_e/Q_{nom}(t)$	$[-]$

Table 5.2: Seven summarising steps in the analyses of experiments

Koushan comparisson The model is subjected to an engine-speed setpoint $n_{e,set}$ = 13.3 $[s^{-1}]$ and a wave with an amplitude ζ_a = 1.4 [m] with a period of T = 4.8 [s]. This results in:
- a period of encounter T_e = 2 [s], equal to the experiments by Koushan (2007).
- an average advance ratio $\bar{J}$ = 0.4 [-], larger than Koushan (2007) [21] at bollard-condition J = 0 [-].
- a range of immersion ratio that is deeper, but equally large: $h/R_{max} - h/R_{min} = 2[-]$.
- as the rotational speed of the engine and propeller is nearly constant, the rotational Froude number Fr_p is nearly constant, as shown in figure 5.10.
- An regime of unstable ventilation events as shown in figure 5.9.

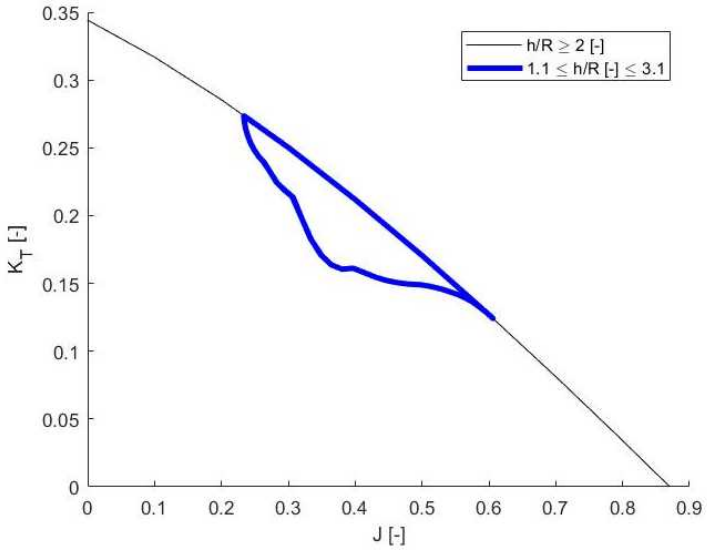

Figure 5.9: Open-water diagram for model subjected to ventilating load.

Results of the Koushan comparisson Figure 5.11 shows the response of the model subjected to this cyclical ventilating load. The beginning of this ventilation cycle shows that:

- An imposed wave results in a reduced immersion h/R from 402.5 [s]. This reduction results in the occurrence of ventilation, as can be seen in figure 5.9, and a sudden large reduction of thrust and torque. This reduction is of the same order as reductions of propeller thrust as reported for constant immersions by Koushan (2007) [21].
- The error in engine speed $e[s^{-1}]$ increases, which leads to an increase of injected fuel to the cylinder. After $\pm$ 0.5 [s], the increased injection of fuel is followed by a rise of the charge-air pressure. This response to a positive error $e[s^{-1}]$ of the rotational speed is to be expected in this range and time frame, as the governor is intended to increase fuel-injection.
- As the propulsion system is subjected to a sudden and significant drop of thrust and torque, the prime-mover responds by slightly increasing the amount of produced torque in this range and time frame. Figure 5.10 shows that the engine operates just within it's static envelope under these conditions.

- The second half of the ventilation cycle is characterised by a non-steady increase of K_T. The whole ventilation cycle occurs within a comparable time frame of [s] as reported by Koushan (2007) [21] and numerous others.

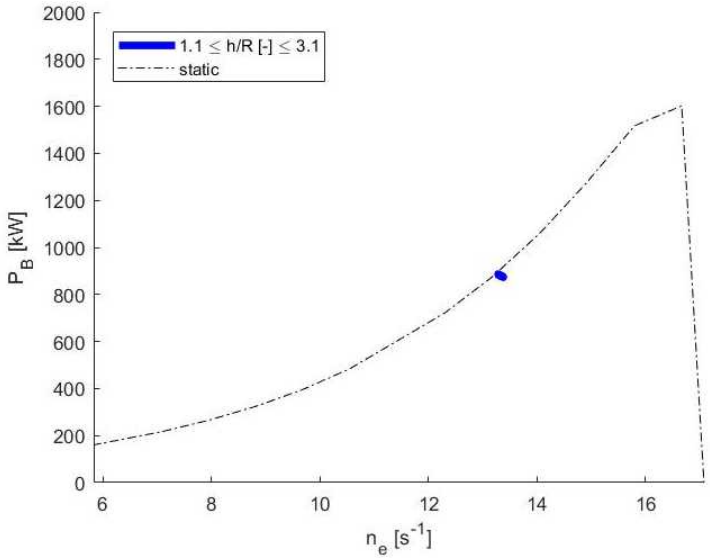

Figure 5.10: Envelope and operational point for model subjected to ventilating load.

In conclusion, the model describes the response to induced ventilation loads in a way that:
- shows realistic variations of propeller functioning including reduction of thrust in the range described by Koushan (2007) [21] for constant reduced immersions, and time frame as for his dynamic experiments. These results are also in the range described by Guoqiang *et al.* (1989) [7].
- shows a realistic response in a range and time frame comparable to descriptions of the prime-mover and it's components as described by Wärtsilä (2017) [10] and Miedema and Lu (2002) [34].

It is therefore concluded that the model describes the response to these loads sufficiently accurate.

5.7. Conclusion

This chapter described key-points in the verification process of the model in chapter 4.

- *Firstly*, the intent of verification was described: to ensure that the model described in chapter 4 provides a true, accurate and valid description of the modelled system and it's functioning.

- *Secondly*, input signals were discussed: Correct engine-speed setpoints were described and the functioning of the waves-block by Fossen and Perez (2004) [8] was verified. It was found to produce accurate and realistic descriptions of single waves, bichromatic waves and different wave-spectra.

- Section 5.3 showed in two steps that the vessel-motion sub-model describes the causal relations on which it is built realistically and accurately: Figure 5.2 showed the response of the hull-speed dependent on positive and negative forces and accelerations, whilst figure 5.3 showed the coupled response of heave- and pitch-displacements z and ϑ.

- Section 5.4 showed in two steps that the propeller sub-model describes the influence of occurring ventilation on the production of thrust and torque accurately.

- Section 5.5 verified the functioning of two characteristic components of the prime-mover, the governor and the turbo-charger, before the prime-mover itself was verified by describing its response to static variations of load-torque and speed setpoint across its nominal domain.

- The previous section compared the functioning of the propeller modelled with the quasi-static method with experimental results by Koushan (2007) [21] and engine limits published by Wärtsilä (2017) [10]. It was found that the model described both propeller functioning and engine responses realistically and in reasonable time frames.

This shows that the model produces the outcomes that can be expected based on the relations upon which it was built in chapter 4. The source-data that was used to describe the three sub-models does not have its origin in one and the same physical ship: it was combined from three in itself realistic sources.

Appendix H described how these three sources were matched based on the work of Klein-Woud and Stapersma (2002) [11]. Although well-matched, this combination of three realistic sources reduces the accuracy of the model. Section 7.3 lists a number of points related to a possible validation study that can help determine the accuracy of this model.

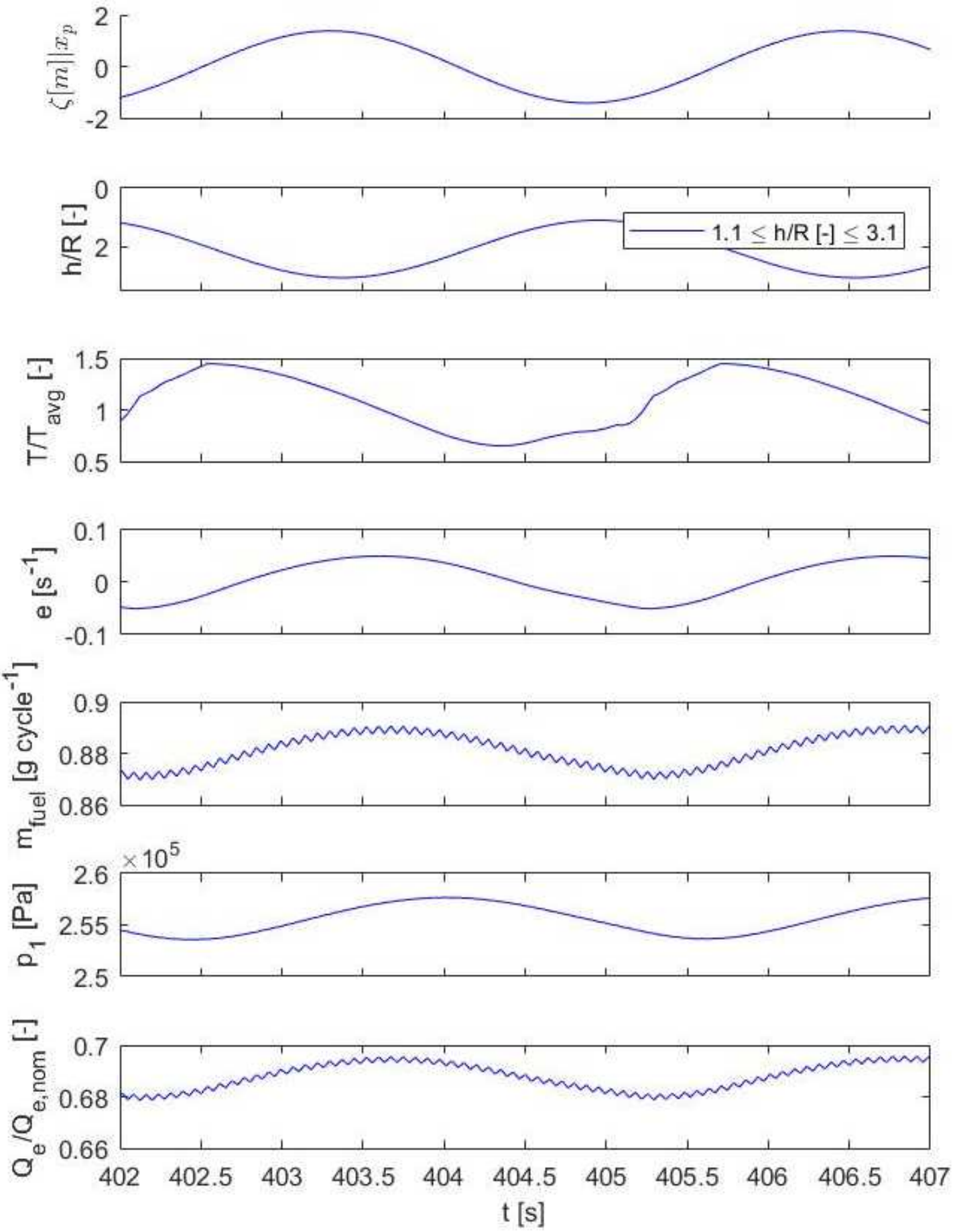

Figure 5.11: Response of the model subjected to ventilating load.

6

Experiment by simulation

The previous chapter verified the functioning of a model that describes the functioning of a vessels propulsion system as it is subjected to different wave-loads and engine-speed setpoints. This chapter intends to use this model to reach the goal of this work:

Goal: *Increased understanding of the relation between wave properties, -height and -frequency, and the response of a marine Diesel engine, -speed and -torque, subjected to wave-induced ventilation*.

Chapter 6 is divided in six sections. The first section discusses the *Experimental setup and hypotheses*, and is followed by four sections,6.2-6.5, with different experiments. These sections treat the results of the experiments that vary the input waves [+] and engine speed setpoint $n_{e,set}$ to the model. The final section 6.6 interprets these results in more detail.

6.1. Experimental setup and hypotheses

This section describes experiments that can answer the main research question. *Firstly*, a review of research questions is done. *Secondly*, an experimental setup is posed that is intended to confirm four hypotheses per experiment. *Finally*, the hypotheses are posed to confirm relations between the input- of the modelled system and the systems response.

Review of research questions Seaway and the vessel motions induced by this seaway result in variations of the sink length l_s, as show in figure figure 4.4, and propeller shaft immersion ratio h/R following figure 4.5. A sufficient reduction of h/R enables the occurrence of ventilation as defined in definition 1: *Ventilation is the transport of a mass of air through the propeller plane*. In particular air coming from the water surface along the waterline of the vessel.

Question 2. *How do vessel motions in a seaway induce propeller ventilation?*

The answer to question 2 is that vessel motions induce a reduction of immersion that allows for the transport of air from the water surface along the water line "*and through the propeller plane before they can dissolve or rise through the water surface again*" (from page 2, based on Carlton (2007) [15]). Different research efforts such as those by van Beek van van Terwisga (2006) [29], Koushan (2007) [21] and Califano (2010) [30] as detailed in section 3.2 confirm the mechanism in this answer.

Question 3. *Can static-immersion propeller ventilation data be used to accurately describe ventilation under varying immersion conditions?*

Static-immersion data as the measurements published by Guoqiang *et al.* (1989) [7] describe K_T as a function of $(J, h/R, Fr_p)$. These measurements are repeated for a number of static immersion ratio's h/R and rotational Froude numbers Fr_p. The quasi-static approach presented in section 4.1 describes how interpolation of static-immersion ventilation data can be applied to describe ventilation and its

influence on K_T as h/R varies in time. Multiple sources including Guoqiang *et al.* (1989) [7] and Koushan (2007) [21] state that K_T- and K_Q-variations are comparable. Validation efforts as detailed in section 7.3 can confirm the accuracy of this approach to describe ventilation under varying immersion conditions.

These answers to questions 2 and 3 leave the main research question:

Question 1. *Main research question: How does a marine Diesel engine respond to off-design loads, and in particular to frequently varying loads resulting from propeller ventilation?*

Experimental setup This question is answered with four experiments, A-D, consisting of simulations that vary different parameters.

A Regular head waves with lower wave frequencies ω and an engine speed setpoint $n_{e,set}$ of 13.3 $[s^{-1}]$. These are of interest in relation to wave loads and vessel motion as indicated by figure 6.1. Encounter frequencies of interest lie in the range $0.25 \leq \omega_e \leq 1.25[rads^{-1}]$, and the green, dotted red and blue line indicate three of the performed simulations in this range.

B Regular head waves with higher wave frequencies ω and an engine speed setpoint $n_{e,set}$ of 13.3 $[s^{-1}]$. These are of interest in relation to characteristic frequencies of engine components such as the turbo charger. Encounter periods of interest lie in the range $0.5 \leq T_e \leq 2.5[s]$.

C Regular head waves with different wave amplitude's ζ_a and an engine speed setpoint $n_{e,set}$ of $16.7[s^{-1}]$. These are of interest in relation to other varying engine loads. A wave period of $T_i = 11[s]$ is selected. This is considered to be a realistic peak value for adverse wave spectra as per table 1.4.

D Head seas with a long-crested adverse Torsethaugen wave spectrum as defined in table 1.4 and realised in figure J.6. Adverse spectra form a boundary condition in relation to EEDI-regulation as described by the IMO-MEPC (2016) [45].

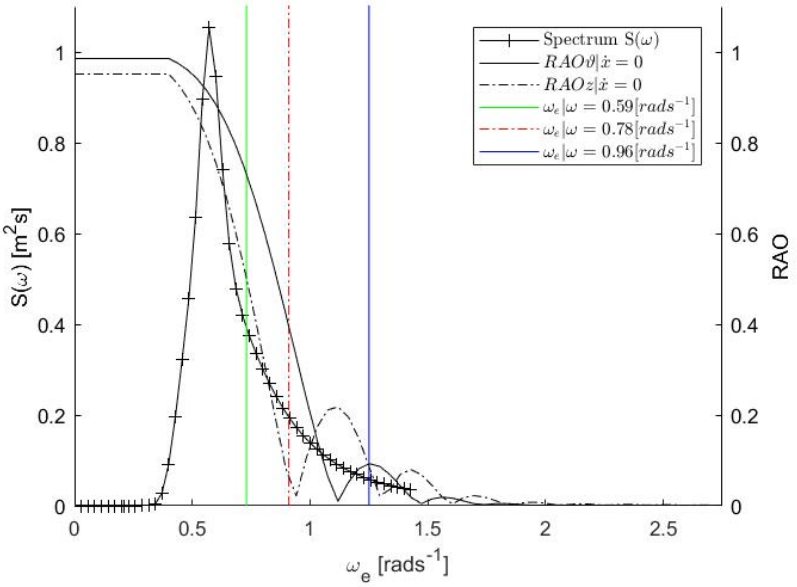

Figure 6.1: Adverse Torsethaugen spectrum, response amplitude operators and ω_e-values for experiment A.

The input of the model, $(waves[+], n_{e,set}[s^{-1}])$, is varied by imposing regular head-waves with wave amplitudes, -frequencies and engine speed setpoints, $(\zeta_a, \omega_i, n_{e,set})$, that result in these variations. Table 6.1 lists the input values that lead to the aforementioned variables of interest (ζ_a, ω_e, T_e).

	$\zeta_a[m]$	$\omega_i[rads^{-1}]$	$n_{e,set}[s^{-1}]$
A	1	[0.59 0.78 0.96]	13.3
B	0.5	[1.40 2.32 3.70]	13.3
C	[0.3 0.8 1.3]	$2\pi/11$	16.7
D	$H_{1/3} = 4[m]$	$T_p = 11[s]$	16.7

Table 6.1: Variation of input-parameters for experiments A-D.

Hypotheses For every of the four experiments A-D, four hypotheses are posed in tables 6.2-6.5. As listed below, these describe relations between the input (waves [+], $n_{e,set}$) and: vessel-motion, the propeller, the prime-mover and the response of the whole system.

Hypotheses H regarding relation between load (waves [+], $n_{e,set}$) and:							
low ω_e		high ω_e		ζ_a		adverse spectrum	
a1	- vessel-motion	b1	- vessel-motion	c1	- vessel-motion	d1	- vessel-motion
a2	- propeller	b2	- propeller	c2	- propeller	d2	- propeller
a3	- prime-mover	b3	- prime-mover	c3	- prime-mover	d3	- prime-mover
a4	- system response	b4	- system response	c4	- system response	d4	- system response

Table 6.2: For experiment A, the hypotheses are posed that:

H-a1 ...different lower wave frequencies result in different frequencies of the immersion ratio h/R as displacement-RAO's vary with the frequency of encounter ω_e, as shown in figure 6.1.
H-a2 ...different frequencies of the immersion ratio h/R result in different variations of the propeller load resulting from different types of ventilation.
H-a3 ...different variations of propeller torque result in different responses of the prime-mover. In particular different variations of the fuel-injection $m_f[gcycle^{-1}]$ and the charge-pressure $p_1[Pa]$.
H-a4 ...different lower wave frequencies result in different significant fluctuations of produced engine torque Q_e and the rotational engine speed n_e.

Table 6.3: For experiment B, the hypotheses are posed that:

H-b1 ...different smaller waves with higher frequencies result in less vessel motion. Secondly, they result in an immersion ratio h/R which varies at higher frequencies.
H-b2 ...different higher wave frequencies with a lower amplitude ζ_a result in a larger advance ratio J, and thereby in less propeller ventilation.
H-b3 ...different high-frequency variations of the propeller load for higher advance ratio J result in variations of fuel injection m_f and charge-pressure p_1, not at the limit of the envelope.
H-b4 ...different high-frequency wave loads result in some fluctuations of the produced engine torque Q_e and minor fluctuations of the rotational engine speed n_e.

Table 6.4: For experiment C, the hypotheses are posed that:

H-c1 ...larger wave amplitudes result in larger vessel-motions and immersion ratio's h/R.
H-c2 ...larger wave amplitudes result in lower advance ratio's J and larger immersion ratio's h/R and thereby in more significant ventilation.
H-c3 ...larger wave amplitudes result in increased fuel injection and charge pressure, possibly to their respective limits. Thereby, larger wave amplitudes can reduce engine speed n_e and operation beyond the prime-mover's static envelope.
H-c4 ...larger wave amplitudes result in larger loads and production of engine torque Q_e. In response to these larger, transient loads and as a result of the increased and possibly limited fuel injection and pressure-charging, operation may take place at reduced engine speed n_e and outside the prime-mover's static envelope.

Table 6.5: For experiment D, the hypotheses are posed that:

H-d1	...adverse irregular wave loads result in irregular vessel-motions and -immersion ratio h/R.
H-d2	...adverse irregular wave loads a resulting irregular immersion ratio induce different types of propeller ventilation and large irregular variations of the propeller loads.
H-d3	...a maximum engine speed setpoint and large irregular variations of the propeller load result in a high engine loading on- or beyond the static envelope of the prime-mover.
H-d4	...adverse irregular waves and a maximum engine speed setting can result in an overload of the prime-mover. This happens by producing more torque Q_e to reach the intended speed $n_{e,set}$, whilst the load increases.

In conclusion, this section has reviewed research questions and discussed an experimental setup to answer the main research question and general goal of this research effort. Finally, hypotheses regarding the response of different system components and the system itself have been posed in tables 6.2-6.5.

6.2. Experiment A: Lower wave frequencies ω

This section intends to show how lower wave frequencies influence the functioning of the prime-mover as it is subjected to possible ventilation events. The input listed in table 6.1 lists constant regular head waves with an amplitude ζ_a = 1 [m], three lower wave frequencies that result in encounter frequencies as displayed in figure 6.1 and is used to create a longer simulation of which 20 representative seconds are displayed in figures 6.2-6.5 below. This section analyses the cyclic response of the system to the blue ($\omega = 0.96[rads^{-1}]$) wave at seven points A-G.

Imposed waves Waves with different lower frequencies in the first step of figure 6.5 show:
- equal amplitudes of ζ_a = 1 [m].
- different wave frequencies ω resulting in the required encounter frequencies ω_e:
$\omega = 0.59[rads^{-1}]$ (green), $\omega = 0.78[rads^{-1}]$ (dotted red) and $\omega = 0.96[rads^{-1}]$ (blue) and $K_{T,ship}$ (same colours, thinner, near-horizontal lines).
- the waves have different phase shifts as a result of the different speeds of the vessel.

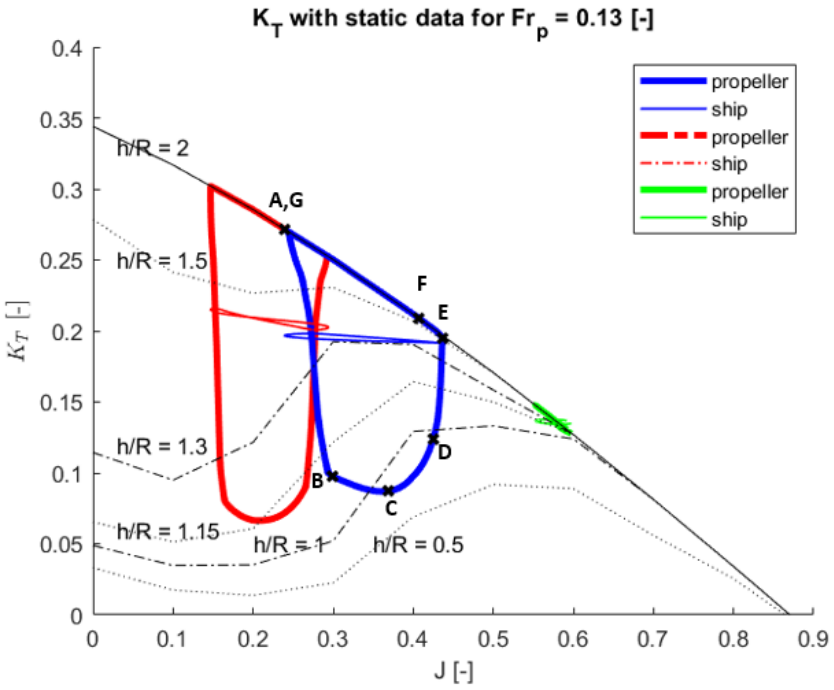

Figure 6.2: Open-water diagram for experiment A.

From immersion to ventilation Immersion ratio's $h/R[-]$ in the second step of figure 6.5 show:
- amplitudes of h/R are not equal as h/R is a function of both wave height and vessel-motion.
- phase shifts between wave-height and immersion ratio occur due to two reasons:
Firstly the upwards positive definition of wave height in h/R and *secondly* the phase shift between wave height and vessel-motions. The red dotted lines for $\omega = 0.78[rads^{-1}]$ illustrate this shift.

Figures 6.2 and the fourth step of figure 6.5 show a sudden and significant drop of thrust in a $\pm 0.5[s]$ timeframe between A and B, in a $\pm 5[s]$ cycle. This characteristic drop is described by van Beek and van Terwisga (2006) [29] as a characteristic property of ventilation: *"Typical and well known characteristics in the occurrence of ventilation is that the beyond the point of ventilation a significant drop in thrust and torque of the propeller occurs."*.
Figure 6.2 further shows how the occurrence of ventilation transforms propeller operation from a line on the deep-immersion $h/R = 2[-]$ K_T-line, to a counter-clockwise cycle. This cycle is forced by the combination of J,h/R, and its shape further influenced by Fr_p. This results in a new equilibrium between $K_{T,propeller}$ and $K_{T,ship}$: Dependent on the specific ventilation that occurs, the rotational engine speed n_e and advance velocity v_a shift.
Koushan (2007) [21] describes the same mechanism for thrusters experiencing heave-motion and ventilation: *"...it is the ventilation which is the primary cause of loading fluctuations rather than the heave motion. Of course, the heave motion acts as a generator and transporter of ventilation."* The link between heave-motion and ventilation that Koushan described is also found in these simulations for fixed-pitch propellers subjected to surge-, heave- and pitch motions.

Successively, the values of K_T and J, the time-average operational points of the propeller in figure 6.2 reach a different equilibrium with $K_{T,ship}$. These different equilibria:
- reduce the vessel speed and increase the variation of n_e.
- are time-average, dynamic equilibria instead of instantaneous ones.
- result in a shift of the operational point of the prime-mover. This will be shown in figures 6.3 and 6.4 and will be explained below.

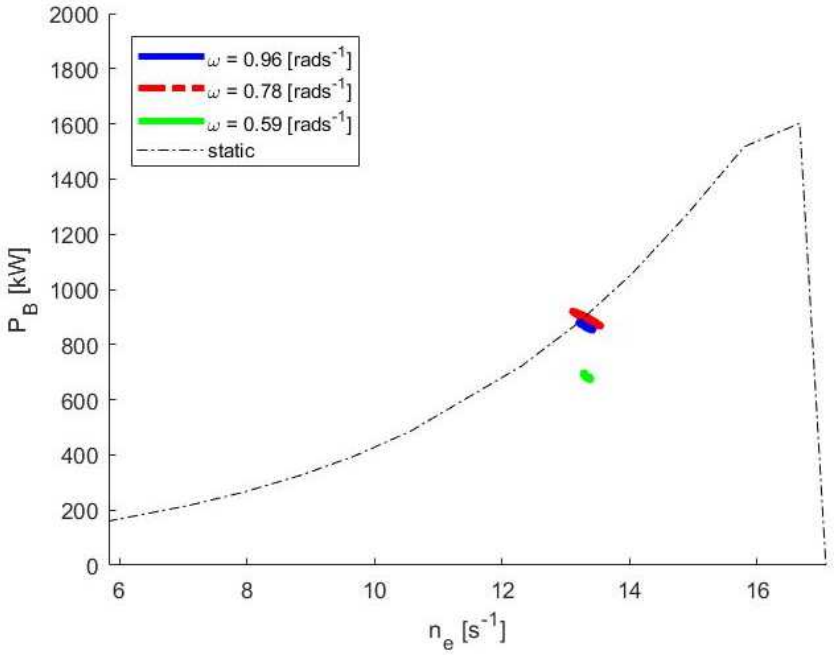

Figure 6.3: Prime-mover response during 20 [s] time frame for experiment A.

From ventilation to engine functioning The open-water diagram in figure 6.2 showed that the green line does not exhibit ventilation. Although the immersion ratio h/R is reduced slightly below 2 [-], ventilation is not induced as the advance ratio J remains sufficiently high.
The dotted red and blue lines show increasingly severe ventilation events with decreasing values of

the advance ratio J. The third step of figure 6.5 shows that these events result in large and sudden drops of propeller thrust between A-B and less sudden increases between C-G. Propeller torque Q_p varies equally sudden.

The fourth step of figure 6.5 shows the rotational speed error $e[s^{-1}]$. All three waves result in an error that in time is both positive and negative. Blue is positive from A-C and before G. It is further remarked that the waves inducing ventilation, result in larger errors e that are characterised by sudden drops and slower increases.
These errors e and different variations of the propeller load result in different engine responses.

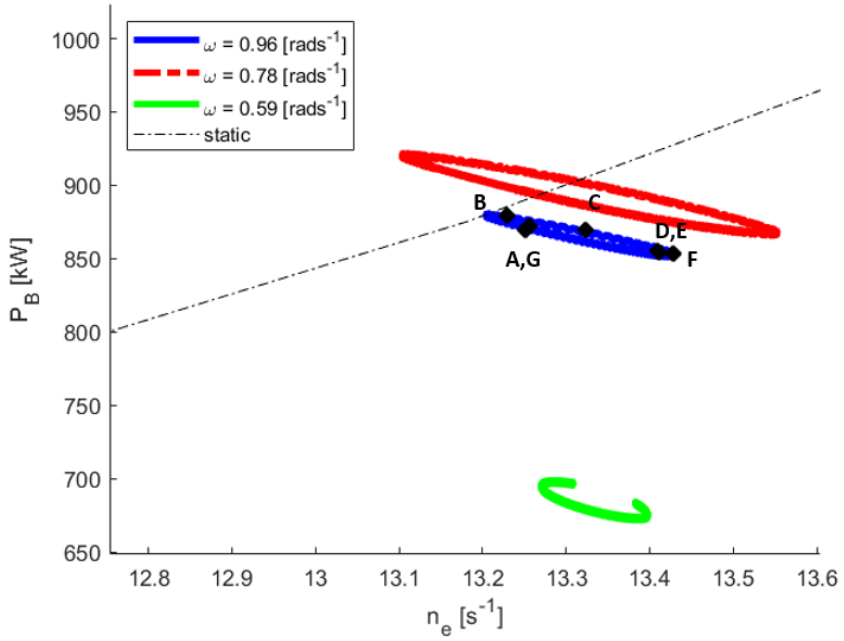

Figure 6.4: Detail of figure 6.3.

From engine functioning to engine response Steps 5 and 6 in figure 6.5 describe the fuel rack setpoint and -limit $X[mm]$ and $X_{limit}[mm]$ for this simulation as well as the charge pressure $p_1[Pa]$. The fuel rack follows the speed error and is significantly less for the non-ventilating (green) load. The same can be said for the charge pressure p_1. The relation between the error e and the charge-pressure p_1 shows a delay in the range of $\pm 0.5[s]$.

The 7^{th} step shows how the produced amount of engine torque Q_e is larger and varies more for the wave loads that induce ventilation. Figure 6.3 confirms this by showing how the prime-mover response varies with the imposed wave frequency ω.

Figures 6.3 and 6.4 show the prime-mover response to different ventilating loads. Figure 6.3 shows that the different waves with equal amplitudes $\zeta_a = 1[m]$ result in different operational points and variations of n_e and P_B. Figure 6.4 shows the cyclic responses in detail
More severe the ventilation events result in larger produced amount of brake power Pb. Secondly, more severe ventilation events result in larger variations of both engine speed n_e and brake power P_B. As depicted by the red line in figure 6.4, the prime-mover is forced to function transiently outside the border of the static envelope during $\pm 1[s]$ of the $\pm 7[s]$ red cycle: The system input ($n_{e,set}$, waves [+]), loads the system intermittently whilst operating near the static envelope. Simulations with other frequencies in the frequency domain described here confirm these characteristics.

In conclusion Certain wave frequencies result in more significant reductions of the immersion ratio h/R and can thereby result in more significant ventilation events. The propeller load variations resulting from these events do not load the prime-mover in a constant manner. As a result of these

load variations, the prime-mover can show significant variations of the fuel injection, charge-pressure and operational point. This confirms the relations described by the hypotheses in table 6.2.

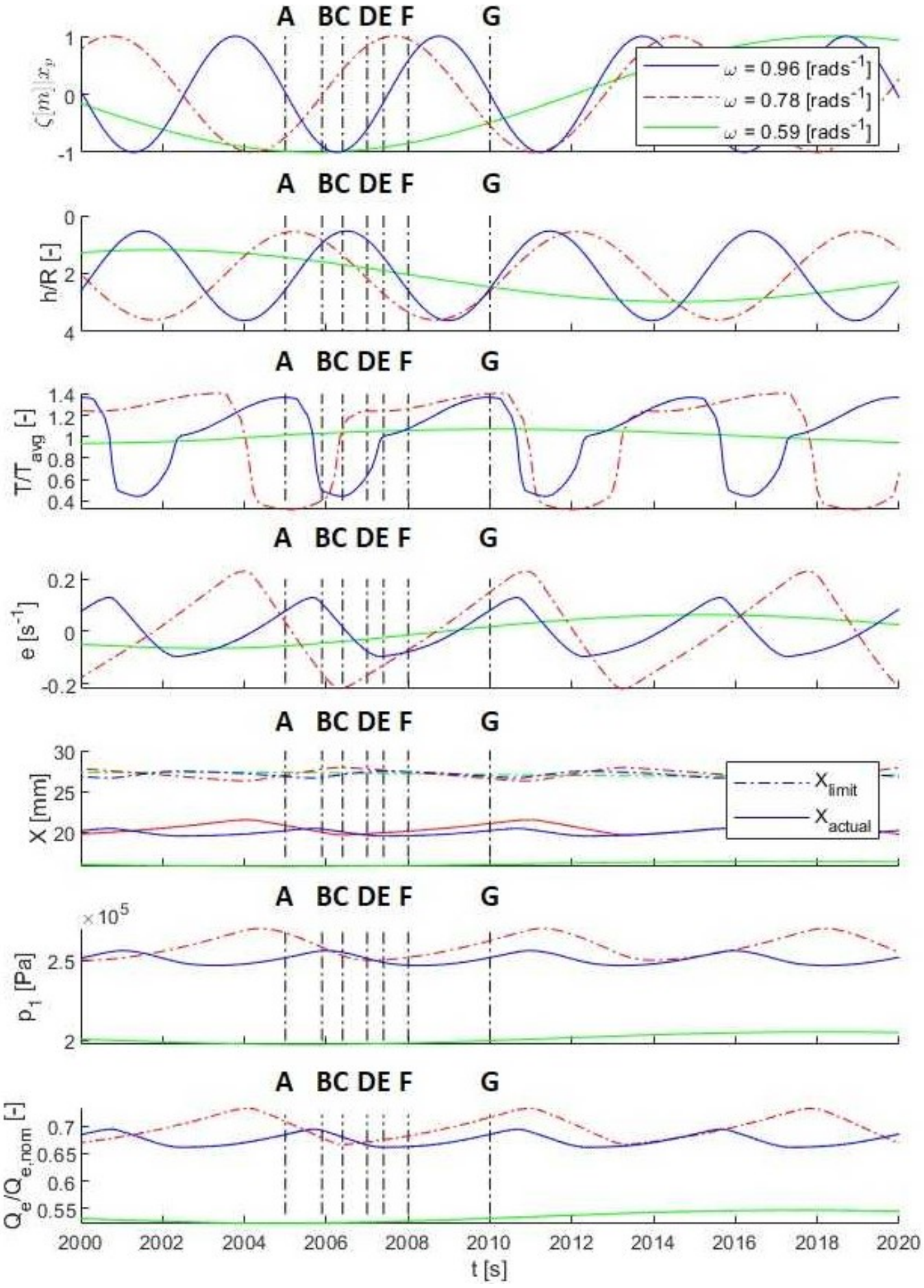

Figure 6.5: Results for lower wave frequencies ω in experiment A.

6.3. Experiment B: Higher wave frequencies ω

This section intends to show how higher wave frequencies influence the functioning of the prime-mover as it is subjected to possible ventilation events. The input listed in table 6.1 lists constant regular head waves with an amplitude $\zeta_a = 0.5[m]$, three higher wave frequencies that span a range covering characteristic frequencies of different prime-mover components such as the governor and the turbo-charger. A representative time frame of 3 [s] is selected from a longer simulation to study the response of the system, as shown in figures 6.6-6.8.

Imposed waves The first step of figure 6.8 shows higher-frequency waves characterised by:
- amplitudes of $\zeta_a = 0.5[m]$, smaller than the waves in experiment A.
- different encounter frequencies ω_e spanning the range including characteristic component-frequencies.
- the waves have accumulated different phase shifts during a 2000 [s] time frame.

From immersion to ventilation The second step in figure 6.8 shows the immersion ratio h/R which is mostly influenced by the imposed waves and less-so by vessel motions. Although the immersion ratio is regularly less than 2 [-], ventilation is not induced. The open-water diagram in figure 6.6 shows that the advance ratios vary, but remain so high that ventilation is not induced. This is deemed to be a result of the lower wave amplitude of ζ_a = 0.5 [m].

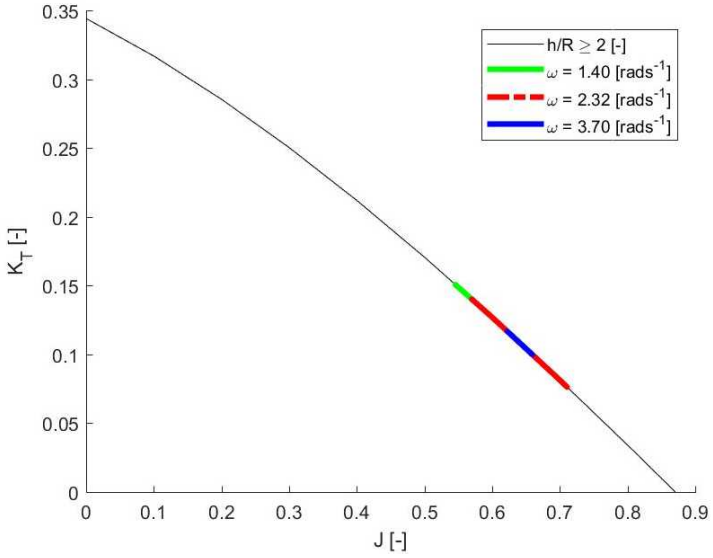

Figure 6.6: Open-water diagram for experiment B.

From ventilation to engine functioning The open-water diagram in figure 6.6 shows that the absence of ventilation events results in load variations as a result of the varying advance ratio J. These variations seem to reduce with an increase of wave-frequency ω. The third step in figure 6.8 shows propeller load variations decreasing with an increase of wave frequency ω.

The fourth step in figure 6.8 shows relatively small engine speed errors e that decrease for higher wave frequencies. This is explained by the reducing variations of the advance ratio J. Figure 6.7 shows the envelope of the prime-mover in experiment B. The depicted loads are nearly equal and vary relatively little in the depicted 20 [s] time frame.

From engine functioning to engine response As the prime-mover functions without much load-variation, the fuel injection m_f is reasonably stable. The fifth step in figure 6.8 shows a slightly larger fuel injection for the largest load, for the smallest wave frequency ω. The sixth step, describing charge-pressure p_1 and seventh step describing engine torque Q_e show the same characteristics: Near-constant operation with larger charge pressure and torque production for the larger load.

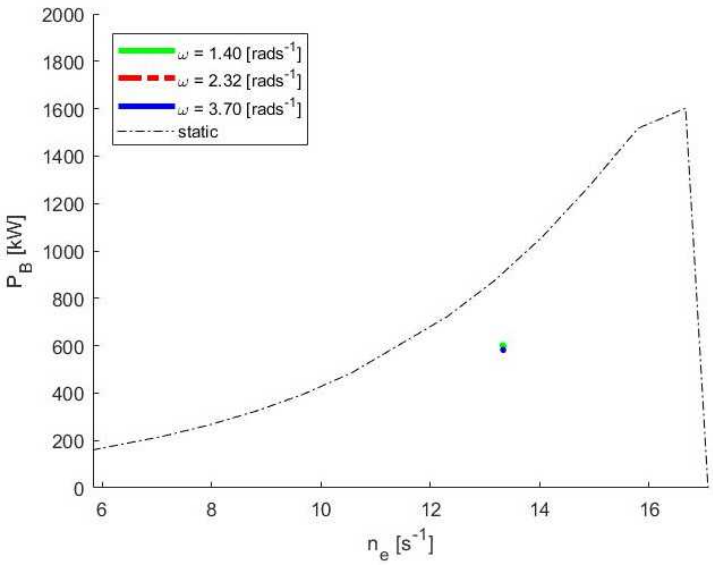

Figure 6.7: Prime-mover response for experiment B.

In conclusion Higher wave frequencies in the domain posed in table 6.1 do not lead to ventilation with the wave amplitude $\zeta_a = 0.5[m]$. Although immersion h/R is temporarily less than 2 [-], ventilation is not induced as the advance ratio remains sufficiently high for this wave-load. The relations described by the hypotheses listed in table 6.3 have been confirmed by these results.

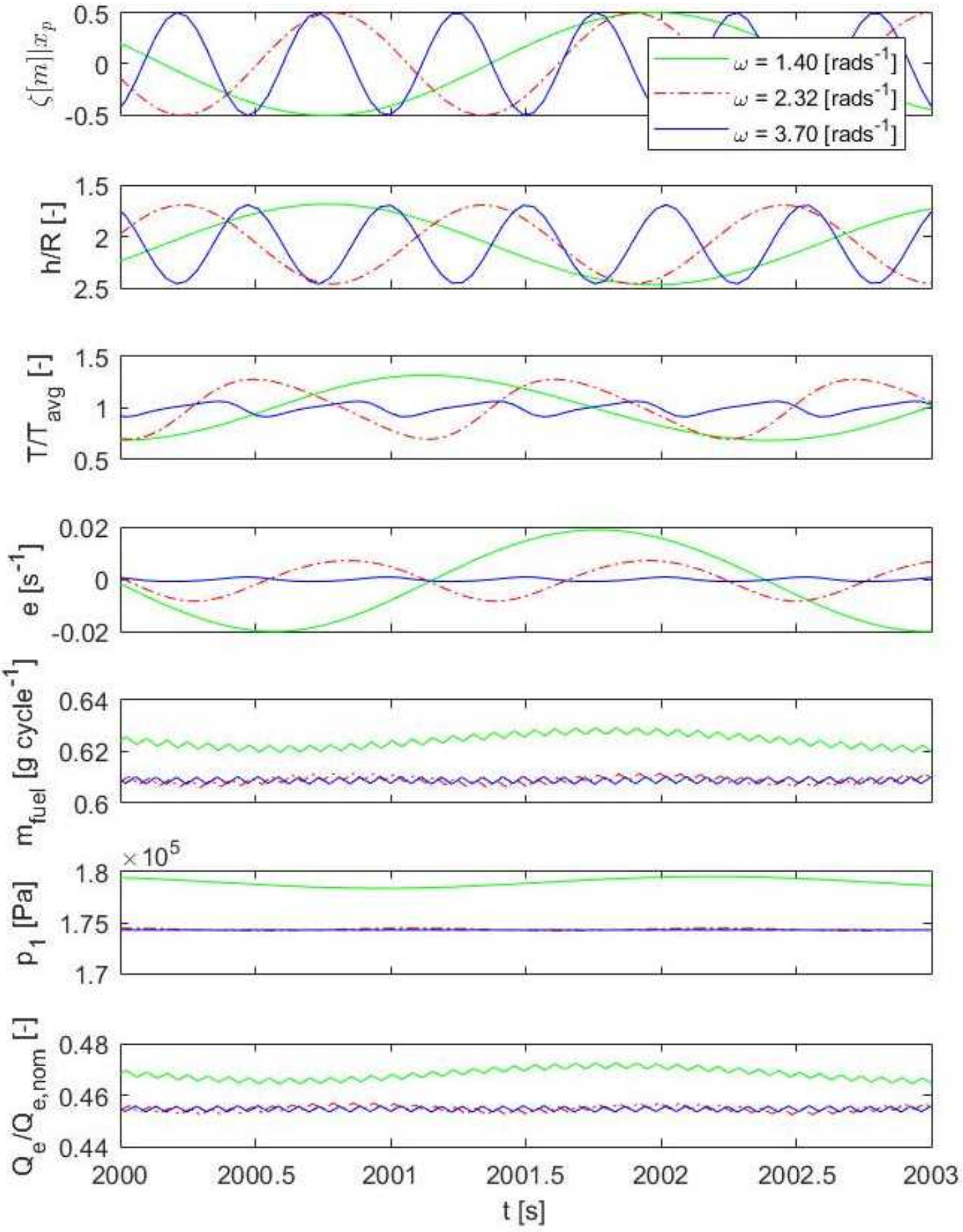

Figure 6.8: Results for higher wave frequencies ω in experiment B.

6.4. Experiment C: Wave amplitude ζ_a

This section intends to show how different wave amplitudes ζ_a influence the functioning of the prime-mover as it is subjected to possible ventilation events. The input listed in table 6.1 lists regular head waves with a realistic period of 11 [s], the peak of an adverse spectrum as described in table 1.4. The engine speed setpoint $n_{e,set}$ is set to the maximum of 16.7 $[s^{-1}]$ as the engine load will increase for larger imposed waves. These settings are used to create longer simulations of which a representative 20 [s] time frame is selected and shown in figures 6.9-6.11 below.

Imposed waves The first step of figure 6.11 shows waves with different amplitudes further characterised by different phase shifts during a 2000 [s] time frame.

From immersion to ventilation The second step in figure 6.11 shows that the imposed waves result in reductions of immersion that increase with wave amplitude ζ_a. The open-water diagram in figure 6.9 further shows that advance ratio J decreases with wave amplitude. For the largest simulated wave amplitude, J and h/R are reduced so much that ventilation occurs.

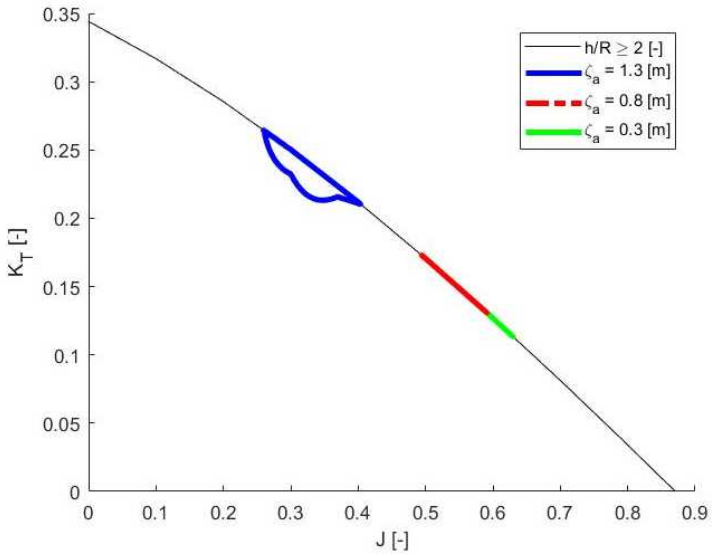

Figure 6.9: Open-water diagram for experiment C.

From ventilation to engine functioning The ventilation event in the open-water diagram in figure 6.9 can be recognised in the thrust signal in the third step of figure 6.11. It is characterised by a sudden and non-linear drop of thrust which is followed by a steady increase of thrust. The propeller loading for these different waves result in two distinctly different speed errors e in the fourth step of figure 6.11: Non-ventilating e of $\pm 0[s^{-1}]$ and ventilating e continuously positive.
The envelope in figure 7.4 summarises this well:

- the smaller wave amplitudes ζ_a result in their maximum-set speed setpoint $n_{e,set}$ on the right (static) limit of the envelope.
- the larger wave amplitude and resulting larger wave load result in engine functioning pushed beyond the static limit. The higher speed setpoint $n_{e,set}$ and load which by ventilation has been intermittently increased, result in this operating point on the prime-mover's dynamic limit.
- The specific part of the limit is governed by the torque-limit from table 3.4. The position of this limit has been determined with the prime-mover's dynamic response in section 5.5.

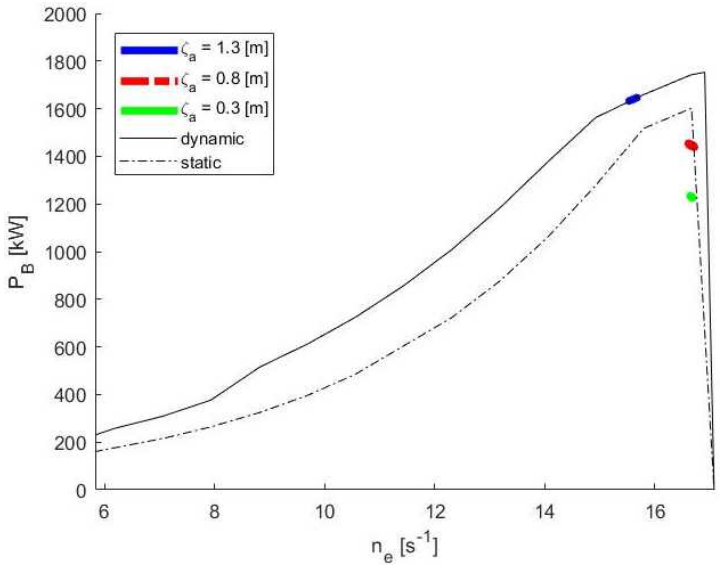

Figure 6.10: Prime-mover response for experiment C.

From engine functioning to engine response These three different responses of the prime-mover function differently:

- Lower wave amplitudes ζ_a without ventilation show lower fuel injection m_f and p_1 charge pressure values in the fourth and fifth steps of figure 6.11.
- Higher wave amplitudes ζ_a that induce ventilation, result in a larger fuel injection m_f, shown in the fourth step of figure 6.11, resulting from the continuously positive speed-error value e. The ventilation event that results in prime-mover functioning beyond the static limit, also results in a charge pressure risen to the value of $4 \cdot 10^5$ [Pa]. This is the value selected as the upper limit of the charge pressure to describe the functioning of an overflow-valve. as further detailed in section 4.4 and appendix G.

Operation of the engine under these conditions with no- or minor ventilation results in minor variations of the engine torque Q_e as shown in the seventh step of figure 6.11.

In conclusion Experiment C has shown that the imposed waves and engine speed setpoint from table 6.1 can shift the operational point of the propeller to a point where ventilation can occur and the engine can be inhibited to function steadily within its static limit. The relations described by the hypotheses listed in table 6.4 have been confirmed by these results.

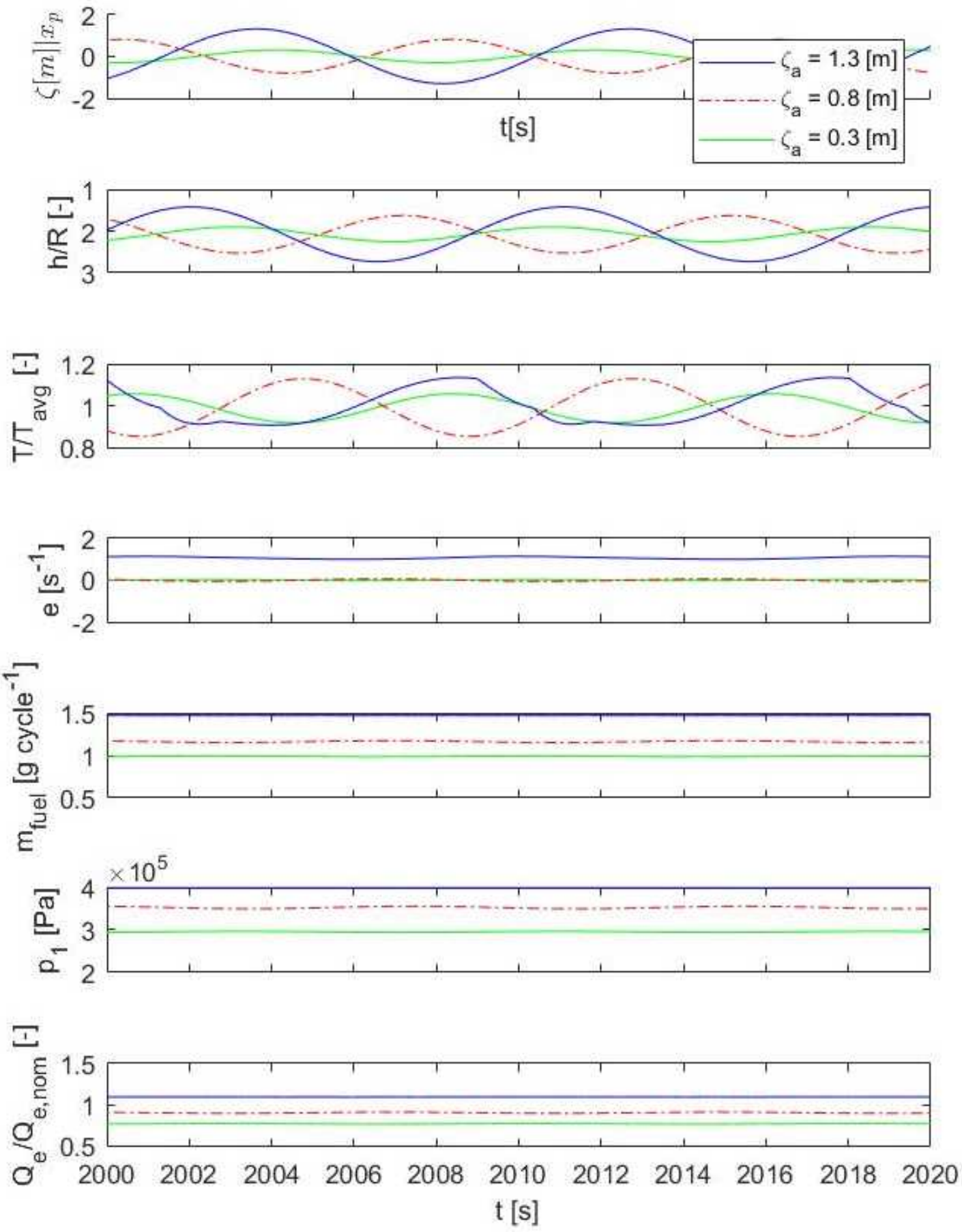

Figure 6.11: Results for different wave amplitudes ζ_a in experiment C.

6.5. Experiment D: Adverse Torsethaugen wave spectrum

This section intends to show how adverse wave spectra influence the functioning of the prime-mover as it is subjected to possible ventilation events. The input listed in table 6.1 lists an adverse Torsethaugen spectrum of long-crested head seas with a significant wave height $H_{1/3} = 4[m]$ and a peak period of 11 [s] as posed by the IMO-MEPC (2016) [45]. A 50-component realisation of this spectrum is shown in figure J.6 and is used to simulate a longer time frame of which 30 representative seconds are displayed in figures 6.12-6.14 below.

Imposed waves The first step in figure 6.14 shows the modelled wave height above the propeller, which is more clearly illustrated by the same 50-component seastate realisation in figure J.6.

From immersion to ventilation The second step in figure 6.14 shows three significant and different reductions of the immersion ratio h/R. These occur as a result of both a low wave height and vessel motions. The open-water diagram in figure 6.12 shows:
- advance ratio J is relatively low which enables ventilation.
- the three ventilation events have distinct, different characteristics.
- operation with a deeply-submerged propeller between ventilation events can be distinguished.

These ventilation events show the same characteristics as simulations A and C did and are

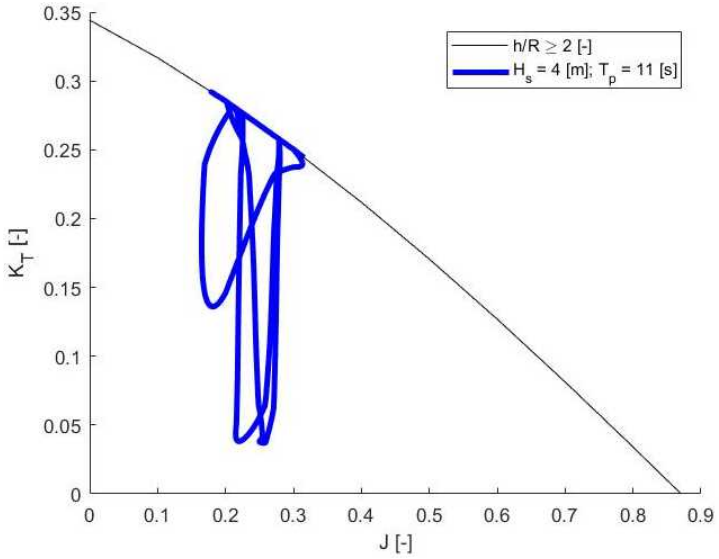

Figure 6.12: Open water diagram for experiment D.

comparable to and in the range of the findings gathered in table 6.6.

characteristic	comparable to
- process buildup	van Beek and van Terwisga (2006) [29]
- amplitudes of thrust- torque variations	Califano (2010) [30]
- time range of steps in a ventilation cycle	Koushan (2007) [21]

Table 6.6: Characteristic properties of a ventilation event.

From ventilation to engine functioning The three distinct ventilation events in the open-water diagram in figure 6.12 can easily be recognised as the sudden and significant drops of thrust in the third step of figure 6.14.These sudden drops of propeller thrust, and equally, propeller torque, result in a sudden but brief drop of the error $e[s^{-1}]$, as the propeller accelerates during ventilation events. This is shown in the fourth step of figure 6.14. The figure also shows that the error is nearly continuously larger than zero. The operational envelope in figure 6.13 confirms this: The prime-mover is intermittently pushed to function beyond its static limit by ventilation loads.

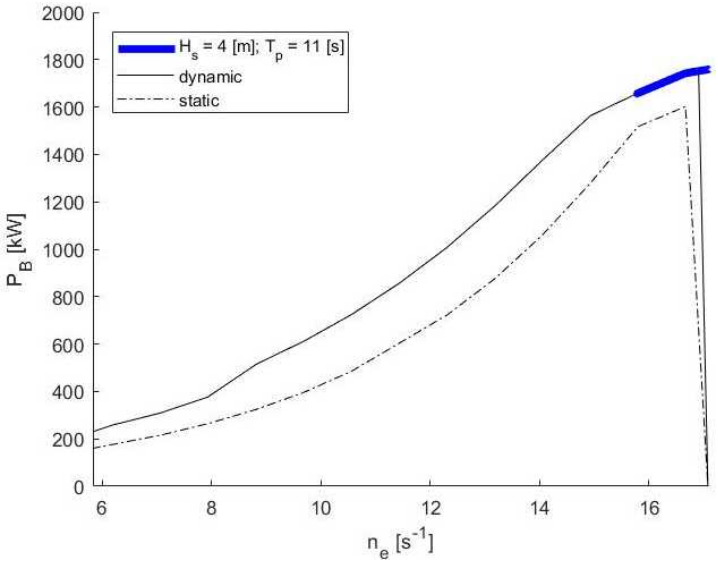

Figure 6.13: Prime-mover response for experiment D.

From engine functioning to engine response During this response, the fifth step in figure 6.14 shows that the fuel injection m_f is continuously at maximum with the exception of the two ventilation events that reduce the speed error e temporarily. The fifth step of figure 6.14 shows that the turbo-charger is continuously producing its maximum pressure of $4 \cdot 10^5[Pa]$. These parameters result in the functioning of the prime-mover shown in the seventh step of figure 6.14: An engine torque Q_e slightly above nominal with small decreases in a delayed response to the larger ventilation events.

In conclusion This experiment with the adverse input conditions as listed in table 6.1 results in a temporary overload of the engine as a result of a large wave load, a high engine speed setpoint and intermittent ventilation events. The relations described by the hypotheses listed in table 6.5 have been confirmed by these results.

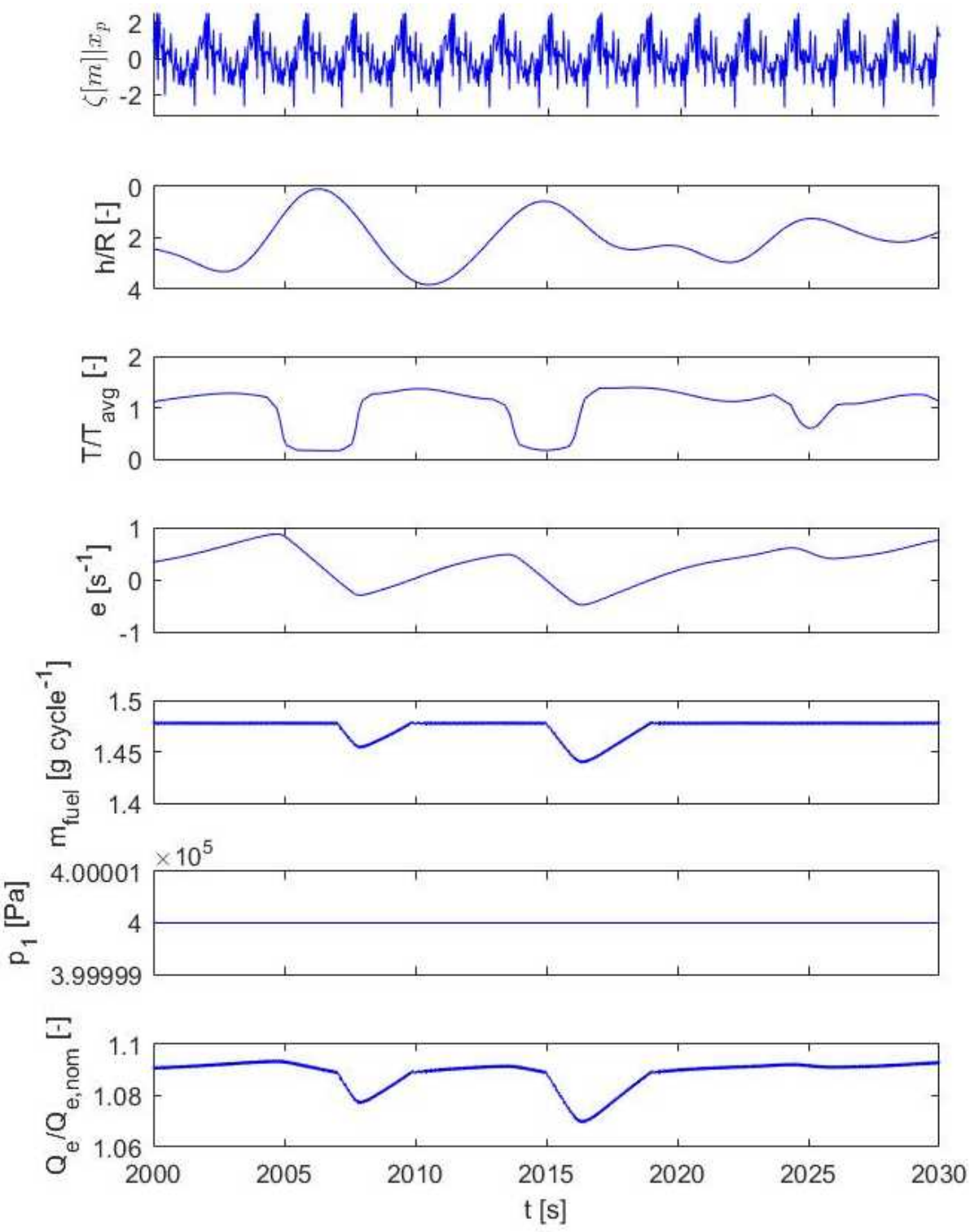

Figure 6.14: Results for an adverse Torsethaugen spectrum in experiment D.

6.6. Interpretation of results

This section interprets the results of experiments A-D by gathering findings from those results in three groups: Results regarding all ventilation responses, regarding smaller load ventilation response and regarding larger-load ventilation response. Finally, these characteristics are gathered in a six-point list.

- **Regarding all ventilation responses** The mechanism that induces all ventilation events:
  - is forced by the waves to which the system is subjected. As experiments A, C and D show, ventilation is equally cyclic or repetitive in nature as the waves that induce it.
  - consists of imposed waves that induce a reduction of the immersion ratio h/R.
  - requires a sufficiently low value of the advance ratio J. This can result from both larger wave loads and the temporary increase of engine speed n_e.
  - shows load variations in all examples in experiments A, C and D. These are characterised by a sudden decrease of load and a slower increase of propeller loads. These characteristics are slightly less pronounced then in certain publications, but unmistakably present.
  - shows a prime-mover response to all ventilation events with a brief increase of rotational engine speed n_e, followed by a decrease once the immersion ratio h/R increases again.
- **Smaller load ventilation response** These ventilation events are characterised by a response which is not limited by any of the limits listed in table 3.4. Different events in experiment A ,B and C have shown that these events are characterised by:
  - reduced values of the advance ratio J.
  - sudden variations of the rotational engine speed n_e.
  - variations of the amount of injected fuel m_f as a result of these engine speed variations.
  - delayed variations of the charge-pressure p_1.
  - resulting variations of produced engine torque Q_e and brake power P_B.
- **Larger load ventilation response** is also shaped by dynamic and transient effects related to the prime-mover limits listed in table 3.4 and discussed in section 5.5. These responses in experiments C and D show that:
  - ventilation events with larger reductions of propeller thrust and -torque.
  - reductions and larger variations of rotational engine speed n_e.
  - nearly-continuous nominal fuel-injection m_f and maximum charge pressure p_1.
  - the prime-mover and its components can be forced to operate on or beyond static limits by significant transient loads.

More simulations have been performed in the discussed domains and the results of these simulations are in line with the results that have been shown in this chapter. Section 7.2 uses the findings gathered in this section to answer the main research question of this thesis.

7

Conclusions and recommendations

This chapter summarises this research effort in three sections of which the first covers a brief summary. It is followed by a section regarding conclusions and the answer to the main research question. The final section treats recommendations for improvements, validation and further research.

7.1. Brief summary of research

This section summarises this thesis by describing the problem that is addressed, the model that is applied and the experiments that were performed by simulation.

Problem Propeller ventilation is consists of the transport of masses of air through the propeller plane. It poses a problem with theoretical and practical relevance as:

- a propeller experiences significant load variations as a result of ventilation events.
- the influence of propeller ventilation on the functioning of the rest of the propulsion system remains a missing theoretical description.
- the design of a propulsion system does not take ventilation into account.
- reduced amounts of installed power are favoured by EEDI-legislation, whilst other IMO-MEPC legislation favours a sufficient amount of installed power in adverse condition that may induce ventilation.

This thesis investigates the response to propeller-ventilation by a monohull-coaster with a medium speed marine Diesel engine and a reduction gearbox connected to a fixed-pitch propeller. It moves with a positive forward speed into long-crested head seas.

Question 2 *How do vessel-motions in a seaway induce propeller ventilation?*

Vessel motions induce a reduction of immersion ratio h/R. That allows for the transport of air from the water surface along the water line *"and through the propeller plane before they can dissolve or rise through the water surface again"* (from page 1, based on Carlton (2007) [15]. Vessel-motions thereby vary the operational point of the propeller in the open-water diagram. This variation of J and resulting varies the required engine speed n_e required for to induce ventilation.
Experiment D and in particular steps 2 and 3 of figure 6.14 show that the waves resulting in certain vessel-motions and variations of the immersion ratio, result in repetitive losses of thrust.

Model Research question 3 investigates the application of static ventilation data to describe ventilation. The immersion is described as proposed by Journée and Massie (2001) [19]. This is the core of the quasi-static approach. The interpolation of static-immersion thrust-data describes the influence of ventilation on the functioning of the propulsion system.

Question 3 *Can static-immersion propeller-ventilation data be used to accurately describe ventilation under varying immersion conditions?*

The model uses input consisting of an engine speed setpoint and the description of waves or a wave-spectrum. Three sub-models determine vessel-motions, the functioning of the propeller and the response of the prime-mover. The output of the model consists of engine-speed- and -torque-data. Verification has shown that the model provides results comparable to, and in the time frame of, the published experimental results of Koushan (2007) [21]. Furthermore, table 6.6 has listed characteristic properties of ventilation events that simulations A, C and D showed and were comparable to different experimental findings.

Experiments by simulation Four experiments were performed with different input.
For reduced constant engine speed setpoints, lower wave-frequencies were varied with a constant wave amplitude of 1 [m] in experiment A, and higher wave-frequencies were varied with a constant wave amplitude of 0.5 [m] in experiment B.
For nominal constant engine speed setpoints, wave amplitudes were varied with the peak-frequency of a realistic adverse spectrum as the wave-frequency in experiment C, and a 50-component realisation of an adverse Torsethaugen spectrum in experiment D.

The simulations of experiment A showed both non-ventilating- and ventilating responses of the model system. Experiment B showed how the imposed input results in different non-ventilating responses. Experiment C resulted in both non-ventilating and ventilating responses on or just beyond the static operating limit of the prime-mover. The simulation in experiment D showed the response of the propulsion system to consecutive ventilation events with different characteristics.

7.2. Conclusions and answers to main research question

This section lists findings and gathers eight statements that are used to answer the main research question based on the experimental results of chapter 6, before the uncertainty and limitations of this thesis are stipulated.

Frequently varying loads resulting from propeller variation can induce:

- a shift of the propellers operational point in the open-water diagram.
- a different, dynamic and time-average equilibrium between $K_{T,propeller}$ and $K_{T,ship}$.
- a possibly significant resulting increase of the variation of engine speed n_e and -torque Q_e.
- increased prime-mover loads and load variations with increasing severity of the ventilation events.
- prime-mover functioning temporarily beyond the static limit of the operational envelope.
- possible transient functioning beyond the static limit of the prime-mover and resulting reductions of rotational engine speed n_e.

Conclusions Based on experimental result from input-variations of the constructed model, we can answer main research question 1 with the following eight statements:

1. Significant drops of propeller thrust and torque induce significant variations of the rotational engine speed n_e, as shown an experiment with lower wave-frequencies.
2. More severe ventilation results in more severe sudden reductions of propeller thrust and -torque. This is shown in experiments applying different wave-frequencies, -amplitudes , an adverse wave spectrum and different speed setpoints.
3. Small variations of input can result in large variations of the engine response. An experiment varying wave amplitude at a higher engine speed setpoint indicates possible operation in a partially-ventilating regime. A second experiment with comparable amplitude but variation of

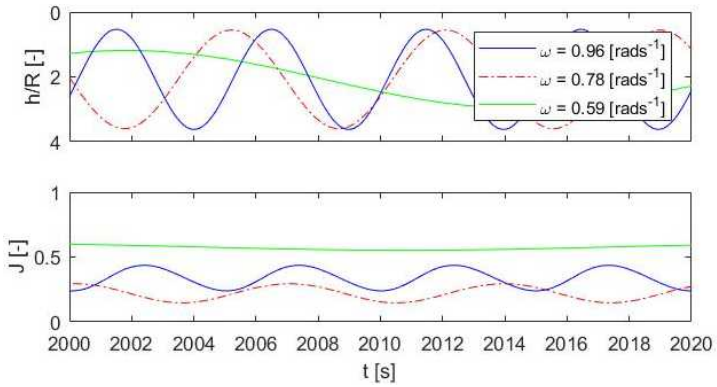

Figure 7.1: Propeller-shaft immersion ratio h/R and advance coefficient J in experiment A. (Reproduced from figures 6.2 & 6.5).

wave-frequencies and a reduced speed setpoint, does not show ventilation. This indicates functioning near the boundary between non- and partially ventilating regimes.

4. Reductions of only the advance ratio J or immersion ratio h/R do not result in ventilation. Higher frequency waves with limited amplitude

   result in variations of the propeller's operational point, but not in ventilation. Figure 7.1 shows variations of advance ratio J in a 20 [s] time frame that could induce ventilation. Simultaneous variations of h/R could also induce ventilation, but the open-water diagram for these loads in figure 7.2 does not show ventilation in all those simulations. Both the advance ratio and immersion ratio must be reduced sufficiently.

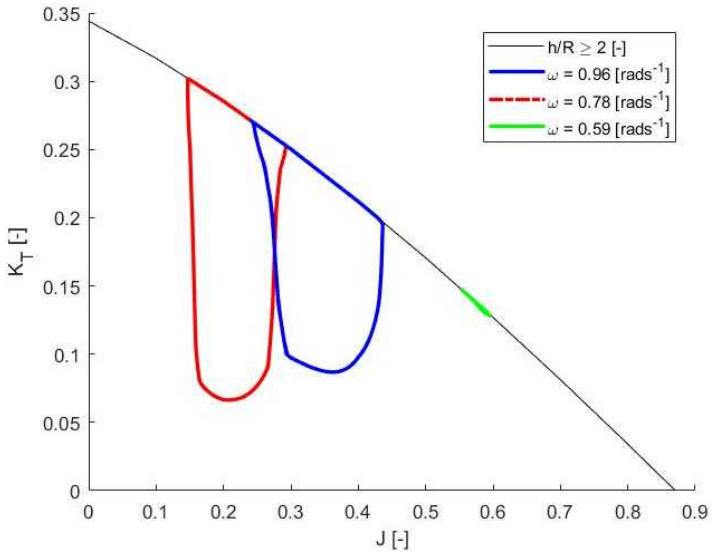

Figure 7.2: Open-water diagram for experiment A. (Figure 6.2 reproduced).

5. Sudden drops of propeller thrust and torque result in an increase of the prime-mover load. This was shown in the experiment discussed in point 4 that varied lower wave-frequencies resulting in the prime-mover response depicted in figure 7.3.

6. Propeller-load variations of significant ventilation events can force the prime-mover to respond with transient operation on- or outside the static operating envelope. This is shown in figure 7.3. It confirms that evaluation of ventilation response in design of propulsion systems can cross the contrary design ideal to minimise installed power.

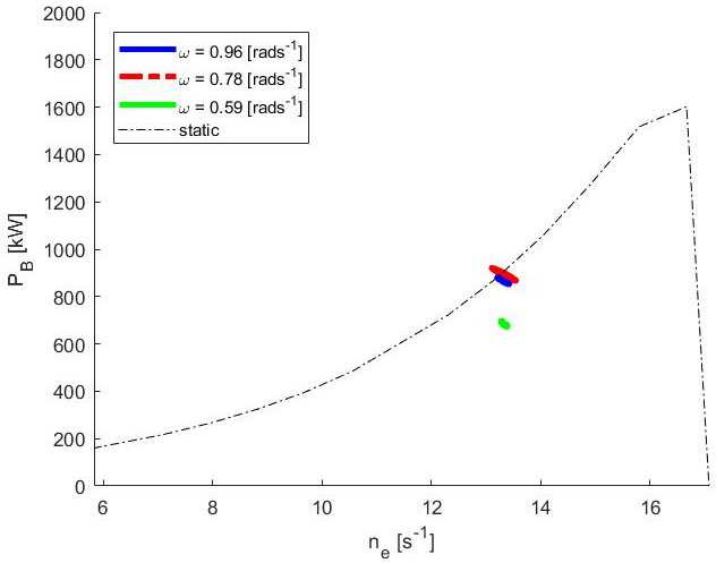

Figure 7.3: Prime-mover response during 20 [s] time frame for experiment A. (Figure 6.3 reproduced).

7. Response to increased loads resulting from ventilation events can be limited by the prime-movers limits. The rotational engine speed can be reduced by the imposed ventilation loads. Experiments that varied wave-amplitude and ones that applied an adverse wave-spectrum confirmed this and figure 7.4 illustrates this.

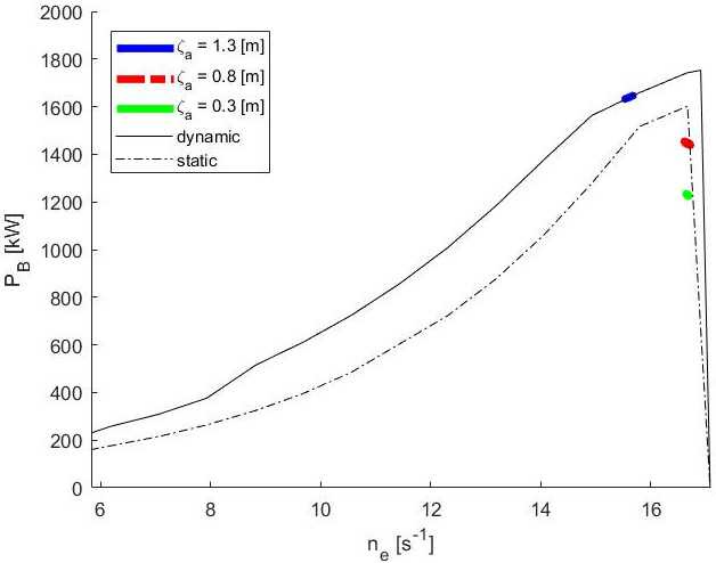

Figure 7.4: Prime-mover response for experiment C. (Reproduced figure)

8. Successive reductions of the immersion ratio, with a sufficiently low advance ratio, result in different successive ventilation events with different significant drops of thrust. Figure 7.5 shows these load variations and the resulting transient response of the prime-mover. This transient response lies outside the static operational limit. This is partially the result of the noticeable variations of the engine speed, as depicted with its error $e[s^{-1}]$. It is further remarked that successive variations of the thrust-drops show nearly the same cyclic and repetitive nature as the immersion ratio that induces them.

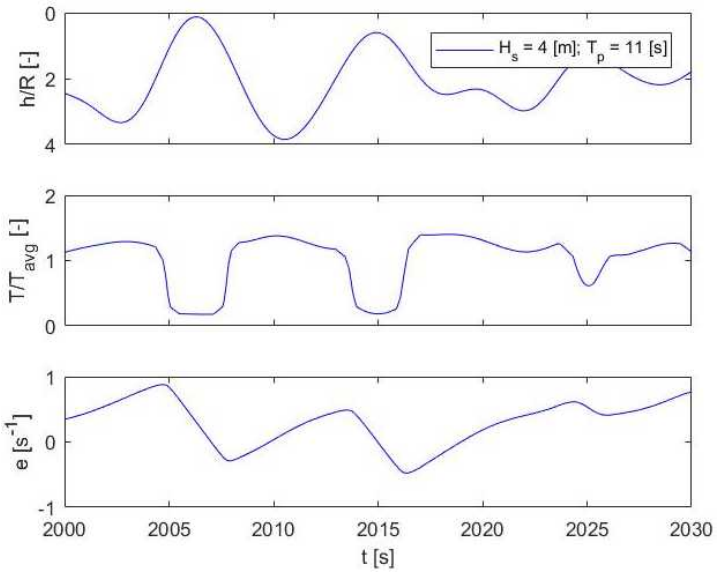

Figure 7.5: Results for an adverse Torsethaugen spectrum in experiment D. (Reproduced from figure 6.14)

Main research question 1 *How does a marine Diesel engine respond to off-design loads, and in particular to frequently varying loads resulting from propeller ventilation?*

Frequently varying loads resulting from propeller ventilation can induce a significant shift in the operational point in the propellers open-water- and engines PV diagram and increase of the variation of engine speed n_e, -torque Q_e.

Uncertainty As indicated in section 5.7, the accuracy of the results produced with the presented model, is dependent on the three main sources of applied data and the quality of the matching process. Although appendix H describes a reasonably-well matched design, the model only describes an approximation of a vessel. This introduces the largest source of uncertainty and should be addressed with validation-efforts as treated in section 7.3.

Limitations Section 4.6 listed three limitations to the described model regarding the range of vessel speeds, the application of 1^{th} quadrant propeller-data and the prime-mover envelope. These limitations have in common that they could be reduced with the application of better information.

7.3. Recommendations

This section gathers possible improvements that can help increase the quality of the model and suggests possibilities to improve it, to help validate it or to apply it in further research.

Improvements

The quasi-static method provides a well-balanced method to describe ventilation loads on a marine Diesel engine. More detail could be brought to bear in the description of the vessel motions, the propeller and the prime-mover.

Vessel motions Vessel motions and imposed wave-loads are described with three equations of motions and undisturbed wave fields. Two improvements are recommended for a more realistic description of ventilation-response:

- The inclusion of more degrees of freedom and specifically the inclusion of yaw- and roll-motions as they are likely to effect the funnel length l_s as that would be included instead of the estimated shaft immersion $\hat{h}/R$.
- The model should include more degrees of freedom to accurately describe vessel motions as a

result of wave spectra with a larger number of wave-directions. An inclusion of yaw- motions is also recommended as this allows more detailed seakeeping analysis linking ventilation events to the functioning of the propulsion system under different vessel headings, instead of only pure head seas.

Propeller Propeller functioning could be described in more detail. In particular the definition of estimated propeller shaft immersion ratio $\hat{h}/R$ could be replaced with a funnel length l_s, that describes the distance between a point on a rotating propeller blade and the nearest point on surface of the water along the hull.
Secondly, an improved estimate of the water entrained by the ventilating propeller could improve the models description of the propeller- and engines rotational speed.

Prime-mover The prime-mover was modelled with a computationally efficient Diesel-A description following Stapersma (2009) [41]. It is adapted with a relatively simple PI-controller governing the fuelrack-setpoint and a heat-to-pressure estimate of the charge-pressure as posed by Miedema and Lu (2002) [34]. These descriptions could be improved with a more detailed description such as the Diesel B method if enough data is present to describe the functioning of the specific Diesel engine.

A second improvement to the modelling of the prime-mover lies in the application of more realistic control strategies that better reflect how the crew or partially-automated control-system respond to ventilation events and a more detailed description of the different operational limits as described in section 4.4.

Validation

Validating efforts are intended to inform to which degree a model describes reality. The *quasi-static method* consists of three main sub-models that each to some degree are based on measured- or estimated properties. This introduces errors that differ principally from errors in the method itself. The latter are to be determined by a comparison of the resulting Q_p, with the propeller torque as measured in a *well-documented* ventilation event. This can be registered by a vessel in practise or in an experimental setup.
A *well-documented* event needs to record at least input information regarding all components of the quasi-static method. Resulting propeller torque needs to be registered so that it can be compared with the response estimated by the quasi-static method. This is only possible indirectly by measuring shaft- or engine-torque.
Secondly, attention is drawn to the functioning of the propeller under the hull. An accurate open water diagram needs to be determined for different immersion ratio's.

data	parameter	application
- wave-data	$\zeta(x,y,t)$	vessel-motion, propeller
- propeller- and ventilation data	n_p, h/R, Q_p	propeller
- hull-properties	w, t, $R_{sw}(\dot{x})$, RAO's	vessel-motion
- engine-data	n_e, m_f, p_1 or (m_1, T_6), Q_e or P_B	prime-mover

Table 7.1: List of data-types, parameters and applications of

Table 7.1 gathers a number of parameters, that should be gathered in reality, to compare the functioning of a specific propulsion system with the outcome of the model.

Further research

- Advanced control strategies could be implemented to describe the response of prime-movers in more realistic scenarios.
- New advanced control strategies could be developed to respond better to possible ventilation events. This could allow propulsion system designers to apply smaller prime-movers and lower a designs EEDI-value.
- New advanced control strategies could be combined with wave-sensing techniques as described by Naaijen (2017) [66].

- Particle image velocimitry or PIV-techniques could be applied to measure and describe the propeller-inflow under ventilating conditions more accurately.
- Research regarding the possible implementation of the study of ventilation-response in the design of propulsion systems.

᾽Ω̃ Κρίτων, ἔφη, τῶ᾽ Ἀσκληπιῶ᾽ ὀφείλομεν
ἀλεκτρυόνα ἀλλά ἀπόδοτε καὶ μὴ ἀμελήσητε.

Socrates

(O Crito, we owe a cock to Asclepius;
make this offering to him and do not forget it.)

Bibliography

[1] Dang, J., Koning, J., Brouwer, J. and de Jong, J., "Dynamic loads on mechanical azimuthing thrusters," 2013.

[2] IMO-MEPC, "2013 interim guidelines for determining minimum propulsion power to maintain the manoeuvrability of ships in adverse conditions, as amended..." pp. 1–8, 2015.

[3] Davis, J. P., Eisenhardt, K. and Bingham, C. B., "Developing theory through simulation methods," pp. 480–499, 2007.

[4] Shi, W., "Dynamics of energy system behaviour and emissions of trailing suction hopper dredgers," 2013.

[5] Bentley Systems, "Maxsurf Resistance - Windows Version 20 User Manual," 2014.

[6] ——, "Maxsurf Motions - Windows Version 20 User Manual," 2014.

[7] Guoqiang, W., Dashan, J., Meiliang, C. and Zhenbang, S., "Propeller air ventilation and performance of ventilated propeller," pp. 6–1 – 6–8, 1989.

[8] Fossen, T. I. and Perez, T., "Marine systems simulator (mss) <http://www.marinecontrol.org>," 2004.

[9] Damen shipyards group, "Product sheet damen combi freighter 3850," Product_Sheet_Damen_Combi_Freighter_3850_05_2017.pdf, 2017.

[10] Wärtsilä Finland OY, "Wärtsilä 20 product guide," Wärtsilä 20 product guide.pdf, 2017.

[11] Klein Woud, H. and Stapersma, D., "Design of propulsion and electric power systems," 2002.

[12] ——, "Matching propulsion engine with propulsor," pp. Vol.4, Issue 2, pp. 25 – 32, 2005.

[13] Smogeli, Ø. N., "Control of marine propellers," 2006.

[14] Leduc, M., "Power to the water [picture]," http://www.dieselduck.info/machine/02%20propulsion/shafting/index.htm, 12-05-2017.

[15] Carlton, J. S., "Marine propellers and propulsion," 2007.

[16] Hydromechanics subcommittee of the technical and research committee of the society of naval architects and marine engineers, "Nomenclature for treating the motion of a submerged body through a fluid," 29 West 39th Street, New York, N.Y., apr 1950.

[17] Stapersma, D., "Interaction between propulsor and engine," 2000.

[18] Faltinsen, O. M., "Sea loads on ships and offshore structures," 1993.

[19] Journée, J.M.J. and Massie, W.W., "Offshore hydromechanics," 2001.

[20] van Lammeren, W.P.A., van Manen, J.D. and Oosterveld, M.W.C., "The wageningen b-screw series," 1969.

[21] Koushan, K., "Dynamics of propeller blade and duct loading on ventilated thrusters in dynamic positioning mode," 2007.

[22] Babicz, J., *Wärtsilä Encyclopedia of ship technology*. Wärtsilä corporation, 2015.

[23] Sen, P. C., "Principles of electric machines and power electronics," 2012.

[24] Pedersen, E. and Engja, H., "Mathematical modelling and simulation of physical systems," 2010.

[25] Fossen, T. I., *Handbook of marine craft hydrodynamics and motion control*. John Wiley & Sons Ltd., Chichester, 2011.

[26] Flying focus, "*A coaster in head seas*," http://www.flyingfocus.nl/, 2017.

[27] Haver, S., "A possible freak wave event measured at the draupner jacket january 1 1995," 2004.

[28] Koushan, K., Spence, S. and Savio, L., "Ventilated propeller blade loadings and spindle moment of a thruster in calm water and waves," june 2011.

[29] van Beek, T. and van Terwisga, T., "Ventilation or cavitation: An experimental study to determine dynamic loads on controllable pitch propellers," 2006.

[30] Califano, A., "Dynamic loads on marine propellers due to intermittent ventilation," 2010.

[31] M. van der Leij, "Experimental and numerical research into propeller thrust breakdown due to ventilation," 2019.

[32] Minsaas, K. J., Faltinsen, O. M. and Persson, B., "On the importance of added resistance, propeller immersion and propeller ventilation for large ships in a seaway," Tokyo & Seoul, 1983.

[33] Grote, K.-H. and Feldhusen, J., "Dubbel - taschenbuch für den maschinenbau," 2007.

[34] Miedema, S.A. and Lu, Z., "The dynamic behavior of a diesel engine," june 2002.

[35] Sørensen, A. J., "Marine control systems," 2013.

[36] Vrijdag, A., Stapersma, D. and van Terwisga, T., "Systematic modelling, verification, calibration and validation of a ship propulsion simulation model," pp. 3–20, 2009.

[37] Welman, Kruger and Mitchell, "Research methodology," 2005.

[38] Wochner, M.S., Gravell, L.R., De Leon, S. and Patterson, R.A., "Underwater noise reduction system using open-ended resonator assembly and deployment apparatus," https://www.google.com/patents/US9410403, Aug. 9 2016, US Patent 9,410,403.

[39] Koushan, K., "Environmental and interaction effects on propulsion systems used in dynamic positioning, an overview," p. pp. 1013 – 1020, 2004.

[40] IMO, "International shipping facts and figures - information resources on trade, safety, security, environment," International%20Shipping%20-%20Facts%20and%20Figures.pdf, 2012.

[41] Stapersma, D., "Diesel engines: A fundamental approach to performance analysis, turbocharging, combustion, emissions and heat transfer : Including thermodynamical principles. pt. 1. diesel engines a : Performance analysis and turbocharging : Wb4408a. performance analysis," 2009.

[42] Hoornaert, M., "Performance of a propulsion system in the seaway -design for service-," 2014, MSc. thesis Technische Universiteit Delft.

[43] International organization for standardization, "Iso 8217:2017 petroleum products - fuels (class f) - specifications of marine fuels," https://www.iso.org/standard/64247.html, 24-10-2017, 2017.

[44] IMO-MEPC, "Description of the package of technical and operational reduction measures for ships agreed by mepc59," pp. 1–8, 2009.

[45] ——, "Air pollution and energy efficiency - a study on minimum power requirements (MacRAW)," 2016.

[46] ——, "Amendments to marpol annex VI on regulations for the prevention of air pollution from ships by inclusion of new regulations on energy efficiency for ships," 2011.

[47] Vrijdag, A. and Stapersma, D., "Extension and application of a linearised ship propulsion system model," pp. 50–65, 2017.

[48] Journée, J.M.J., "Quick strip theory calculations in ship design," 1992.

[49] Brandt, H., "Gutachten für das Befahren von Flachwassergebieten mit Kleinfahrzeugen unter Motor in besonderer Hinsicht auf den Saaler Bodden bis zum Achterwasser von Usedom und die Gewässer um Hiddensee," 1999, (in German).

[50] Minsaas, K. J., "Ship design for fuel economy - propulsion in service conditions influence of hull deterioration, waves, wind and steering," 1983.

[51] Godjevac, M., "Wear and friction in a controllable pitch propeller," 2009.

[52] Rammell, C., Wedgeworth, L., Brown, C., Combley, R., Hewitt, C., Raybould, H., Todd, J. and Williams, J., "Collins cobuild learners dictionary," 1996.

[53] Boyce, W.E. and DiPrima, R.C., "Elementary Differential Equations and Boundary Value Problems," 2012.

[54] Bretschneider, C.L., "Generation of waves by wind," 1964.

[55] Pierson, W.J. and Moskovitz, L., "A proposed spectral form for fully develloped wind seas based on the similarity theory of s. a. kitaigorodskii," 1964.

[56] Torsethaugen, K., Haver, S. , "Simplified double peak spectral model for ocean waves," Touson, France, 2004.

[57] Gourlay, T., von Graefe, A., Shigunov, V. and Lataire, E., "Comparison of aqwa, gl, rankine, moses, octopus, pdstrip and wamit with model test results for cargo ship wave-induced motions in shallow waters," 2015.

[58] Pape, W., "Handwörterbuch der griechischen sprache," p. 1243, 1914.

[59] Shiba, H., "Air-drawing of marine propellers," p. 9:1–320, 1953.

[60] MacPherson, D.M., Puleo, V.R. and Packard, M.B., "Estimation of entrained water added mass properties for vibration analysis," www.hydrocompinc.com/knowledge, 2007.

[61] Geertsma, R.D., Negenborn, R.R., Loonstijn, M.A. and Hopman, J.J., "Pitch control for ships with diesel mechanical and hybrid propulsion: Modelling, validation and perforance quantification," 2017.

[62] Ding, Y., "Characterising combustion in diesel engines using parameterised finite stage cylinder process models," 2011.

[63] Schulten, P.J.M., "The interaction between diesel engines, ship and propellers during manoeuvring," 2005.

[64] Haugen, F., "The good gain method for pi(d) controller tuning," 2010.

[65] Schwanecke, H., "Gedanken zur frage der hydrodynamischen schwingungserregung des propellers und der wellenleitung," 1963.

[66] P. Naaijen, "Deterministic prediction of waves and wave induced vessel motions. future telling by using nautical radar as a remote wave sensor." 2017, thesis under embargo until 31-12-2022.

[67] Stapersma, D. and Klein Woud, H., "Matching propulsion engine with propulsor," pp. 25–32, 2014.

A

EEDI - Energy efficiency design index

The simplied formulation of the EEDI as provided in equation 1.1 is a summary of the actual definition as described in equation A.1 below. Source: [44]

$$\frac{\left(\Pi_{j=1}^{M} f_j\right)\left(\Sigma_{i=1}^{nME} P_{ME(i)} \cdot C_{FME(i)} \cdot SFC_{ME(i)}\right) + \left(P_{AE} \cdot C_{FAE} \cdot SFC_{AE^*}\right) + \left(\left(\Pi_{j=1}^{M} f_j \cdot \Sigma_{i=1}^{nPTI} P_{PTI(i)} \Sigma_{i=1}^{neff} f_{eff(i)} \cdot P_{AEeff(i)}\right) C_{FAE} \cdot SFC_{AE}\right) - \left(\Sigma_{i=1}^{neff} f_{eff(i)} \cdot P_{eff(i)} \cdot C_{FME} \cdot SFC_{ME}\right)}{f_i \cdot Capacity \cdot V_{ref} \cdot f_w} \tag{A.1}$$

B

Fourier transform equations

$F(t)$ in equation B.1 describes a time dependent signal that repeats itself after a period T. It uses equations B.2 to B.4 per value of component n, which is a positive integer. As in the description of a wave under **b2.** in section 3.1, use is made of the definition that $\omega = 2\pi T$. This allows a description of the signal F(t) in the domain from t to $t + T$.

$$F(t) = a_0 + \Sigma_{n=1}^{\infty} (a_n cos(n\omega t) + b_n sin(n\omega t)) \tag{B.1}$$

$$a_0 = \frac{1}{T}\int_t^{t+T} F(t)dt \tag{B.2}$$

$$a_n = \frac{2}{T}\int_t^{t+T} F(t)cos(n\omega t)dt for n > 0 \tag{B.3}$$

$$b_n = \frac{2}{T}\int_t^{t+T} F(t)sin(n\omega t)dt \tag{B.4}$$

C

Dimensionless parameters

This appendix elaborates on dimensionless parameters, dimensionless numbers applied to describe a specific flow. After a summarising table C.1, their sources, physical importance and possible use in the description of propeller ventilation are discussed.

number	definition	ratio	note	source
$Fr\ [-]$	$= \frac{v_a[ms^{-1}]}{\sqrt{g[ms^{-2}]\cdot L[m]}}$	inertial / gravitational	hull	[11]
$Fr_p[-]$	$= \frac{g[ms^{-2}]}{(n[s^{-1}])^2\cdot D[m]}$	gravitational / inertial	propeller	[7]
	$= n[s^{-1}]\cdot\sqrt{\frac{D[m]}{g[ms^{-2}]}}$	inertial / gravitational	propeller	[31] and others
$J\ [-]$	$= \frac{v_a[ms^{-1}]}{n[s^{-1}]\cdot D[m]}$	advance velocity / circumferential speed	propeller	[11]
$\sigma[-]$	$= \frac{p-p_v[Nm^{-2}]}{\frac{1}{2}\cdot\rho[kgm^{-3}](n[s^{-1}])^2\cdot(D[m])^2}$	$p - p_v$	propeller	[36]
$h/R[-]$	$= \frac{\zeta+h_p}{R}$	shaft centerline immersion / diameter	propeller	[21]
$Re\ [-]$	$= \frac{\rho[kgm^{-3}]\cdot v_S[ms^{-1}]\cdot L[m]}{\eta[kgm^{-1}s^{-1}]} = \frac{v_S[ms^{-1}]\cdot L[m]}{\nu[m^2s^{-1}]}$	inertial / viscous	propeller	[11]
$We[-]$	$= n_p[s^{-1}]\cdot D[m]\sqrt{(\frac{\rho[kgm^{-3}]\cdot D[m]}{S[Nm^{-1}]})}$	inertial / surface tension	propeller	[15]

Table C.1: Dimensionless parameters.

Froude number $Fr[-]$ (hull)

As described by Klein Woud and Stapersma (2002) [11], "*the Froude number Fr represent ... the dynamic (waves) effects on resistance (and power)*". It characterises the relation between inertial forces and the gravitational forces in a flow of water. The physical importance of Fr lies in the fact that it, as put by van der Leij (2019) [31], is a "*parameter which indicates the potential of free surface deformation.* As waves can play a significant role in the immersion of a propeller, next to other factors such as static-immersion, they also play a significant role in the description of ventilation. Although this description of the Froude number is undisputed in the description of hull-resistance, it is not used directly in this work. Instead, the propeller- or rotational-Froude number below is selected to describe the influence of waves on propeller-ventilation.

Froude number $Fr_p[-]$ (propeller- or rotational-)

Equations $Fr_p[7]$ and $Fr_p[31]$ in table C.1 are described as squared-inverses and are therefore other definitions of the same parameter: $Fr_p[7] = \frac{1}{\sqrt{Fr_p[31]}}$. This Froude number, applied to a propeller instead of the wetted hull, describes the relation between gravitational- and inertial-forces in the flow. The physical importance of this parameter in the field of propeller ventilation is that it characterises the tendency of the flow to disturb the free surface of the flow around the propeller.

Propeller ventilation is defined as "*the transport of a mass of air from the water surface through the propeller plane*" on page 1. Following that definition, Fr_p can be used undiputedly to describe the tendency of the flow to deform the water surface above, and thereby the tendency to incept or sustain a ventilating regime.

Advance ratio $J[-]$

The advance ratio (Klein Woud and Stapersma (2002) [11]) or advance coefficient (Guoqiang *et al.* (1989) [7]) characterises the inflow conditions of water at the propeller blade. As the propeller blades do not experience an undisturbed flow, but one disturbed by the presence of the hull Klein Woud and Stapersma (2002) [11] note that "*it is proportional to the tangent of the angle between advance velocity v_a and the circumferential speed of the propeller.*" In other words, it describes the relation between advance velocity and the circumferential speed (Klein Woud and Stapersma (2002) [11]) of a propeller blade.
This relation has physical importance as it characterises the inflow regime of the propeller and in particular the amount of slip that occurs. As discussed by Guoqiang *et al.* (1989) [7], slip in turn can be used to characterise different ventilation regimes. It is concluded that the advance ratio characterises the inflow conditions of water at the propeller blade as they vary with different ventilation regimes and -events. All consulted sources on propeller ventilation confirmed the significant relation between the advance ratio and the type of ventilation that might occur.

Cavitation number $\sigma[-]$

The cavitation number in table C.1 as posed by Vrijdag (2009) [36], is used by many other sources before and after, amongst which Guoqiang *et al.* (1989) [7]. Following Vrijdag (2009) [36], it describes "*the nondimensional pressure at mean shaft immersion.*" In other words, it is a non-dimensional pressure difference between the ambient pressure at the propeller shaft centerline p and the vapour pressure of the medium p_v This parameter governs the inception of cavitation and describes a pressure ratio, which is done under the assumption of a water-column present above the propeller. Van Beek and van Terwisga (2006) [29] found that "*cavitation has a strong damping effect*" on the occurrence of ventilation. As this attenuating effect of cavitation can dampen the effect that ventilation has on blade- and propeller loading. As this work treats a worst-case ventilation-loading, this influence is neglected. *Secondly*, the inception of ventilation is governed more by the disturbance of the water surface than by this pressure difference, or the surface tension forces discussed under $We[-]$, below. In summary, the cavitation number σ does not characterise ventilation directly or significantly and is neglected as simultaneous cavitation only has a damping influence on ventilation loads.

Immersion ratio $h/R[-]$

Koushan (2007) [21] defines h/R as the vertical distance between a location on the still-water level and the water-surface at that location. Applied to a propeller, it describes the relation between vertical distance between the centreline of the propeller-shaft and surface of the water above: $h/R[-] = (h_p(t)[m] + \zeta(t)[m])/R[m]$. As immersion h (below still-water) and wave height ζ (above still-water) are defined in opposite directions (see figure 4.5B), $h/R[-]$ can be negative for reduced values of h and out-of-water-events.

Reynolds number $Re[-]$

Klein Woud and Stapersma (2002) [11] describe that "*the Reynolds number Re represent ... the viscous (friction) effects on resistance (and power)*". This description focuses on the application of the Reynolds number to characterise the flow-regime around a wetted hull. The application of Re to characterise a flow around propeller blades equally describes whether the flow is laminar, transient or turbulent in character. In either application, it expresses the relation between inertial- and viscous-forces in the respective flows. In other words, it's physical importance lies in the fact that it describes the amount of transverse flow-components in a flow.
As discussed in more detail by Guoqiang *et al.* (1989) [7], ventilation events are more likely to occur and profound in nature for flows with a larger Reynolds number and a more turbulent flow. Following that work, a Re-limit is imposed to ensure a turbulent flow in the modelled system.

Weber number $We[-]$

Carlton (2007) [15] described the Weber number in table C.1 with S as the air-water surface tension in $[Nm^{-1}]$. It characterises the relation between inertial- and surface tension- forces. Thereby it characterises the likelihood of cavities or air-pockets in a flow to deform, which is governing in early-stage inception. According to Carlton (2007) [15]:
"*Shiba (Reference 46) based on a large set of model measurements concluded that if the Weber number is greater than 180 then its effect is probably insignificant.*"
For lower numbers, effects would be less significant or delayed. The system described in this work, requires an engine speed of $n_e = 83.3[rpm]$ to render its influence insignificant. As this is less than the minimum speed of the engine as defined in figure E.1, the influence and physical importance of We are "*probably insignificant*" at the notably larger rotational speeds described in this work. It is therefore not selected as a characteristic or governing parameter in this work regarding ventilation.

Conclusion

Remark The mentioned *Ship*- and *advance*-velocities characterise the velocity of the undisturbed flow surrounding the hull of the ship, and the inflow condition of the propeller blade. They differ by a factor w [-], the wake-factor, that characterises the flow-disturbance in the wake of the hull.

D

Damen Combi freight carrier 3850

The following data was published by Damen (2017) [9] in a product-sheet characterising a contemporary coaster design. This data is published here with permission from the Damen shipyards group and is used to characterise the design and propulsion system of a realistic current design. This specific design is chosen based on the criteria discussed in section 2.6. It is powered by a single medium speed marine Diesel engine that powers an FPP.
Table D.1 presents the designs principle particulars. It is followed by table D.2 which characterises the propulsion system. Table D.3 characterises the propulsive qualities of the design which can be seen in figure D.1.

Figure D.1: Combi freighter 3850 standard. Source: [9]

Dimensions		[unit]
Length overall	88,60	m
Length b.p.p.	84,99	m
Beam moulded	12,50	m
Depth moulded	7,00	m
Draft design	5,42	m
Deadweight	3.800	t
Tonnage measurement	2.545	GT

Table D.1: Dimensions from Damen combi freighter 3850 product sheet. Source: [9]

Propulsion system	[unit]
Main engines	Diesel (MGO), 1.520 kW at 1.000 rpm
Gearbox	Reverse reduction type
Stern tube	Oil lubricated
Propeller	Fixed pitch, 2.600 mm
Steering gear	Electric hydraulic
Rudder	Spade type
Bow thruster	Electric, fixed pitch, 220 kW

Table D.2: Propulsion system from Damen combi freighter 3850 product sheet. Source: [9]

Performances		[unit]
Speed, d=3,20 m 100% MCR approx.	12,5	kn

Table D.3: Performances from Damen combi freighter 3850 product sheet. Source: [9]

E

Wärtsilä 20

The following data was published by Wärtsilä (2017) [10] describing the Wärtsilä 20 engine range. Wärtsilä's W 8L20 engine is an 8-cylinder engine design with the cylinders in line (L) and a cylinder bore of 20 [cm]. The engine operates at a speed of 1.000 [rpm] and produces 1.600 [kW] brake power. This is comparable with, and sufficient for the 1.000 [rpm] and 1.520 [kW] required characteristics mentioned in table D.2. Tables E.1 to E.3, selected from Wärtsilä (2017) [10] characterise the design of Wärtsilä's W 8L20 engine. Figure E.1 depicts the operational envelope of the engine while figure E.2 depicts the engines maximum temporary recommended load increase. Section 2.3.2.1 Maximum instant load steps, from [10] also states that: *"The maximum permissable load step is 33% MCR for an engine without SCR and 25% MCR if the engine is equipped wit an SCR. The resulting speed drop is less than 10% and the recovery time to within 1% of the steady state speed at the new load level is max. 5 seconds*". The maximum recommended load increase rates for variable speed engines are shown in figure E.2.

Wärtsilä 8L20		ME Tier 2 mode
Cylinder output	kW	200
Engine speed	RPM	1000
Speed mode		Variable
Engine output	kW	1600
Mean effective pressure	Mpa	2.73

Table E.1: Selection of general data from subsection 3.3 Technical data - Wärtsilä 8L20. ME = Engine driving propeller, variable speed. Source: [10]

Wärtsilä 8L20		ME Tier 2 mode
Combustion air system (Note 1)		
Flow at 100% load	kg/s	3.15
Temperature after air cooler (TE601)	^{0}C	50...70

Table E.2: Selection of combustion air system data from subsection 3.3 Technical data - Wärtsilä 8L20. Note 1 At ISO 15550 conditions and 100% load. Flow tolerance 5%. Source: [10]

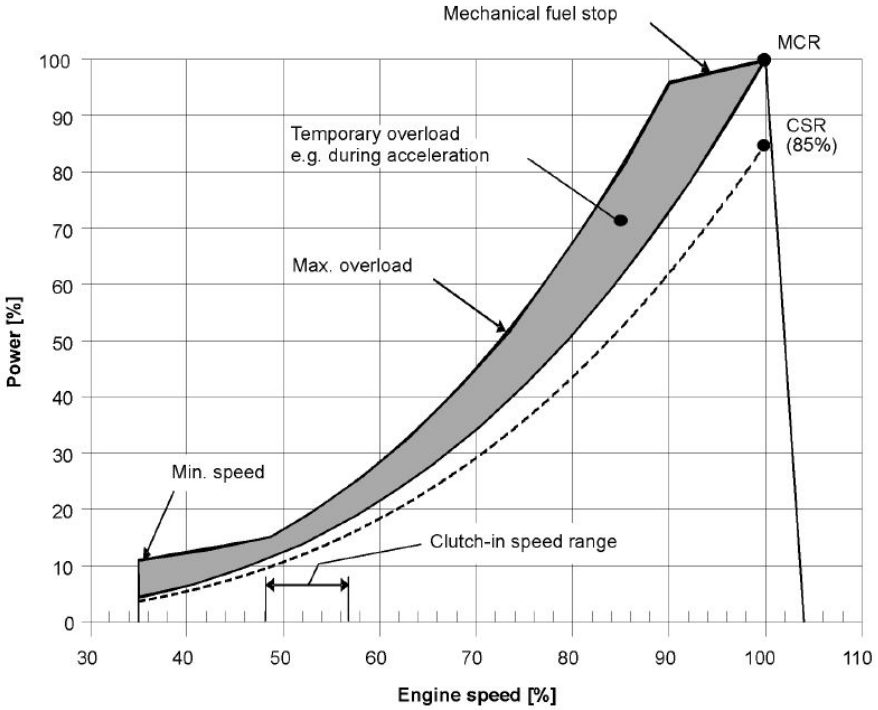

Figure E.1: Operating field for FP Propeller (DAAF007340). Source: [10]

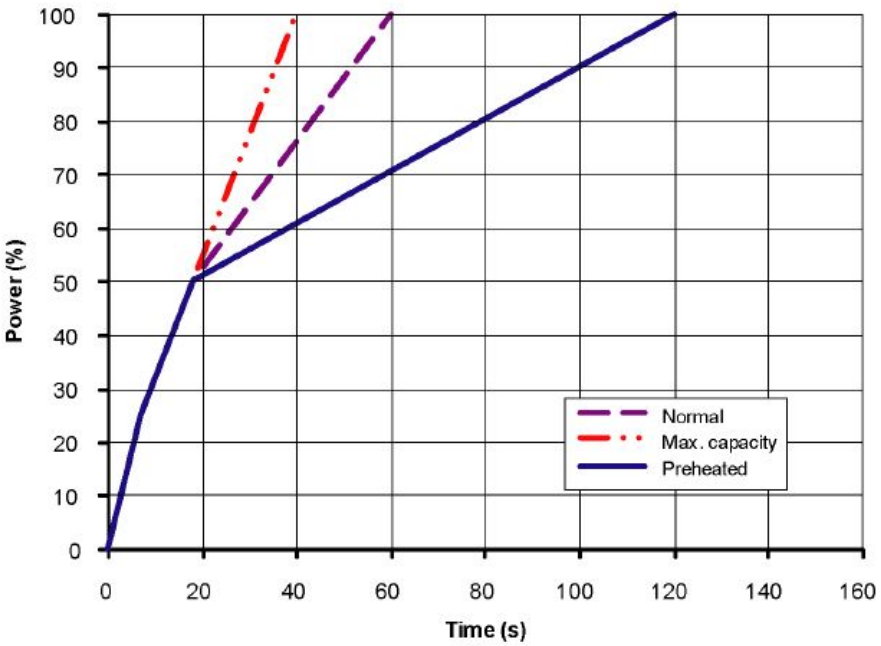

Figure E.2: Maximum recommended load increase rates for variable speed engines. Source: [10]

Wärtsilä 8L20		ME Tier 2 mode
Exhaust gas system (Note 2)		
Flow at 100% load	kg/s	3.11
Flow at 85% load	kg/s	2.77
Flow at 75% load	kg/s	2.4
Flow at 50% load	kg/s	1.61
Temperature after turbocharger, 100% load	^{0}C	370
Temperature after turbocharger, 85% load	^{0}C	340
Temperature after turbocharger, 75% load	^{0}C	350
Temperature after turbocharger, 50% load	^{0}C	385
Backpressure, max.	kPa	5.0
Calculated pipe diameter for 35 m/s	mm	453

Table E.3: Selection of exhaust gas system data from subsection 3.3 Technical data - Wärtsilä 8L20. Note 2 At ISO 15550 conditions. Flow tolerance 5% and temperature tolerance 10^0C. Source: [10]

F

Different modelling details

Fuel-pump setpoint
The limiter and fuel-pump relate the engine's required- and provided- fuel-rack setting according to equation F.1.

$$X_{set}[mm] = X_{nom}[mm] \cdot (0.1 + 0.9 \cdot X_{req}[-] | \{\leq X_{lim}\}) \tag{F.1}$$

Wave-frequency limiting
Sørensen (2013) [35] describes how insignificant wave components can be neglected by implementing equation F.2. It limit's the wave-frequency with a maximum value, dependent on the spectrums peak-frequency ω_p and a cutoff factor ξ [-]. The value of ξ = 2.5 [-] is used in this work and considered to be sufficient for the intents and purposes of the seastate to be described.

$$\omega_{max}[rads^{-1}] = \xi[-] \cdot \omega_p[rads^{-1}] \tag{F.2}$$

Regarding the advance velocity v_a

Assumptions
Following Carlton (2007) [15], the classical description of the advance velocity of the propeller blades, $v_a[ms^{-1}]$, as used in equation 2.6, is usually described as equation F.3.

$$v_a[ms^{-1}] = v_s[ms^{-1}] \cdot (1 - w(v_s))[-] \tag{F.3}$$

Sørensen (2013) [35] elaborates with equation F.4, where index w indicates the wake fraction caused by wave motion of the water particles, p the wake fraction caused by potential effects in an ideal fluid and v the wake fraction resulting from viscous effects resulting from the presence of boundary layers along the hull. (Sørensen (2013) [35])

$$V_a = U[ms^{-1}] \cdot (1 - (w_w + w_p + w_v) \tag{F.4}$$

Sørensen (2013) [35] further remarks that "*One should notice that (F.4) only must serve as a rough estimate, since it does not account for the interactions between the vessel motion and the actual wave particle flow.*"
Perhaps the most important assumption behind these descriptions of the advance velocity is, as described by Sørensen (2013) [35], that "*For a ship moving forward, V_a is less than U since the after-body flow changes its magnitude between ship speed near the vessel and zero far from the vessel.*" Or, in other words, the assumption that there is *no flow* present far from the vessel.
Sørensen (2013) [35] implements the disturbance by waves in w_w, whilst Stapersma (2000) [17] provides another example, in figure F.1 below. It explicitly shows these 'Disturbances' to the advance velocity v_a by influences on the wake of a vessel with a Controllable Pitch Propeller.
Description of a wave
To describe this influence of present waves on the advance velocity v_a, this work *firstly* assumes a uniform *zero-velocity* field, or still-water. *Secondly*, this is superposed with the explicit presence of an

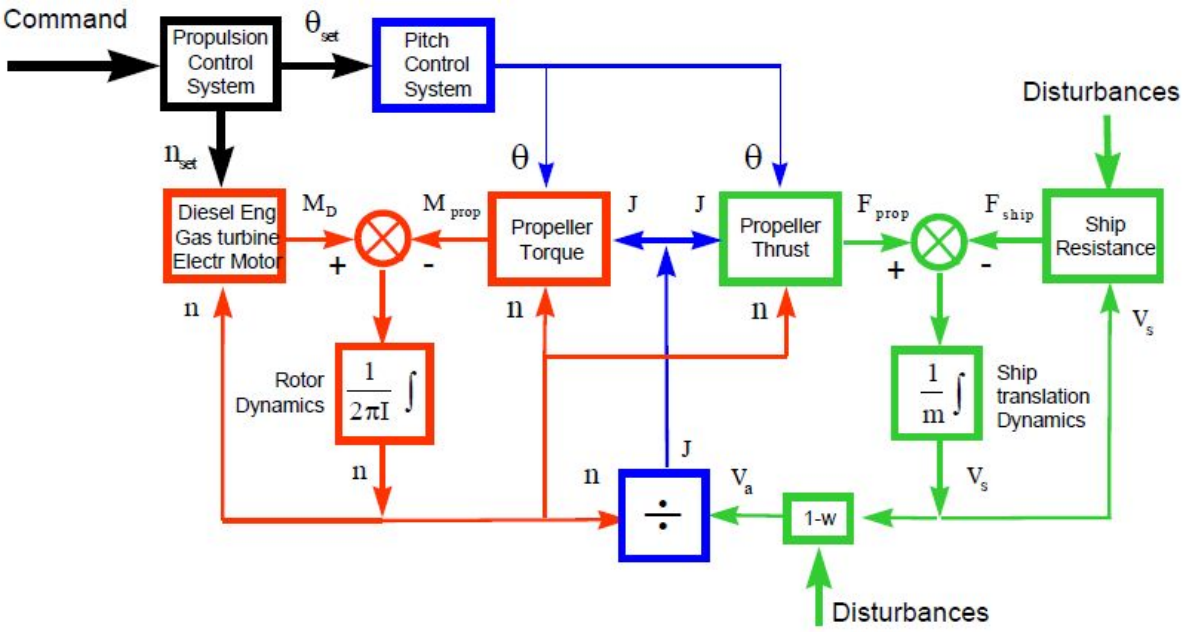

Figure F.1: Block diagram of ship dynamics. Source: [17]

explicitly-described wave-field. The wave-field is implemented with the Marine Systems Simulation-(MSS) toolbox by Fossen and Perez (2004) [8] which is verified in section 5.2, using appendix J. This in term follows the use of the Couchy-Poisson boundary condition (F.5) as discussed by Journée and Massie (2001) [19]. They use it to describe the displacement and motion of water-particles in a wave moving in an x-z reference-frame:

$$\Phi_w(x,z,t) = \Phi_w(x,z) \cdot sin(\omega t) \tag{F.5}$$

The assumed potential flow of a water particle in equation F.5 is used to derive u, the horizontal flow speed of the particle in x-direction, with equation F.6. Further assumptions of the dispersion relation in equation F.7 and deep water ($h >> 1$)[1] in equation F.8, result in a description of the horizontal flow speed u of an infinitesimal small water particle.

$$u = \frac{\delta\Phi}{\delta x} = \frac{dx}{dt} = \zeta_a \frac{kg}{\omega} \frac{coshk(h+z)}{coshkh} cos(kx - \omega t) \tag{F.6}$$

$$u = \zeta_a \omega \frac{coshk(h+z)}{sinhkh} cos(kx - \omega t) \tag{F.7}$$

$$u = \zeta_a \omega e^{kz} cos(kx - \omega t) \tag{F.8}$$

From particle to wave-field

This description of the motion of a single particle in the x,z-reference frame is further expanded to an x,y,z-reference frame by the inclusion of wave component direction ψ and relative direction μ, according to figure 3.3a, in equation F.9. Owing to the equations linearity, it can be used to superpose descriptions for i = q [-] different wave components i in a wave-field, each characterised by their respective values of $\zeta_{a,i}, \omega_{e,i}, k_i, \epsilon_i$ and $\mu_i = \psi_i - \psi_{hull}$. Equation F.10, thereby constitutes a complete description of horizontal flow speed $u_w[ms^{-1}]$ of multiple wave components in the x,y,z-reference frame, in x-direction. The description is given as a function of (x,z)-displacements and time: $u_w = f(x,z,t)$.

[1] h As used by Journée and Massie (2001) [19] does not refer to the immersion of the propeller shaft, but the water depth measured between still-water level and bottom.

$$u = \zeta_a \omega e^{kz} cos(kxcos(\mu) - \omega t + \epsilon) \tag{F.9}$$

$$u_w = \Sigma_{i=1}^{q}\, u_i = \Sigma_{i=1}^{q}\, \zeta_{a,i} \omega_i e^{k_i z} cos(k_i xcos(\mu_i) - \omega_{e,i} t + \epsilon_i) \tag{F.10}$$

$$u_w = \Sigma_{i=1}^{q}\, \zeta_{a,i} \omega_{e,i} e^{-k_i \frac{h}{R} R} cos(k_i xcos(\mu_i) - \omega_{e,i} t + \epsilon_i) \tag{F.11}$$

The influence of a wave-field on the wake

Carlton (2007) [15] describes that "*assuming a mean wake fraction for the vessel*" is a reasonably practised as a first-estimate to find propeller forces and moments in the early stage of design. This premise leads to $(x_p, \frac{h}{R}R)$[2], the time variant (x,z) location of the propeller shaft heart-line, as the point that is evaluated with equation F.11. The final step between *zero-flow* and a sufficiently accurate description of the advance velocity v_a of the propeller lies in the inclusion of this horizontal flow speed u_w.

The horizontal flow speed of the waves u_w can now be calculated with the waves-block data from the MSS-toolbox by Fossen and Perez (2004). It can then be used to describe the disturbances on the advance velocity v_a, as shown in figure 3.23 by implementing it in the model with equation F.12.

$$v_a = (U - u_w(x, h/R, t)) \cdot (1 - w(U - u_w)) \tag{F.12}$$

[2]h meaning propeller shaft immersion in equation F.11 and onwards.

Submodel (system)	Process	Formula	Output	Assumption
Turbine-compressor	amb - t			
Inlet manifold	ic - inl	$T_{inl}[^{\circ}K]$		$T_1[^{\circ}K]$
Intercooler (open)	b-c(=1)	$T_c[K]$ $p_c[Pa] - p_{loss,IC}[Pa]$?	$T_c[K]$ $p_b[Pa]$	Ideal intercooler
Inlet volume		$\int(\dot{m}_C - \dot{m}_{cyl,in})dt[kg] \cdot (V_{inl}[m^3])^{-1} R[J(kgK)^{-1}] \cdot T_{inl}[K]$	$p_c[Pa]$	
Heat-release & 5-stage Seiliger (closed)	1-2		$T_2[K]$ $p_2[K]$ $w_{12}[Jkg^{-1}]$	Isentropic (adiabatic and reversible) compression of air (as ideal gas).
Heat-release & 5-stage Seiliger (closed	2-3		$T_3[K]$ $p_3[Pa]$	Constant-volume heat-release
Heat-release & 5-stage Seiliger (closed)	3-4			Constant-pressure heat-release
Heat-release & 5-stage Seiliger (closed)	4-5			Isothermal heat-release
Heat-release & 5-stage Seiliger (closed)	5-6			Polytropic expansion
Heat-release & 5-stage Seiliger (closed)	6-1			Constant-volume heat release
Turbine-compressor (open)	6-1	$p_{atm}[Pa] \cdot (\frac{\eta_{com}[-] \cdot q_{61,cyc,kg,cyl}[Jkg^{-1}]}{c_{p,a}[Jkg^{-1}K^{-1}] \cdot T_{amb}[^{\circ}K]} - 1)^{\frac{n_{TC}[-]}{n_{TC}[-]-1}}$	$p_{1,est}(t)[Pa]$	Isentropic expansion

Table F.1: Summary of modelled prime-mover components and processes.

$I_{xx} = k_{xx}^2 \cdot \rho\nabla$
$I_{yy} = k_{yy}^2 \cdot \rho\nabla$
$I_{zz} = k_{zz}^2 \cdot \rho\nabla$
$k_{xx} \approx 0.30 \cdot Bto0.40 \cdot B$
$k_{yy} \approx 0.22 \cdot Lto0.28 \cdot L$
$k_{zz} \approx 0.22 \cdot Lto0.28 \cdot L$
From Journée and Massie (2001) [19], (see equation 8.2).

G

On turbo-charger modelling

Different parts of the prime-mover model The closed-cylinder process follows a certain p-v-(pressure versus volume-) -relation, as depicted in figure 3.16. This is modelled in two parts: *Firstly*, the p-v relation for the closed-system work-stroke as depicted in figure 4.10. *Secondly*, the open-system of the turbocharger that defines the varying value of $p_1[Pa]$.
Regarding the inlet- and exhaust-receivers An engine's inlet- and exhaust receivers gather mass to be transported to- and from the engine's cylinders. They have to distinct effects on these masses: *Firstly* they change the temperature of the passing masses as the receiver walls have a different temperature than the masses. *Secondly*, as mass is distributed between multiple cylinders and a single receiver, pressure fluctuations are dampened by the presence of the receiver. This effect is strengthened by the medium's compressibility.
Miedema and Lu (2002) [34] further characterise the functioning of a turbocharger by a turbocharger-specific delay. This delay is introduced by the turbocharger's rotational inertia. It is modelled in the frequency domain s with a cut-off frequency that neglects variations of the pressure with higher frequencies than the cut-off frequency. Using equation G.1, this frequency is rewritten as a period.

$$f_{TC}[s^{-1}] = \frac{1}{T_i[s]} \tag{G.1}$$

Implementation within prime-mover model As figure 2.14a depicts, the turbo-charger raises the cylinder charge pressure ($p_1[Pa]$) by expanding hot exhaust gasses leaving the cylinder. To limit the range of $p_1[Pa]$, a bypass- and overflow-valve are implemented. If the turbo-charger $p_1[Pa]$ would fall below atmospheric pressure, this bypass-valve would ensure that $p_1 = 1 \cdot 10^5[Pa]$, the assumed atmospheric pressure. The overflow-valve limits $p_1 \leq 4 \cdot 10^5[Pa]$, which is the selected design-value, deemed to be realistic. A charge-pressure delay, originating from the rotational inertia of the turbocharger is implemented as a static delay of $\tau_{tc} = 2[s]$.
The functioning of the turbo-charger Regarding the implementation of upper- and lower limits and a delay to the charge-pressure p_1, the functioning of the turbocharger can be described using equation **??**, following the work of Miedema and Lu (2002) [34]. Three notable differences are the fact that Miedema and Lu (2002) [34] described p_1 explicitly as a function of the delay, *and* that they simplified the closed-cylinder process to a 5-point description, instead of the more detailed 6-point description. *Finally*, and albeit unusual, Miedema and Lu (2002) [34] describe a *specific* charge-pressure, dependent on m_1 and thereby the massflow of the closed-cylinder process.
A final remark regarding this method is the assumption of conservation of mass: it is assumed that the complete mass $m_{1,cyc,cyl}[kg]$ undergoing the closed cylinder process, passes through the turbocharger or it's overflow valve.
Fourier-transformed pressure variations Sørensen (2013) [35] describes three essential applications of signal filtering techniques: *Filtering of measurement noise*, *reconstruction of non-measured data* and *dead-reckoning*. The charge-pressure (p_1) signal between the turbocharger and the different cylinders is damped and delayed. The damping and delay of this signal can be described by the application of such *filtering*-techniques.

The damping and delay of the calculated p_1 variations of a single cylinder find their origin in three physical properties of the turbocharger-system:

1. Rotational inertia of the turbocharger.
2. Geometry of- and heat-transfer by the inlet- and exhaust-receivers.
3. Properties of the medium such as it's compressibility and behaviour as an assumed-to-be ideal gas.

Point (a) introduces a time-delay of the p_1-signal, whilst points (b) and (c) dampen the variations of the p_1-signal.
Miedema and Lu (2002) describe this delay and damping with a first-order non-ideal low-pass filter, summarised in equation **??**. This filter describes the delay and damping in the frequency-domain (s) instead of the time-domain (t). Parameter $\tau_{TC,cutoff} = \tau_{TC}$ can be determined empirically, or estimated alongside η_{com}.

H

Propulsion system matching

This appendix follows the method of Stapersma and Woud (2014) [67] to match components of the propulsion system. Relations H.1-H.5 link together which steps are taken in this matching-process.

The dichotomy of still-water resistance

This work is characterised by two still-water resistance curves, $R_{sw} = f(\dot{x}$. One curve describing the resistance of a hull in a, horizontally trimmed, trial or ballast condition. This is the same relation that was previously shown in figure **??**. The other one more representative of a hull in regular operation. The first is estimated with a Maxsurf Holtrop estimate. The latter, for the sake of simplicity, is estimated roughly as a multiple of this function. Figure H.1 shows that these functions, in first assumption, can roughly be represented with a 2^{nd}-order function. To determine the amount of brake engine power P_b required to propel the hull, in either or another condition, R_{sw} is used to determine the hulls required dimensionless thrust: $K_{T,ship}$ [-]. This is done under the assumption that $K_{T,ship} = \frac{c_8}{\rho \cdot D^2} \cdot J^2 = c_7 \cdot J^2$ [-], which is summarised in relation H.1.$K_{T,ship}$ in figure **??** depicts this curve.

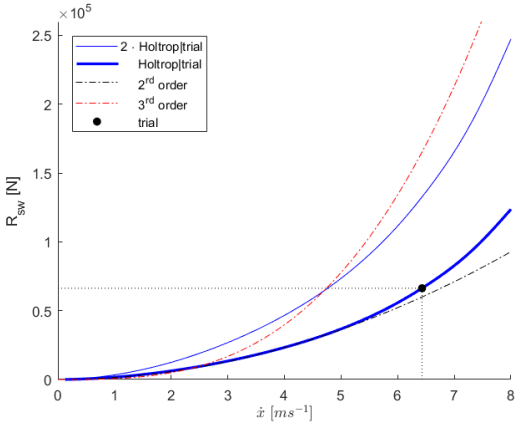

Figure H.1: Maxsurf-Holtrop based predictions, 2^{nd} order and 3^{rd} order still-water resistance curves.

A propulsion system design such as that proposed by Damen (2017) [9] is likely based on a representative *operational* resistance curve. In turn, every design can be characterised by the size of it's margins. As a result, not all characteristics of the proposed design are known in the public domain. What is known, is that the resistance curve found with Maxsurf and the Holtop method in trial condition, is significantly smaller. As a result, based on it's ventilation-related merits, the selected trial condition *is not* expected to be a showcase match. And although smaller, it does represent a realistic and in this respect, both interesting and relevant case.

Resistance to torque

$K_{T,ship}|Holtrop$ in figure **??** depicts this curve. It leads to the operational point of the propeller, by matching[1] thrust T and resistance R_{sw}, or K_t and $K_{T,ship}$ in $J_{op} = 0.62[-]$. This operational point represents the functioning of the hull under trial condition, instead of the usual match under operational condition, closer to the origin of the graph. Table H.1 lists the resulting thrust-, torque- and open-water efficiency characteristics of both these operational points. This in term is summarised in relation H.2.

[1]Remark: Note that matching of thrust and resistance, or K_T and $K_{T,ship}$, is done under non-ventilating trial condition.

Torque to power
With K_Q resulting from the now determined operational point, the propeller load M_p can be determined as a function of n_p: $M_p = \frac{\rho \cdot D^5}{\eta_R} \cdot K_Q \cdot n_p^2$. This in turn can be written as a relation between propeller power P_p and rotational speed n_p (summarised with relation H.3) which, using the transmission efficiency η_{TR}, can be rewritten as a relation between P_p and n_p. Relation H.4 summarises this. The final step to describe the load curve describes $P_{b,load}$ as a function of n_e under the assumption of the constant gearbox ratio i_{gb}.

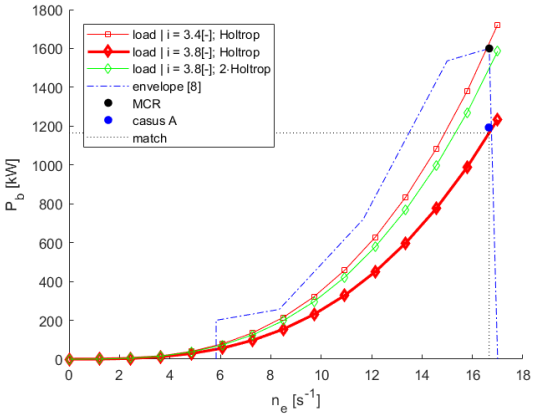

Figure H.2: Operational envelope of diesel engine with propeller load curves for different gearbox ratio's i_{gb} and resistance estimates.

Above, the single load-curve $(R_{sw}, \dot{x})$ for the hull in trial condition is rewritten as a load curve for the engine: $(P_{b,load}, n_e)$. Once this is done, the gearbox ratio i_{gb} can be determined based on the requirements that, for a well-designed propulsion system, *the load $P_{b,load}$ is smaller than MCR at nominal engine speed $n_{e,nom}$*. This ensures the implementation of a sea margin for an $(R_{sw}, \dot{x})$ load-curve the vessel is subjected to during it's operational lifetime. Relation H.5 summarises this whilst figure H.2 shows graphically how different gearbox-ratio's load the engine for the same $(R_{sw}, \dot{x})$ load-curve.

Second to this, figure H.2 also shows a load line for the larger resistance curve with the same gearbox ratio. This load line represents an *operational condition* of the same hull. It shows a near-perfect match with the engine's maximum continuous rating MCR.

In summary, trial measurements and design data of an actual vessel, described by Damen (2017) [9] are used to describe a realistic model of the propulsion system of such a vessel. Uncertainties such as the actual resistance-curve, propeller pitch P/D and gearbox-ratio i_{gb}, introduce small discrepancies between the product-sheet data and the model. However, the model provides a realistic and more detailed description of such a propulsion system. Table H.1 summarises these details and assumptions behind them.

$$R(\dot{x})|trial \rightarrow T(\dot{x}) \rightarrow K_{T,ship}(J) \quad \text{(H.1)}$$
$$K_{T,ship}(J) \rightarrow J_{op}|K_T = K_{T,ship} \rightarrow K_Q \quad \text{(H.2)}$$
$$K_Q \rightarrow M_p(n_p)|\eta_R \rightarrow P_p(n_p) \quad \text{(H.3)}$$
$$P_p(n_p) \rightarrow P_B(n_p)|\eta_{TR} \quad \text{(H.4)}$$
$$P_B(n_p) \rightarrow P_B(n_e)|i_{gb} \quad \text{(H.5)}$$

Parameter	unit [dimension]
Assumed efficiencies	
Relative rotative efficiency η_R [67]	0.99 [-]
η_{gb} [17]	0.98 [-]
η_s [17]	0.99 [-]
Transmission efficiency $\eta_{tr} = \eta_{gb} \cdot \eta_s$ [17]	0.97 [-]
Product sheet [9]	
Realised ship speed v_s ([9])	6.43 [ms^{-1}]
[9]	(12.5 [kts])
Engine 100% MCR	1520 [kW]
Estimations based on [9] and fig. **??** | trial	
$\dot{x}$	7.39 [ms^{-1}]
R_{sw}	$96.8 \cdot 10^3$ [N]
Wake fraction w	0.043 [-]
Thrust deduction t	0.082 [-]
Effective towing power P_E	715 [kW]
Factor $c_1 = \frac{R}{v_s^2}$	1773 [kgm^{-1}]
Factor $c_8 = \frac{c_1}{(1-t)(1-w)^2}$	2018 [kgm^{-1}]
Estimated operational point based on fig. **??**	
$J \approx$	0.621 [-]
$K_T \approx$	0.117 [-]
$K_Q \approx$	0.0179 [-]
$\eta_o \approx$	0.65 [-]
Estimations based on fig. H.2 | trial	
i_{gb}	3.8 [-]
P_B|trial	1193 [kW]
Engine n_e|trial	16.7 [s^{-1}]
$P_{P,load}$|trial	1157 [kW]
n_p|trial	4.39 [s^{-1}]
Theoretical ship speed v_s|trial	$\pm$ 7.39 [ms^{-1}]
	($\pm$ 14.4 [kts])

Table H.1: Data regarding design- and trial conditions
of the hull, propeller and engine. Adapted from [11] and [12]

I

Propeller air ventilation and performance of ventilated propeller

This appendix lists information regarding propeller-ventilation behaviour as published by Guoqiang *et al.* (1989) [7]. Section provides data regarding ventilating propellers. It is followed by section I which discusses data related to the implementation of the data from Guoqiang *et al.* and a comparison with experimental data by Koushan (2007) [21], illustrating the quasi-static approach.

Ventilation-related data

Table I.1 lists the different propeller designs that were described and figures I.1 describe the influence of submerged depth on open water characteristics for different rotational speeds $n_p[rps]$. Figures I.2 and I.3 finally show what can also be recognised in the first figures: For a certain immersion ratio, the increase of rotational speed $n_p[rps]$ leads to a drop of the produced thrust ratio. The influence of ventilation leads to significant drops of the thrust ratio. The truly nonlinear relation between K_T and J for lower immersion ratio's, limit's the possibilities to describe propeller-functioning under these conditions as a shift in J or K_T.

serial number of propeller model	diameter (mm)	pitch ratio	number of blades	expanded area ratio
MP8701	214.6	0.788	4	0.6
MP8702	139.5	0.788	4	0.6
MP8703	103.3	0.788	4	0.6
MP8704	140.0	0.9	4	0.5

Table I.1: Main particulars of the propeller. Source: [7]

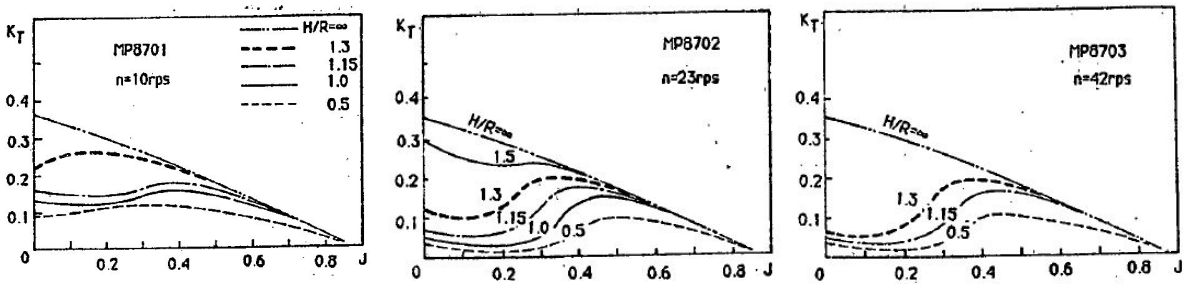

(a) (MP8701) (Reprint of fig. 2.9) (b) (MP8702) (c) (MP8703)

Figure I.1: Influence of submerged depth on open water characteristics. Source: [7]

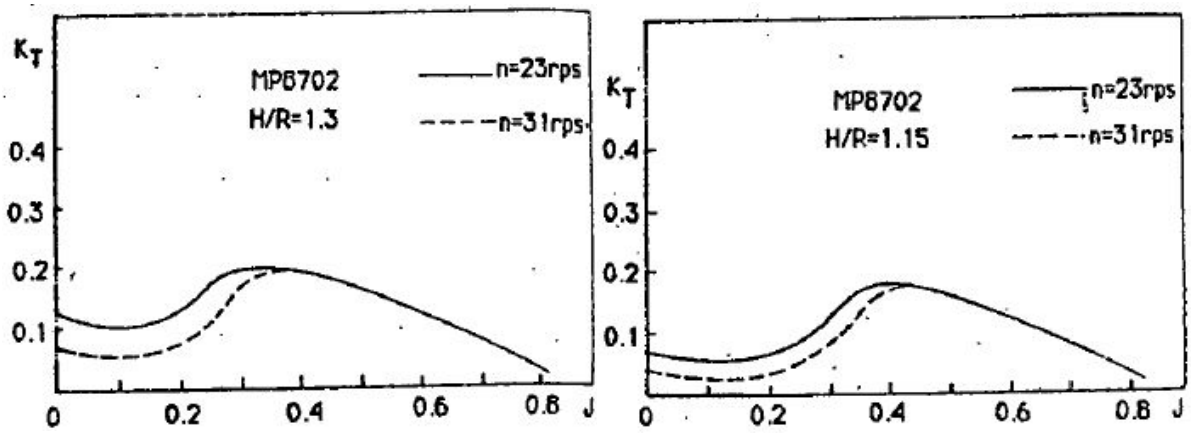

(a) (MP8702 at H/R=1.3) (b) (MP8702 at H/R=1.15)

Figure I.2: Rate of revolution on open water characteristics. Source: [7]

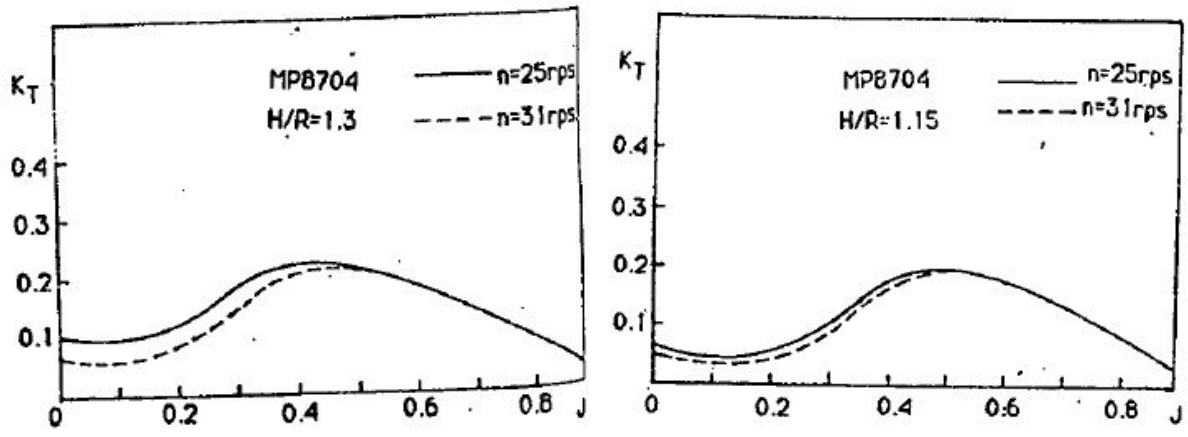

(a) (MP8704 at H/R=1.3) (b) (MP8704 at H/R=1.15)

Figure I.3: Rate of revolution on open water characteristics. Source: [7]

Implementation of ventilation-related data

To implement the aforementioned ventilation-related data regarding thrust losses, information regarding the propeller's torque-related characteristics must be added. Guoqiang *et al.* (1989) [7] state that *"all the results in the tests show that the variation tendency of K_T with J is similar to that of K_Q. So for simplicity the K_T value is used to investigate the problem of propeller air ventilation. It is obvious that the conclusions drawn from the analysis of are suitable to K_Q."* The propeller with the same number of propeller blades (4 [-]) and nearest pitch (0.788 [-]) has an expanded-area ratio A_e/A_0 of 0.6 [-]. The most-comparable propeller-torque characteristics from the Wageningen-B propeller series as published by van Lammeren, van Manen and Oosterveld in (1969) [20] are used as an estimate for the torque-characteristics at immersion ratio $h/R = \infty[-]$. These can be found under the B4-55 propeller description. For other immersion ratios, the torque breakdown as a result of occurring ventilation is estimated as an equal percentage in breakdown as the thrust-breakdown.

Comparison

The quasi-static method as treated in section 4.1, intends to describe immersion continuously (red line in figure I.5) by linear interpolation of the static-data (green crosses in figure I.4). This is done by:

- Describing immersion h/R continuously by linear interpolation of the static-data (green crosses h/R), as a function of (J, Fr_p).
- Use static-immersion ventilation data K_T (black lines in figure I.4) for varying immersions h/R (green crosses).
- Estimate thrust variations (blue line in figure I.5) of dynamic-immersion (red line in figure I.5).

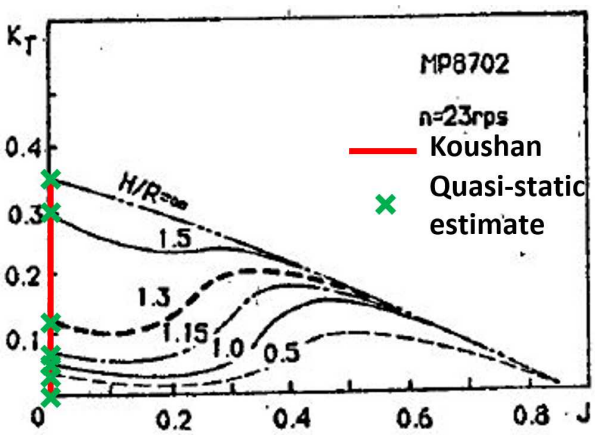

Figure I.4: Adapted from source: [7]

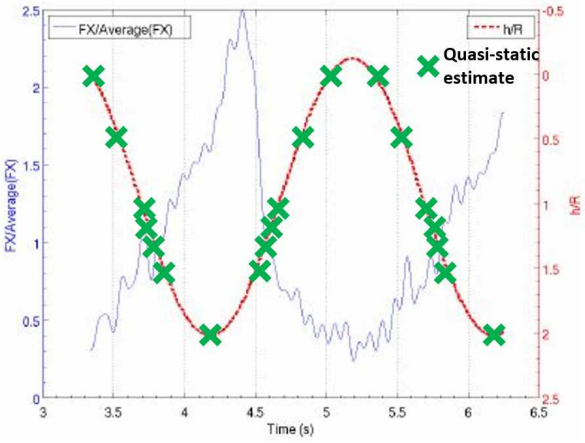

Figure I.5: Adapted from source: [7]

Two remarks are made regarding this application of static-immersion ventilation data:

- Figure I.4 assumes static immersion and thereby nearly static thrust production.
- By continuously interpolating h/R between known experimental data $(K_T, h/R)|(Fr_p, J)$, the *known systematic error* in the description of K_T is limited.

J

Modelling waves

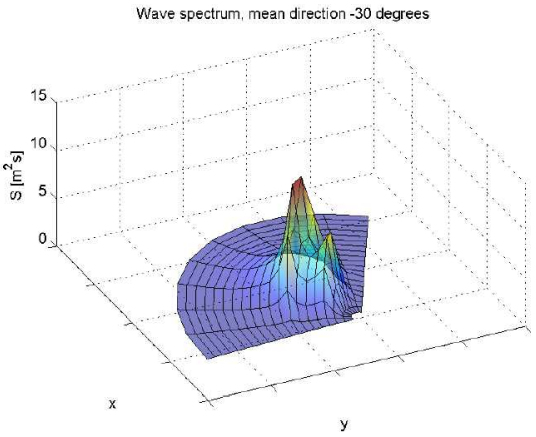

(a) Source: [35]

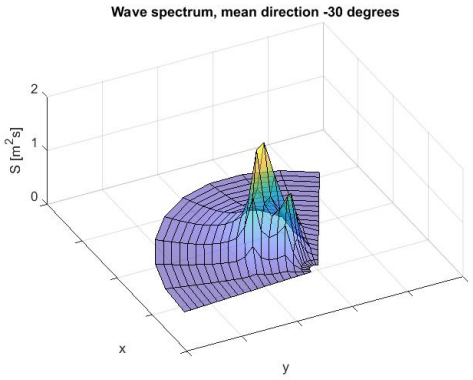

(b) By author, using [8].

Figure J.1: Torsethaugen frequency spectrum with H_s = $4m$ and ω_p = $1rad/s$, spreading function with ψ_0 = -30° and s = 4, number of frequencies and directions N = 20 and M = 10, frequency cutoff factor ξ = 2.5 and wave direction limit ψ_{lim} = 20°.

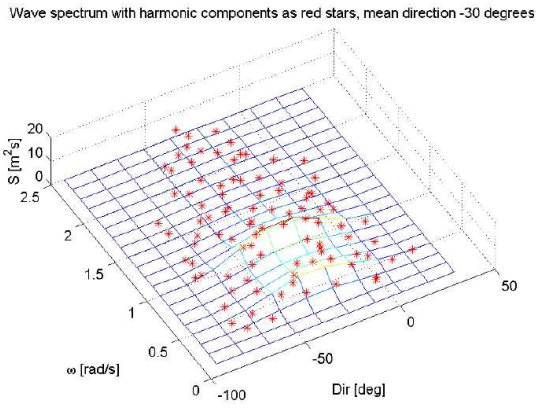

(a) Source: [35]

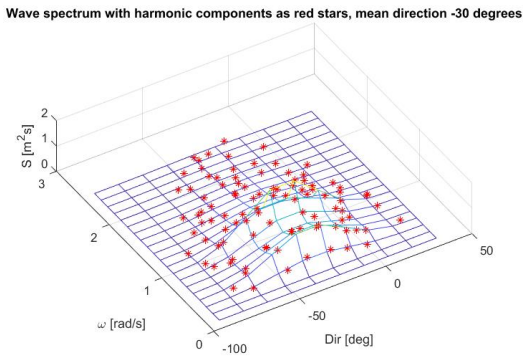

(b) By author, using [8].

Figure J.2: Wave spectrum with wave energy limit κ = 0.005. The frequencies and directions of the components, which are shown as red stars, are chosen at random

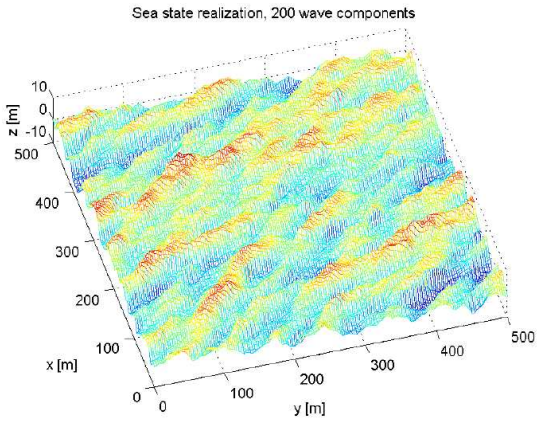

(a) Source: [35]

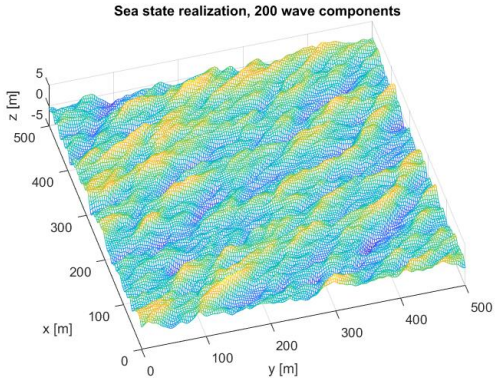

(b) By author, using [8].

Figure J.3: Realization of a Torsethaugen spectrum with 200 wave components.

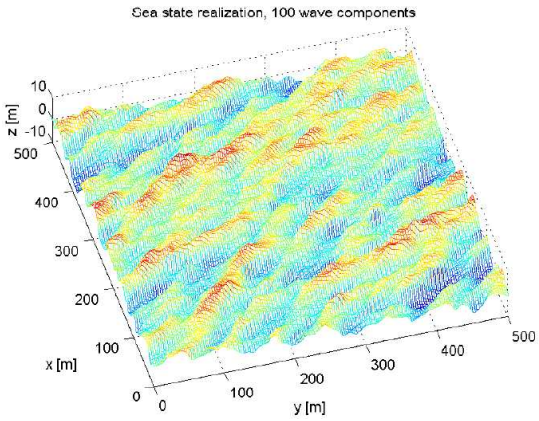

(a) Source: [35]

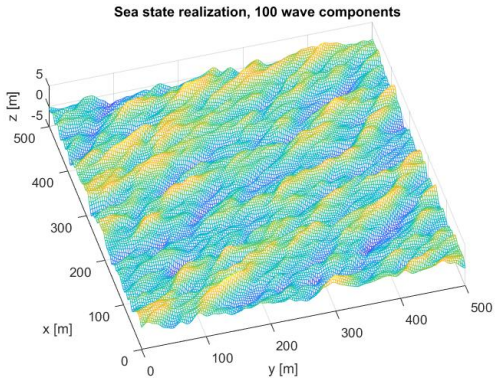

(b) By author, using [8].

Figure J.4: Realization of a Torsethaugen spectrum with 100 wave components.

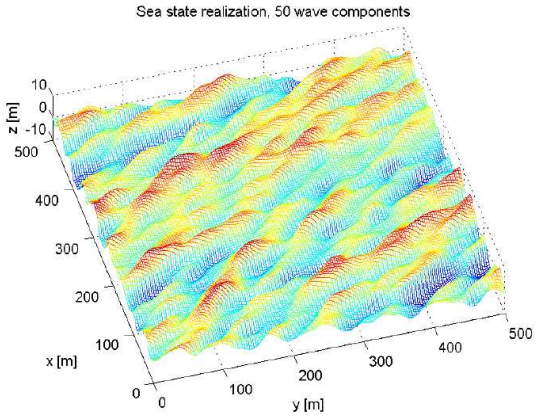

(a) Source: [35]

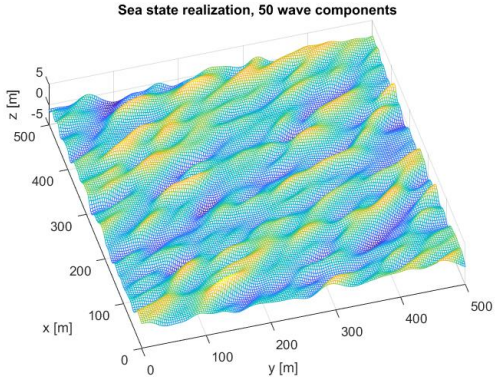

(b) By author, using [8].

Figure J.5: Realization of a Torsethaugen spectrum with 50 wave components.

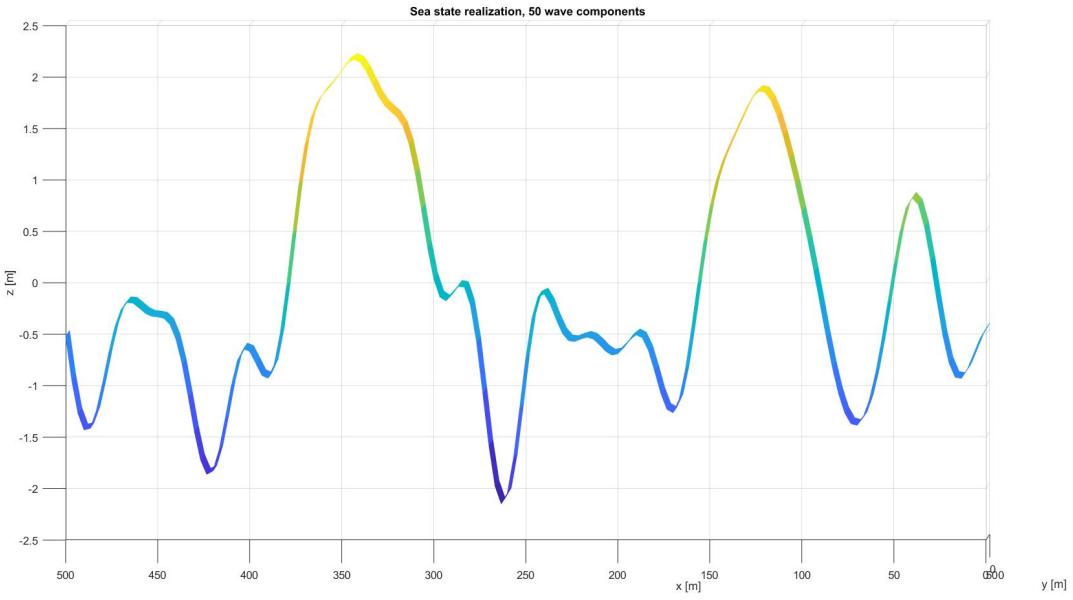

Figure J.6: Realization of an 50-component adverse Torsethaugen spectrum with the MSS-toolbox from [8].

K

Equations of motion and RAO's

Equation K.1 describes the equation of motion of the vessel's CoG in the x-direction in a $NED_{\{e\}}$ reference frame. Equations K.2 and K.3 describe the equations of motion of the vessel's CoG in heave- and pitch-directions in this reference frame.

$$m \cdot \ddot{x} = T_p - R_{sw}(\dot{x}) - R_{aw}(\dot{x}, \omega_i, \psi_i) \tag{K.1}$$

The equilibria for excitating wave forces and moments and the resulting coupled heave- and pitch-motions of a vessel's hull are used to determine A and B. These are the respective complex products describing the heave- and pitch-RAO's and their phase angles. Vice-versa, potential-flow calculations in linear strip-theory software packages such as Maxsurf Motions can be used to estimate A, B, m, I,a_{ij},b_{ij} and c_{ij}. In term, these can be used to determine solutions K.4 and K.7 to equations K.2 and K.3.

$$(m + a_{33}) \cdot \frac{\ddot{z}}{\zeta_a} + b_{33} \cdot \frac{\dot{z}}{\zeta_a} + c_{33} \cdot \frac{z}{\zeta_a} + a_{35} \cdot \frac{\ddot{\vartheta}}{\zeta_a} + b_{35} \cdot \frac{\dot{\vartheta}}{\zeta_a} + c_{35} \cdot \frac{\vartheta}{\zeta_a} = \frac{F_{z,wave}}{\zeta_a} \tag{K.2}$$

$$(I_{yy} + a_{55}) \cdot \frac{\ddot{\vartheta}}{\zeta_a} + b_{55} \cdot \frac{\dot{\vartheta}}{\zeta_a} + c_{55} \cdot \frac{\vartheta}{\zeta_a} + a_{53} \cdot \frac{\ddot{z}}{\zeta_a} + b_{53} \cdot \frac{\dot{z}}{\zeta_a} + c_{53} \cdot \frac{z}{\zeta_a} = \frac{M_{y,wave}}{\zeta_a} \tag{K.3}$$

The $z, \vartheta, F_{z,wave}$ and $M_{y,wave}$ terms above are described by equations K.4 to K.11.

$$z = z_a \cdot cos(\omega \cdot t + \epsilon_{z\zeta}) = Re\left[z_a \cdot e^{i\cdot(\omega\cdot t + \epsilon_{z\zeta})}\right] \tag{K.4}$$

$$\dot{z} = Re\left[i \cdot \omega \cdot z_a \cdot e^{i\cdot(\omega\cdot t + \epsilon_{z\zeta})}\right] \tag{K.5}$$

$$\ddot{z} = Re\left[-1 \cdot \omega^2 \cdot z_a \cdot e^{i\cdot(\omega\cdot t + \epsilon_{z\zeta})}\right] \tag{K.6}$$

$$\vartheta = \vartheta_a \cdot cos(\omega \cdot t + \epsilon_{\vartheta\zeta}) = Re\left[\vartheta_a \cdot e^{i\cdot(\omega\cdot t + \epsilon_{\vartheta\zeta})}\right] \tag{K.7}$$

$$\dot{\vartheta} = Re\left[i \cdot \omega \cdot \vartheta_a \cdot e^{i\cdot(\omega\cdot t + \epsilon_{\vartheta\zeta})}\right] \tag{K.8}$$

$$\ddot{\vartheta} = Re\left[-1 \cdot \omega \cdot \vartheta_a \cdot e^{i\cdot(\omega\cdot t + \epsilon_{\vartheta\zeta})}\right] \tag{K.9}$$

$$F_{z,wave} = F_a \cdot cos(\omega \cdot t + \epsilon_{F\zeta}) = Re\left[F_a \cdot e^{i\cdot(\omega\cdot t + \epsilon_{F\zeta})}\right] \tag{K.10}$$

$$M_{y,wave} = M_a \cdot cos(\omega \cdot t + \epsilon_{M\zeta}) = Re\left[M_a \cdot e^{i\cdot(\omega\cdot t + \epsilon_{M\zeta})}\right] \tag{K.11}$$

Equation K.2 can now be rewritten as K.12 and K.3 as K.13. Once that is done, $Re\left[e^{i\cdot(\omega\cdot t)}\right]$ can be divided out of the equations which in term leads to the complex equations K.14 and K.15.

$$Re\left[(-1\cdot\omega^2\cdot(m+a_{33})+i\cdot\omega\cdot b_{33}+c_{33})\cdot\frac{z_a}{\zeta_a}\cdot e^{i\cdot(\omega\cdot t+\epsilon_{z\zeta})}+(-1\cdot\omega^2\cdot a_{35}+i\cdot\omega\cdot b_{35}+c_{35})\cdot\frac{\vartheta_a}{\zeta_a}\cdot e^{i\cdot(\omega\cdot t+\epsilon_{\vartheta\zeta})}\right]=Re\left[\frac{F_a}{\zeta_a}\cdot e^{i\cdot(\omega\cdot t+\epsilon_{F\zeta})}\right] \quad \text{(K.12)}$$

$$Re\left[(-1\cdot\omega^2\cdot(I_{yy}+a_{55})+i\cdot\omega\cdot b_{55}+c_{55})\cdot\frac{\vartheta_a}{\zeta_a}\cdot e^{i\cdot(\omega\cdot t+\epsilon_{\vartheta\zeta})}+(-1\cdot\omega^2\cdot a_{53}+i\cdot\omega\cdot b_{53}+c_{53})\cdot\frac{z_a}{\zeta_a}\cdot e^{i\cdot(\omega\cdot t+\epsilon_{z\zeta})}\right]=Re\left[\frac{M_a}{\zeta_a}\cdot e^{i\cdot(\omega\cdot t+\epsilon_{M\zeta})}\right] \quad \text{(K.13)}$$

$$(-1\cdot\omega^2\cdot(m+a_{33})+i\cdot\omega\cdot b_{33}+c_{33})\cdot\frac{z_a}{\zeta_a}\cdot e^{i\cdot(\epsilon_{z\zeta})}+(-1\cdot\omega^2\cdot a_{35}+i\cdot\omega\cdot b_{35}+c_{35})\cdot\frac{\vartheta_a}{\zeta_a}\cdot e^{i\cdot(\epsilon_{\vartheta\zeta})}=\frac{F_a}{\zeta_a}\cdot e^{i\cdot(\epsilon_{F\zeta})} \quad \text{(K.14)}$$

$$(-1\cdot\omega^2\cdot(I_{yy}+a_{55})+i\cdot\omega\cdot b_{55}+c_{55})\cdot\frac{\vartheta_a}{\zeta_a}\cdot e^{i\cdot(\epsilon_{\vartheta\zeta})}+(-1\cdot\omega^2\cdot a_{53}+i\cdot\omega\cdot b_{53}+c_{53})\cdot\frac{z_a}{\zeta_a}\cdot e^{i\cdot(\epsilon_{z\zeta})}=\frac{M_a}{\zeta_a}\cdot e^{i\cdot(\epsilon_{M\zeta})} \quad \text{(K.15)}$$

Replacing P, Q, R and S from K.16 and K.17 simplifies complex equations K.14 and K.15 to K.18 and K.19:

$$P=(-1\cdot\omega^2\cdot(m+a_{33})+i\cdot\omega\cdot b_{33}+c_{33}) \quad \text{(K.16)}$$

$$Q=(-1\cdot\omega^2\cdot a_{35}+i\cdot\omega\cdot b_{35}+c_{35}) \quad \text{(K.16)}$$

$$R=(-1\cdot\omega^2\cdot(I_{yy}+a_{55})+i\cdot\omega\cdot b_{55}+c_{55}) \quad \text{(K.17)}$$

$$S=(-1\cdot\omega^2\cdot a_{53}+i\cdot\omega\cdot b_{53}+c_{53}) \quad \text{(K.17)}$$

$$P\cdot\frac{z_a}{\zeta_a}\cdot e^{i\cdot(\epsilon_{z\zeta})}+Q\cdot\frac{\vartheta_a}{\zeta_a}\cdot e^{i\cdot(\epsilon_{\vartheta\zeta})}=\frac{F_a}{\zeta_a}\cdot e^{i\cdot(\epsilon_{F\zeta})} \quad \text{(K.18)}$$

$$R\cdot\frac{\vartheta_a}{\zeta_a}\cdot e^{i\cdot(\epsilon_{\vartheta\zeta})}+S\cdot\frac{z_a}{\zeta_a}\cdot e^{i\cdot(\epsilon_{z\zeta})}=\frac{M_a}{\zeta_a}\cdot e^{i\cdot(\epsilon_{M\zeta})} \quad \text{(K.19)}$$

The complexes $A(\omega)=\frac{z_a}{\zeta_a}\cdot e^{i\cdot(\omega\cdot t+\epsilon_{z\zeta})}$ and $B(\omega)=\frac{\vartheta_a}{\zeta_a}\cdot e^{i\cdot(\omega\cdot t+\epsilon_{\vartheta\zeta})}$ are now defined under the assumption of a fixed vessel heading ψ, and thereby the assumption of a fixed relative angle μ between vessel heading and wave(component) direction ψ_i.

$$P\cdot A(\omega)+Q\cdot B(\omega)=\frac{F_a}{\zeta_a}\cdot e^{i\cdot(\epsilon_{F\zeta})} \quad \text{(K.20)}$$

$$S\cdot A(\omega)+R\cdot B(\omega)=\frac{M_a}{\zeta_a}\cdot e^{i\cdot(\epsilon_{M\zeta})} \quad \text{(K.21)}$$

This linear system... of complexes $A(\omega)$ and $B(\omega)$ is solved in equations K.22 and K.23. All parameters on the right side of these equations are known. Parameters $\frac{F_a}{\zeta_a}, \frac{M_a}{\zeta_a}, \epsilon_{F\zeta}), \epsilon_{M\zeta}, a$ and b vary with ω and μ. Complexes $A(\omega)$ and $B(\omega)$ can therefore be solved as a function of ω, for different values of μ.

$$A(\omega) = \frac{z_a}{\zeta_a} \cdot e^{i\cdot(\epsilon_{z\zeta})}$$
$$= \frac{M_a}{\zeta_a} \cdot e^{i\cdot(\epsilon_{M\zeta})} \cdot \left(\frac{1}{S} - \frac{Q}{P \cdot R}\right) \quad \text{(K.22)}$$

$$B(\omega) = \frac{\vartheta_a}{\zeta_a} e^{i\cdot(\epsilon_{\vartheta\zeta})}$$
$$= \frac{F_a}{\zeta_a} \cdot e^{i\cdot(\epsilon_{F\zeta})} \cdot \left(\frac{1}{Q}\right) - \left(\frac{M_a}{\zeta_a} \cdot e^{i\cdot(\epsilon_{M\zeta})} \cdot \left(\frac{P}{Q \cdot S} - \frac{1}{R}\right)\right) \quad \text{(K.23)}$$

$\frac{z_a}{\zeta_a}, \frac{\vartheta_a}{\zeta_a}, \epsilon_{z\zeta}, \epsilon_{z\zeta}$ and $\epsilon_{\vartheta\zeta}$ can now be found with equations K.24-K.27 using the Re- and Im-parts of $A(\omega)$ and $B(\omega)$ and correcting the values of K.25 and K.27 for values in the negative quadrants.

$$\frac{z_a}{\zeta_a} = \sqrt{\mathrm{Re[A]}^2 + \mathrm{Im[A]}^2} \quad \text{(K.24)}$$

$$\epsilon_{z\zeta} = arctan\left(\frac{Im[A]}{Re[A]}\right) \quad \text{(K.25)}$$

$$\frac{\vartheta_a}{\zeta_a} = \sqrt{\mathrm{Re[B]}^2 + \mathrm{Im[B]}^2} \quad \text{(K.26)}$$

$$\epsilon_{\vartheta\zeta} = arctan\left(\frac{Im[B]}{Re[B]}\right) \quad \text{(K.27)}$$

L

Analysis of ventilation events

This work applies two principally different methods to analyse ventilation events. These are called *loop-analysis* and *Olofssen-analysis*, following figure 1.2 as published by Smogeli (2006) [13]. The following sections briefly expand on the structure and application of these methods.

Loop-analysis

What is loop-analysis? As described in section 6.6, ventilation-events can display cyclic nature. Their varying influence on propeller functioning can be described in a (J,K_T)-graph, or open-water plot, as shown in figure **??**. These loops, called *immersion-loops*, describe different ventilation events. They can have different shapes and variations as a continuous function of $(J,h/R)$, characterising the specific event. They generally consist of the following steps.

- A build-up of K_T $[-]$ and thrust in the non-ventilating regime ($h/R \geq 2$ $[-]$, assumption based on Guoqiang *et al.* (year unknown) [7]).
- A relatively sudden drop of K_T $[-]$ and thrust for lower values of J and reducing values of $h/R < 2$ $[-]$.
- A minimal build-up of K_T $[-]$ and thrust for higher and increasing values of J and h/R $[-]$.
- a secondary drop of K_T $[-]$ and thrust for higher and increasing values of $[-]$, whilst $h/R < 2$ $[-]$.
- A build-up of K_T $[-]$ and thrust for decreasing values of J $[-]$ with $h/R \geq 2$ $[-]$.

A ventilation loop can consist of all possible relations in the framework scetched by Guoqiang *et al.* (year unknown) [7], in an unstable regime, even non-continuity of the relation between J and K_T could be possible. The five relations listed above provide a toolbox of sorts that can be used to describe all relations in the (J,K_T) frame-of-reference.

Why is loop-analysis applied? Analysis of these loops provides information regarding the specific loads imposed by specific ventilation events.

Olofssen-analysis

What is Olofssen-analysis? This method describes the input-conditions of a propeller with a $(J,h/R)$-relation. It categorises the expected ventilation-regime of a specific propeller-design for these conditions.

Why is Olofssen-analysis applied? Dependent on interest and intent, the (predicted) functioning of a propeller can be described. This can be especially useful to predict the functioning of the propulsion system in a longer timeframe.

Summary Two methods are described to characterise the same ventilation events. The first method focuses on a detailed description of the specific ventilation event whilst the second focuses on the effect of multiple ventilation events.

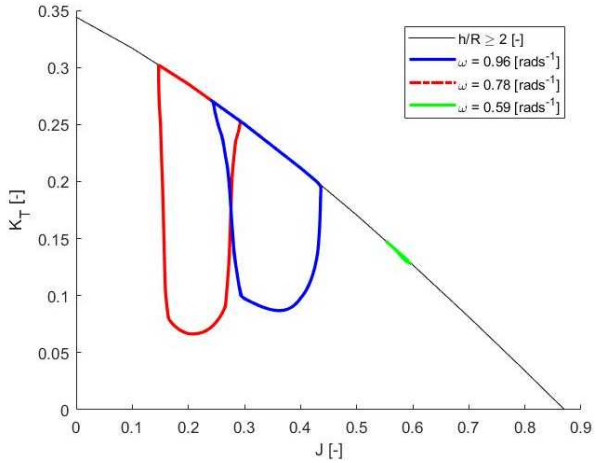

Open-water diagram for experiment A. (Reproduction of figure 6.5)

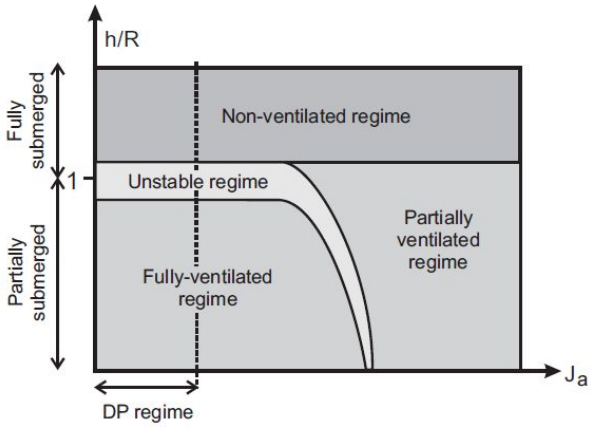

Figure 1.2: Ventilation flow regimes, with the regimes relevant for DP indicated on the Ja axis. Adopted from Olofsson. Source:[13]. (Reproduction of figure 1.2)